Dissertation

Circulating Tumor DNA in Metastatic Hormone Receptor-Positive Breast Cancer Patients With Focus on HER2 Biology

submitted by

Nina DOBRIĆ

for the Academic Degree of

Doctor of Philosophy (PhD)

at the

MEDICAL UNIVERSITY OF GRAZ

Division of Oncology, Department of Internal Medicine

Under the Supervision of:

Univ.-Prof.in Dr.in med.univ.et scient.med.

Marija BALIĆ

2026

STATUTORY DECLARATION

I hereby declare that this thesis has been prepared independently and represents my own academic work. All sources and contributions from other authors have been properly cited and acknowledged. No sources other than those listed in the references have been used. I confirm that I have read and adhered to the regulations concerning academic integrity and plagiarism as defined by the Medical University. In addition, if artificial intelligence tools were utilized in the preparation or revision of any parts of this thesis, their use complied with ethical standards and institutional guidelines. Any such use was limited and applied in a transparent and responsible manner.

Graz, 11.04.2026.

Nina Dobrić

DISCLOSURES

Parts of this thesis have been published in:

Dobrić Nina[1], Hasenleithner Samantha[1], Suppan Christoph[1], Klocker Eva Valentina[1], Hlauschek Dominik[1], Graf Ricarda[2], Beichler Christine[2], Albertini Carmen[3], Egle Daniel[3], Liu Daisong[4,5], Starzer Angelika Martina[6], Bartsch Rupert[6], Moser Tina[2], Rinnerthaler Gabriel[1], Jost Philipp Jakob[1], Heitzer Ellen[2,7], Dandachi Nadia[1,2,8], Balic Marija[1,5]. Integrating Baseline ctDNA-Derived Tumor Metrics Enhances Risk Stratification in HR+/HER2– Advanced Breast Cancer: A Real-World Multicenter Cohort Study from Austria. ESMO Open. 2026. DOI: 10.1016/j.esmoop.2026.106939.

[1]Division of Oncology, Department of Internal Medicine, Medical University of Graz, Austria

[2]Institute of Human Genetics, Diagnostic and Research Center for Molecular Biomedicine, Medical University of Graz, Austria

[3]Department of Gynecology, Breast Cancer Center Tirol, Medical University of Innsbruck, Austria

[4]School of Medicine, Tsinghua Medicine, Tsinghua University, Beijing, China

[5]Division of Oncology, Hillmans Cancer Center, University of Pittsburgh, Pittsburgh, PA, USA

[6]Division of Oncology, Department of Medicine I, Medical University of Vienna, Austria

[7]Christian Doppler Laboratory for Liquid Biopsies for Early Detection of Cancer, Graz, Austria

[8]Research Unit Epigenetic and Genetic Cancer Biomarkers, Medical University of Graz, Graz, Austria

All co-authors have provided their consent for the inclusion of their published data in this dissertation. Figures and illustrations from my own and third-party publications have been reproduced or adapted in accordance with the applicable Creative Commons licenses and are appropriately acknowledged.

The article “Integrating Baseline ctDNA-Derived Tumor Metrics Enhances Risk Stratification in HR+/HER2– Advanced Breast Cancer: A Real-World Multicenter Cohort Study from Austria” (Dobrić et al., 2026) was published Open Access under the Creative Commons Attribution-Noncommercial-NoDerivatives 4.0 International License (CC BY-NC-ND 4.0). This license permits non-commercial sharing and distribution with appropriate attribution, but does not allow modifications of the original work. Accordingly, the figures and corresponding legends included in this thesis are reproduced without modification from the original publication.

Alongside the published work outlined above, this thesis integrates data obtained from an ESR1 testing project conducted on a referral basis. These data have not been formally published but were presented at the European Society for Medical Oncology (ESMO) Congress. The inclusion of anonymized data in this thesis has been approved by the following participating researchers and referring clinicians:

Christoph Suppan[1], Eva Valentina Klocker[1], Tamara Esterl[1], Tina Moser[2], Samantha Hasenleithner[1], Ricarda Graf[2], Sonja Heibl[3], Barbara Töpfer[4], Lukas Weiss[5], Manuel Pörnbacher[6], Carmen Siebenhofer[7], Margit Sandholzer[8], Günther G. Steger[9], Gabriel Rinnerthaler[1], Ellen Heitzer[2,10], Philipp J. Jost[1], Marija Balic[1,11], Nadia Dandachi[1,2,12]

[1]Division of Oncology, Department of Internal Medicine, Medical University of Graz, Graz, Austria

[2]Institute of Human Genetics, Diagnostic and Research Center for Molecular Biomedicine, Medical University of Graz, Graz, Austria

[3]Department of Internal Medicine IV, Klinikum Wels-Grieskirchen GmbH, Wels, Austria

[4]Department of Internal Medicine and Hematology and Internal Oncology, Landesklinikum Wiener Neustadt, Wiener Neustadt, Austria

[5]Third Medical Department with Hematology and Medical Oncology, Hemostaseology, Rheumatology and Infectious Diseases, Oncologic Center, Paracelsus Medical University Salzburg, Salzburg, Austria

[6]Oncology Department, Allgemein öffentliches Krankenhaus Spittal/Drau, Spittal/Drau, Austria

[7]Department of Gynecology, Konventhospital Barmherzige Brüder, Graz, Austria

[8]Department of Internal Medicine II, Academic Teaching Hospital Feldkirch, Feldkirch, Austria

[9]Departement of Internal Medicine I, Division of Oncology, Medical University of Vienna, Vienna, Austria

[10]Christian Doppler Laboratory for Liquid Biopsies for Early Detection of Cancer, Graz, Austria

[11]Division of Hematology/Oncology, UPMC Hillman Cancer Center, Pittsburgh, PA, USA

[12]Research Unit Epigenetic and Genetic Cancer Biomarkers, Medical University of Graz, Graz, Austria

ACKNOWLEDGEMENTS

This work would not have been possible without the support of many people, to whom I am deeply grateful, both professionally and personally, during my time at the Medical University of Graz.

First and foremost, I would like to thank my supervisor, **Prof. Marija Balić**, for giving me the opportunity to conduct my PhD in her group, but also for opening so many doors in my life. From the many professional opportunities and conferences to introducing me to inspiring people and welcoming me into her new lab in Pittsburgh, she has shaped both my professional and personal journey in countless ways. Thank you for inspiring me. You are truly the reason for everything I was able to see, learn, and experience over the past four years, and for that I will be forever grateful.

I would also like to express my deepest thanks to **Prof. Nadia Dandachi**, who has always supported me with valuable advice and inspiring discussions. While you may not have been an official member of my thesis committee, you truly felt like one. I am sincerely grateful for your guidance, supervision, and unwavering support from the very beginning of my PhD.

I am deeply grateful to the members of my thesis committee: Prof. Philipp J. Jost, Prof. Ellen Heitzer, and Dr. Samantha Hasenleithner. **Prof. Jost**, thank you for all the pleasant interactions, insightful discussions, and your constant support. **Ellen**, thank you for making me feel like a real member of your group throughout my time in Graz, for teaching me so much, and for helping me grow as a researcher. **Sam**, thank you for being a guiding star—someone I look up to and whose path and way of thinking I aspire to follow.

I would also like to express my sincere gratitude to the late **Prof. Michael R. Speicher**, who welcomed me in his group so easily and who, in our very first discussion before I even became a student in Graz, sparked my interest in liquid biopsy and its vast potential.

A very special thank you goes to all my friends and colleagues at the Institute of Human Genetics. Thank you (all of you!) for the shared memories, discussions, coffees, but also for the challenging and emotional moments that we got through together in the past four years. **Silvia** and **George**, thank you will never be enough for everything you have done for me—your friendship (and wisdom) mean so much. **Hani**, there's no one I'd rather have had by my side

from day one. **Stefan**, thank you for being both an incredible teacher and a true friend; your words have always encouraged me to keep going.

Finally, I would like to thank my family and my friends. To my biggest support system—my **mom** and **dad**—thank you for being the best example any child can ask for, for always showing me the way forward, and for standing firmly by my side no matter the obstacle. To my **friends**—back home, in Graz, or around the world—I am so lucky to have so many people believe in me even when I find it difficult. I owe the biggest thank you to **Dušan** and **Dušica**, who are the reason I started this journey: thank you for being a piece of my old home in my new home.

PhD Student Nina Dobrić received funding from the Medical University of Graz through the PhD program Molecular Medicine (MolMed). The primary project reported in this thesis was supported by Novartis, AstraZeneca, Daiichi Sankyo and Pfizer (no grant numbers). The work performed within ESR1 testing project was supported by Stemline and AstraZeneca. In addition, this work was supported by the Austrian Federal Ministry for Digital and Economic Affairs (Christian Doppler Research Fund for Liquid Biopsies for Early Detection of Cancer), the OeAD-GmbH Agentur für Bildung und Internationalisierung through the Marietta Blau Grant, and by the Austrian Marshall Plan Foundation through the Marshall Plan Scholarship.

Table of Contents

LIST OF ABBREVIATIONS

1L	First- Line
2L	Second-Line
3L	Third-Line
4L	Fourth-Line
ABC	Advanced Breast Cancer
ADC	Antibody-Drug Conjugate
AI	Aromatase Inhibitor
AIC	Akaike Information Criterion
AKT1	AKT Serine/Threonine Kinase 1
ASCO	American Society of Clinical Oncology
ATM	Ataxia Telangiectasia Mutated
BCL2	BCL2 Apoptosis Regulator
BC	Breast Cancer
BEAMing	Beads, emulsion, amplification, and magnetics
bp	Base Pair
BRCA1/BRCA2	Breast Cancer Susceptibility Gene 1/2
C-index	Uno's Concordance Index
CAF	Cancer-Associated Fibroblast
CAP	College of American Pathologists
CCND1	Cyclin D1
CDK4/6	Cyclin-Dependent Kinase 4/6
cfDNA	Cell-free DNA
CHEK2	Checkpoint Kinase 2
CHIP	Clonal Hematopoiesis of Indeterminate Potential
CI	Confidence Interval
CNA	Copy-Number Alteration
CNV	Copy-Number Variation
CTC	Circulating Tumor Cell

ctDNA	Circulating Tumor DNA
CTLA-4	Cytotoxic T Lymphocyte-Associated Protein 4
Dato-DXd	Datopotamab Deruxtecan
DCIS	Ductal Carcinoma In Situ
DNA	Deoxyribonucleic acid
dPCR	Digital PCR
EBC	Early Breast Cancer
EGFR	Epidermal Growth Factor Receptor
EMA	European Medicines Agency
ER	Estrogen Receptor
ERBB2/3/4	Erb-b2 Receptor Tyrosine Kinase 2/3/4
ESR1	Estrogen Receptor 1
ET	Endocrine Therapy
EV	Extracellular Vesicles
FDA	US Food and Drug Administration
FDR	False discovery rate
FFPE	Formalin-Fixed, Paraffin-Embedded
FGF19	Fibroblast Growth Factor 19
FGFR1	Fibroblast Growth Factor Receptor 1
GISTIC	Genomic Identification of Significant Targets in Cancer
HER2	Human Epidermal Growth Factor Receptor 2
HR	Hormone Receptor
hVAF	Highest Variant Allele Frequency
IHC	Immunohistochemistry
IGF1R	Insulin Like Growth Factor 1 Receptor
ILC	Invasive Lobular Carcinoma
IRR	Incidence Rate Ratio
ISH	In Situ Hybridization
KAT6B	Lysine Acetyltransferase 6B

kDa	Kilodalton
KRAS	KRAS Proto-Oncogene, GTPase
LINE-1	Long Interspersed Nuclear Element-1
LOD	Limit of Detection
mFAST-SeqS	Modified Fast Aneuploidy Screening Test Sequencing System
MBC	Metastatic Breast Cancer
MIR21	microRNA 21
MRD	Minimal Residual Disease
MTB	Molecular Tumor Board
MYC	MYC Proto-Oncogene
NCCN	U.S. National Comprehensive Cancer Network
NIPT	Non-Invasive Prenatal Testing
NF1	Neurofibromin 1
NGS	Next-Generation Sequencing
NST	Carcinoma of No Special Type
OR	Odds Ratio
OS	Overall Survival
P/LP	Pathogenic/likely pathogenic
PALB2	Partner and Localizer of BRCA2
PARPi	Poly(adenosine diphosphate-ribose) Polymerase Inhibitors
PCR	Polymerase Chain Reaction
PD-L1	Programmed Cell Death Ligand 1
PFS	Progression-Free Survival
PIK3CA	Phosphatidylinositol-4,5-Bisphosphate 3-Kinase Catalytic Subunit Alpha
PPV	Positive Predictive Value
PR	Progesterone Receptor
PTEN	Phosphatase and Tensin Homolog
RAB11FIP1	RAB11 Family Interacting Protein 1
RB1	RB Transcriptional Corepressor 1

SERD	Selective Estrogen Receptor Degrader
SERM	Selective Estrogen Receptor Modulator
SG	Sacituzumab Govitecan
SMAD4	SMAD Family Member 4
SNP	Single Nucleotide Polymorphism
SNV	Single Nucleotide Variant
STK11	Serine/Threonine Kinase 11
sWGS	Shallow Whole-Genome Sequencing
TAM	Tumor-Associated Macrophages
TFx	Tumor Fraction
T-DM1	Trastuzumab Emtansine
T-DXd	Trastuzumab Deruxtecan
TDLU	Terminal Duct–Lobular Unit
TNBC	Triple-Negative Breast Cancer
TP53	Tumor Protein p53
TROP2	Trophoblast Cell Surface Antigen 2
VAF	Variant Allele Frequency
WBC	White Blood Cells
WES	Whole-Exome Sequencing
WGS	Whole-Genome Sequencing
WHO	World Health Organization
ZNF703	Zinc Finger Protein 703

ZUSAMMENFASSUNG

Eine präzise Risikostratifizierung zu Beginn der systemischen Therapie ist bei Patient:innen mit HR+/HER2− fortgeschrittenem Mammakarzinom (ABC) weiterhin eine große Herausforderung. Eine verbesserte Identifikation von Patient:innen mit ungünstigem Krankheitsverlauf ist entscheidend für Therapieentscheidungen in frühen Behandlungslinien. Ziel dieser Arbeit war es, die klinische Charakterisierung von HR+/HER2− ABC zu verbessern, indem untersucht wurde, ob plasmabasierte genomische Analysen sowie quantitative Parameter der zirkulierenden Tumor-DNA (ctDNA) die prognostische Einschätzung über konventionelle klinisch-pathologische Faktoren hinaus verbessern. Darüber hinaus wurden potenzielle biologische Unterschiede zwischen HER2-low- und HER2-0-Tumoren untersucht. Ergänzend wurde eine landesweite Initiative zur Evaluation der plasmabasierten *ESR1*-Testung durchgeführt, um die Identifikation geeigneter Patient:innen für eine Therapie mit Elacestrant zu prüfen und Einblicke in die molekulare Heterogenität unter Alltagsbedingungen zu gewinnen.

Mithilfe eines tumoragnostischen plasmabasierten Sequenzierungsansatzes wurden ctDNA-basierte genomische Alterationsmuster charakterisiert und quantitative Parameter analysiert. Die genomischen Profile entsprachen bekannten Merkmalen von HR+/HER2− Erkrankungen, einschließlich häufiger Veränderungen in *PIK3CA*, *TP53* und *ESR1*. *ESR1*-Mutationen traten in späteren Therapielinien häufiger auf, was auf klonale Selektion hinweist. Die Integration mutationsbasierter und genomweiter ctDNA-Parameter erhöhte die Nachweissensitivität und ermöglichte eine umfassendere Charakterisierung der Tumorlast. Die meisten Parameter waren mit klinischen Endpunkten assoziiert und verbesserten in Kombination mit klinischen Basisvariablen die prognostische Stratifizierung. HER2-low- und HER2-0-Tumoren zeigten ähnliche Profile. Die plasmabasierte *ESR1*-Testung erwies sich als praktikabel und klinisch relevant.

Zusammenfassend stellt die ctDNA-basierte Analyse ein minimalinvasives Instrument für das personalisierte Management von HR+/HER2− ABC dar und unterstützt die Risikostratifizierung sowie therapiegeleitete Entscheidungen.

ABSTRACT

Accurate risk stratification at the initiation of systemic therapy remains a major challenge in patients with HR+/HER2− advanced breast cancer (ABC). Improved identification of patients with an unfavorable disease course is essential to guide treatment decisions in early lines. The primary aim of this thesis was to enhance the clinical characterization of HR+/HER2− ABC by evaluating whether plasma-derived genomic profiling and quantitative circulating tumor DNA (ctDNA) metrics improve prognostic assessment beyond conventional clinicopathologic parameters. In addition, potential biological differences between HER2-low and HER2-0 tumors were explored. To address the need for reliable liquid biopsy-based testing and extend the clinical applicability of ctDNA-based analyses, a nation-wide initiative was implemented to evaluate plasma-based *ESR1* mutation testing in patients with HR+/HER2− ABC, assessing its feasibility for identifying candidates for elacestrant while providing insight into molecular heterogeneity in a real-world setting.

Using a tumor-agnostic sequencing approach, the ctDNA-derived genomic landscapes were characterized, and quantitative tumor-derived metrics were assessed. The genomic profiles in the early treatment lines were consistent with known features of HR+/HER2− disease, including recurrent alterations in *PIK3CA*, *TP53*, and *ESR1*. *ESR1* mutations were more frequent in later treatment lines, reflecting therapy-driven clonal selection. Integration of mutation-based and genome-wide ctDNA metrics improved detection sensitivity and enabled a more comprehensive assessment of tumor burden. Most ctDNA-derived measures were associated with clinical outcomes, and their integration with established baseline clinical variables improved prognostic stratification compared with conventional factors alone. Exploratory ctDNA analyses revealed largely similar genomic profiles between HER2-low and HER2-0 tumors. Plasma-based *ESR1* testing proved to be feasible in a more advanced and heterogeneous clinical setting, underscoring its relevance for treatment-guided decision-making.

In summary, ctDNA-based profiling represents a practical and minimally invasive tool for personalized management of HR+/HER2− ABC, enabling improved risk stratification and supporting clinically driven molecular testing to inform treatment selection.

1. INTRODUCTION

1.1. Breast cancer

1.1.1. Epidemiology of breast cancer

Breast cancer (BC) is the most frequent malignancy worldwide and the deadliest cancer in the global female population. It was diagnosed in over 2 million people in 2020, and an estimated 685,000 women have died from it the same year (1-3). While the incidence rates for female BC are much higher in high-income countries (Australia/New Zealand, North America, western and northern Europe) compared to low- and middle-income countries (south-central Asia, central America, eastern and middle Africa), deaths caused by it are more prevalently reported in the latter group, with the highest mortality rates found in the Caribbean, Melanesia, western Africa, and Micronesia/Polynesia (1, 4). This can be explained by the easier access to new therapies and advanced screening methods that facilitate early BC detection, such as mammography, in economically developed countries (5, 6). Additionally, the high-incidence trends in high income countries reflect the higher prevalence of behavioral and lifestyle-related BC risk factors, such as advanced age at first birth, having fewer children, menopausal hormone-replacement therapy, alcohol consumption, obesity, and physical inactivity. However, transitioning countries are following closely behind, with their incidence rates quickly rising (1, 2, 5). BC survival rates vary drastically depending on the healthcare development level of a country/region, stage at diagnosis, subtype, and other features (4, 7). In Europe, when women are diagnosed with early BC (EBC), their 5-year survival rates are around 96%, while when they are diagnosed with metastatic BC (MBC), their 5-year survival probability is around 38% only (8). In the European Union, 3-8% of patients with newly diagnosed BC already have metastatic disease, and 20-30% of patients diagnosed with early-stage BC will later develop metastases (9, 10). These numbers illustrate the urgent need for new studies and clinical trials, in order to find new therapeutic targets and improve the survival of BC patients, especially those diagnosed with MBC.

1.1.2. Biology of breast cancer

The human mammary gland is a highly organized, branched epithelial organ embedded within a fibro-adipose stroma. It consists of a hierarchical ductal network that originates at the nipple and progressively branches, ending in small lobular units known as terminal duct–lobular units (TDLUs), the functional milk-producing units of the breast. Within each TDLU, alveoli (acini) – small spherical sacs with a diameter of a few millimeters – are the basic secretory units. Clusters of adjacent alveoli form a lobule, and each lobule is drained by one or more small intralobular ducts, which merge into larger interlobular ducts and eventually into the main collecting ducts leading to the nipple (11-14). Histologically, the breast epithelium is consisted of two layers. All ducts and secretory units are lined by an inner layer of luminal epithelial cells responsible for milk production, and an outer layer of basal myoepithelial cells, which provide structural support and contractile function. The mammary epithelium is highly dynamic, changing profoundly during the gland ontogeny, in response to hormonal and developmental signals (15-17). Maintenance of the breast tissue homeostasis relies on this bilayered epithelial organization and the precise regulation of epithelial cell differentiation, proliferation, and interactions with the surrounding microenvironment (14). Disruption of these processes plays a critical role in the initiation and progression of BC.

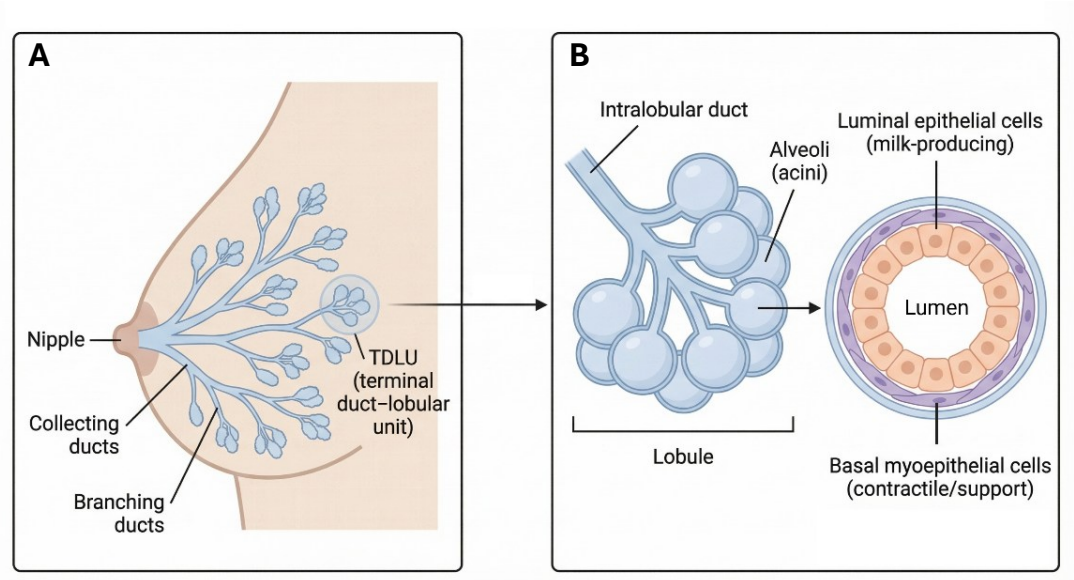

Figure 1. Structure of the human mammary gland. (A) The adult mammary gland consists of a branching ductal tree that terminates in TDLUs, the functional units of the breast. **(B)** Each TDLU contains clusters of alveoli composed of a bilayered epithelium, with an inner layer of luminal epithelial cells and an outer layer of basal myoepithelial cells. Created with BioRender.com

BC is a complex and heterogeneous disease at both the morphological and the molecular level (14). This heterogeneity reflects differences in cellular origin, genetic alterations, hormonal responsiveness, and interactions with the surrounding tissue, and underlies the wide variation in clinical behavior and therapeutic responses observed among patients.

The etiology of BC remains incompletely understood and is shaped by a complex network of genetic, environmental, and lifestyle influences that contribute to tumorigenesis (14, 18) (**Figure 2**). While the most common BC risk factors are associated with altered reproductive behavior, obesity, exposure to exogenous hormones, and alcohol consumption, approximately 10% of BCs are considered to be hereditary and are associated with a family history of the disease. Germline mutations in two high-penetrance tumor suppressor genes, *BRCA1* and *BRCA2*, which code for proteins involved in homologous recombination-mediated DNA repair, promote genomic instability, leading to an approximate 60% higher risk of BC. The prevalence of these mutations varies across populations, ranging from around 0.5% in Asian populations to up to 10.2% in Ashkenazi Jewish families. In addition to *BRCA1* and *BRCA2*, a number of additional high- and moderate-penetrance genes are routinely screened to assess the inherited risk of BC. Many of these genes play key roles in maintaining genomic stability, and include *ATM*, *CHEK2*, *PALB2*, *PTEN*, *STK11*, and *TP53*. Germline mutations in these genes are associated with hereditary cancer syndromes that contribute to a more moderate increase in BC risk (14, 19-21).

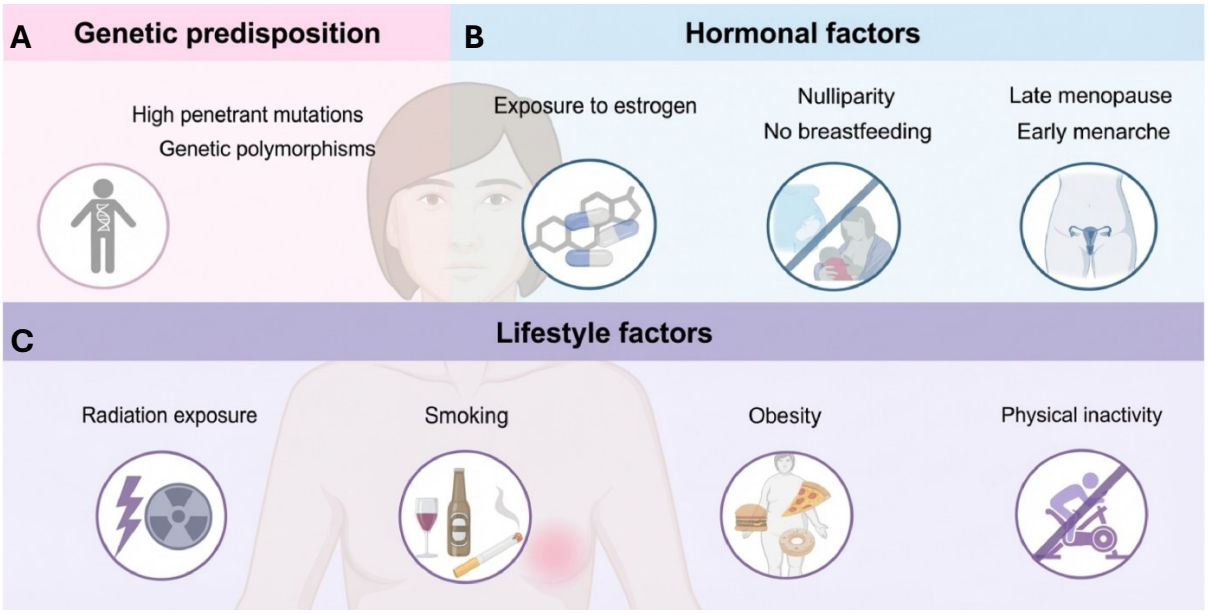

Figure 2. Risk factors for BC. BC risk is influenced by a heterogeneous set of factors, including **(A)** genetic predisposition, **(B)** hormonal influences and **(C)** lifestyle-related factors. BC breast cancer. Figure and legend adapted from Xiong et al. (18), under the terms of the Creative Commons CC BY 4.0 license, https://creativecommons.org/licenses/by/4.0/ . The figure was created with BioRender.com

Looking at the cell of origin, there are two leading models explaining the genesis of BC: the clonal evolution model and the cancer stem cell model. The clonal evolution model hypothesizes that any breast epithelial cell may accumulate stochastic genetic and epigenetic mutations that give them the stem-like abilities to differentiate and self-renew. These cells become selected over time and contribute to tumor generation and progression. In contrast, the cancer stem cell model proposes that only stem and progenitor cells, which inherently possess these proliferation and differentiation abilities, can initiate tumor formation and sustain progression. These models are not considered to be mutually exclusive, as increasing evidence suggests that BC may originate from stem, progenitor, or transit-amplifying cells and subsequently evolve through clonal selection, resulting in dynamic changes in stem-like properties during disease progression (14, 16, 18, 22, 23).

At the molecular level, breast carcinogenesis is driven by alterations in signaling pathways that regulate cell proliferation, survival, and differentiation. The most common drivers include hormone receptor (HR) signaling, growth factor receptor activation, intracellular kinase cascades, and defects in genomic maintenance, which together shape tumor behavior. Estrogen receptor (ER) signaling represents a major oncogenic axis in hormone receptor–positive (HR+) BC, where estrogen-mediated transcriptional programs drive cell cycle progression and support

cell survival. In parallel, amplification of human epidermal growth factor receptor 2 (HER2) results in constitutive activation of downstream pathways, leading to enhanced proliferation and resistance to apoptosis. The PI3K/AKT/mTOR pathway is one of the most frequently altered intracellular signaling pathways in BC, integrating signals from ER and receptor tyrosine kinases such as HER2, EGFR, and IGF1R, and promoting cell growth, metabolic adaptation, and survival. Alterations such as *PIK3CA* mutations or loss of the negative regulator *PTEN* result in pathway hyperactivation and contribute to tumorigenesis and therapeutic resistance (20, 21, 24). Similarly to other cancers, *TP53* mutations are common in BC. This tumor suppressor encodes the p53 protein, a transcription factor that orchestrates cellular responses to stress by regulating genes involved in apoptosis and cell cycle arrest (21). The RAS/MAPK pathway similarly transduces mitogenic signals from the activated growth factor receptors and supports cell division and differentiation, while extensive crosstalk with the PI3K/AKT pathway further enhances oncogenic activity (20, 21). Additional signaling pathways, including Notch, Wnt/β-catenin, JAK/STAT, and NF-κB, contribute to cancer stem cell maintenance, epithelial–mesenchymal transition, and the acquisition of invasive and metastatic traits (20, 24). All these signals frequently converge with defects in DNA damage repair pathways, such as those involving *BRCA1* and *BRCA2*, resulting in genomic instability, intratumoral heterogeneity, and clonal evolution. Genomic and epigenetic changes acquired during tumor evolution—such as copy-number loss, transcriptional downregulation, epigenetic silencing, and whole-genome duplication—facilitate immune escape and adaptation to environmental pressures (18). Collectively, these molecular alterations provide the biological basis for BC initiation and progression and form the foundation for molecular classification and targeted therapeutic strategies.

Exposure to hormonal influences, such as menopausal hormone therapy, elevated dietary estrogen intake, and endocrine dysregulation, is a major contributor to sporadic BC. Estrogen and progesterone regulate the growth and differentiation of epithelial breast cells during puberty, menstrual cycles, and pregnancy. An imbalance in these hormones, particularly prolonged estrogen exposure, enhances epithelial cell proliferation and increases the likelihood of DNA damage. With repeated menstrual cycles, the cumulative burden of DNA damage—particularly when coupled with impaired DNA repair mechanisms—can promote the emergence of premalignant and ultimately malignant cells. In this context, estrogen acts primarily as a tumor promoter, supporting the survival and expansion of transformed epithelial

cells as well as remodeling of the surrounding stromal microenvironment, thereby facilitating BC development (14, 18) (**Figure 3**).

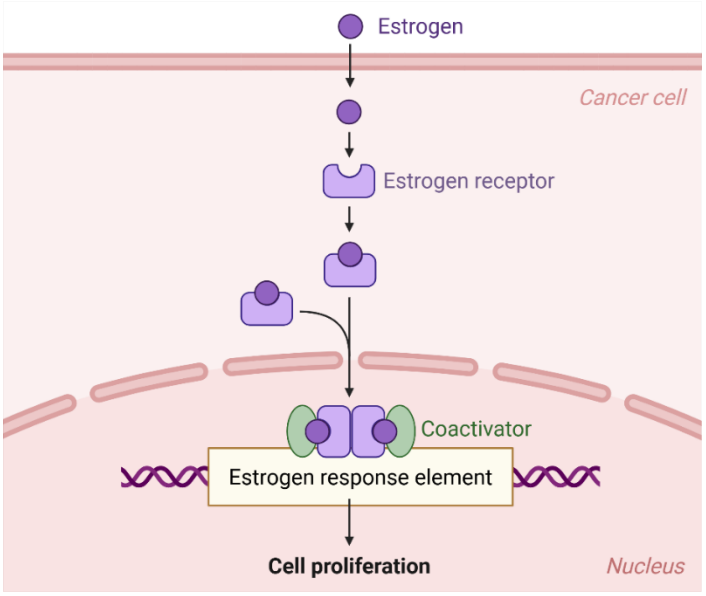

Figure 3. Estrogen as a tumor promoter in BC. Estrogen enters the cell and binds to the ER, a ligand-activated transcription factor. This interaction induces a conformational change, leading to receptor dimerization and nuclear translocation, where ER interacts with estrogen response elements located in target gene promoters. Recruitment of coactivator proteins promotes the transcription of genes associated with cell proliferation and survival. ER signaling can also interact with growth factor pathways, further enhancing proliferative signaling in BC cells (14). BC breast cancer, ER estrogen receptor. Created with BioRender.com

BC develops within a complex tumor microenvironment composed of extracellular matrix and multiple non-malignant cell types, among which cancer-associated fibroblasts (CAFs) are predominant, alongside immune cells such as lymphocytes, tumor-associated macrophages (TAMs), and myeloid-derived cells. During early tumorigenesis, the immune milieu is largely tumor suppressive, mainly due to the effect of cytokines released from the activated cytotoxic CD8+ and helper CD4+ T cells. However, as tumors progress, cancer cells acquire immune-evasive properties, including the upregulation of checkpoint regulators, such as cytotoxic T lymphocyte-associated protein 4 (CTLA-4) and programmed cell death ligand 1 (PD-L1), leading to the suppression of antitumor immune responses. Tumor invasion dynamically reshapes the cellular and cytokine composition of the microenvironment, promoting disease progression. In parallel, BC evolves toward greater genomic complexity and heterogeneity, imposing selective pressures that contribute to variable therapeutic responses and resistance to immunotherapy. Notably, BC cells can exploit mechanisms resembling central nervous system immune privilege to evade immune surveillance, a process dependent on disruption of

immunological synapse formation (14, 18, 25). Together, these interactions between tumor cells and host immunity further reflect the multifaceted and heterogeneous nature of the BC.

Clinically, BC is termed EBC when confined to the breast or regional lymph nodes, whereas MBC represents advanced disease characterized by the spread of disease to distant sites such as liver, bone, lung, or brain (14, 26).

Metastasis is a process that encompasses a series of successive biological events through which malignant cells depart from the primary lesion, invade the surrounding tissue, enter the bloodstream or the lymphatic system, survive transport, and ultimately colonize distant organs (**Figure 4**). This mechanism contributes to the vast majority of cancer-related deaths (> 90%), primarily through the impairment of critical organ function (27).

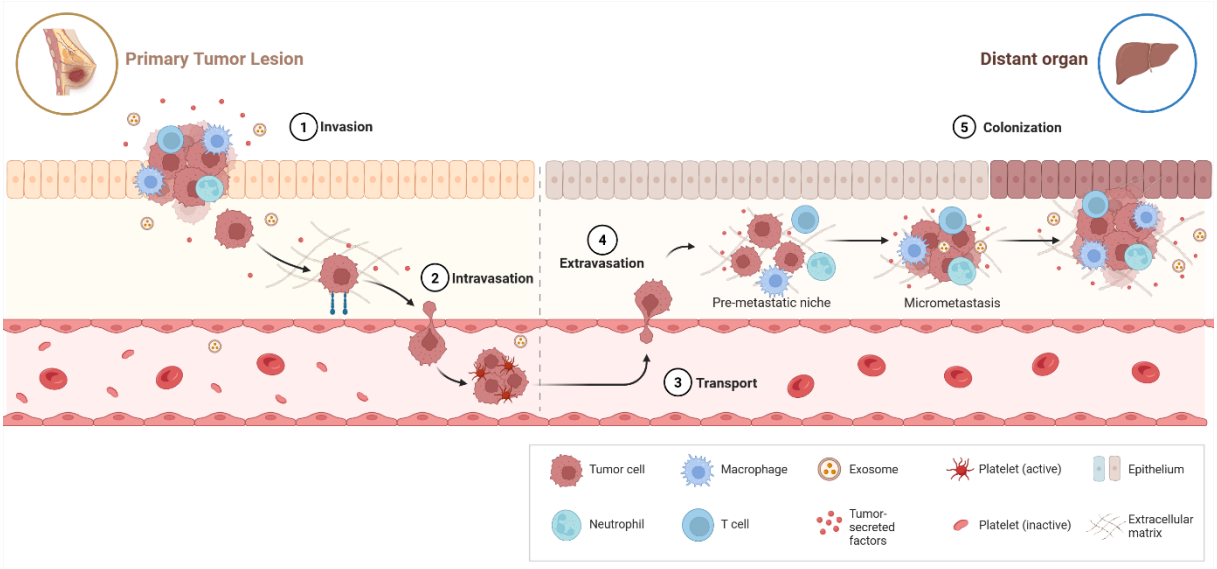

Figure 4. Mechanism of metastasis in BC. The process of metastasis occurs in 3 main stages: **(i)** Escape from the primary tumor lesion and local invasion; **(ii)** Intravasation and survival in the circulation; **(iii)** Extravasation and metastatic seeding. BC breast cancer. Created with BioRender.com

Approximately 25–28% of MBC cases present as de novo metastatic disease at initial diagnosis. More frequently, patients with early-stage disease experience recurrence, with metastases developing months or even decades after initial treatment (14, 27). However, these proportions and absolute numbers vary depending on age, access to screening programs, availability of therapeutic innovations, and the quality of early treatment. In western countries, an estimated 20–30% of stage I–III BC patients experience metastatic recurrence, while 5–10% of patients present with stage IV disease at the time of diagnosis (10, 14). Patients with recurrent MBC

usually have poorer survival outcomes than those with de novo MBC, likely due to prior treatment exposure and the emergence of therapy-resistant tumor clones (10). Prolonged intervals between primary cancer diagnosis and recurrence have been proposed to reflect tumor dormancy, a state in which minimal residual disease (MRD) remains below the limits of clinical detection for extended periods (27). Furthermore, while many of the driver mutations present in the primary tumor are also preserved in the metastases, new genetic alterations may arise at different metastatic sites, resulting in subclonal diversification with potential new driver mutations (14). Consequently, given the systemic spread of metastatic disease, biological heterogeneity, and treatment resistance, MBC is generally incurable and represents a major clinical challenge.

1.1.3. Classification of breast cancers

Due to its large heterogeneity that spans many levels, several classifications of BC are actively used in practice, determined by the molecular and histological profile of the tumor (19).

Histologically, breast tumors are classified as either in situ or invasive carcinomas, depending on whether malignant cells remain confined to the ducts/lobules or have infiltrated the surrounding stroma. Ductal carcinoma in situ (DCIS) accounts for about 10–30% of BC cases and is considered to be pre-invasive BC (25). According to the current World Health Organization (WHO) Classification of Breast Tumors (5th edition), invasive BC comprises nineteen subtypes, of which the most common type is carcinoma of no special type (NST, formerly referred to as ductal carcinoma), diagnosed in around 70-75% of patients. Invasive lobular carcinoma (ILC) accounts for 10–15% of cases, while the remaining patients belong to one of the 17 different rare histotypes (carcinomas of special type), or have mixed histologies (14, 18, 21, 28).

To evaluate prognosis and try to support personalized treatment decisions for patients with BC, it is mandatory that all newly-diagnosed patients are tested for the expression of three key biomarkers: ER, progesterone receptor (PR), and HER2 (14, 29). On the basis of these markers, BC can be broadly divided into three principal subtypes: HR+/HER2-negative (HER2-), characterized by ER and/or PR expression; HER2-positive (HER2+), characterized by overexpression or amplification of HER2; and triple-negative BC (TNBC), which lacks both HRs and HER2 overexpression/amplification. HR+/HER2- BC is the most common subtype,

representing a significant proportion (approximately 70%) of cases, while HER2+ BC includes approximately 20%, and TNBC approximately 10% of BC cases (3, 18, 30, 31).

Starting from the early 2000s, gene expression profiling has expanded our knowledge about BC molecular complexity beyond what is reflected by traditional clinicopathological markers. Unsupervised clustering of tumor gene expression data led to the first molecular classification of BC and the identification of intrinsic subtypes. Subsequent studies further refined the subtypes based on differences in hormone receptor–related gene expression and proliferative activity. In widely used contemporary classification schemes, four principal intrinsic BC subtypes are recognized: luminal A (approximately 50–60% of cases), luminal B (around 10–20%), HER2-enriched (about 15–20%), and basal-like tumors (approximately 10–15% of cases). A normal-like subtype has also been described; it shares transcriptional similarities with luminal A tumors, is associated with less favorable clinical outcomes, and likely represents a minority of cases. With continued advances in sequencing technologies, these intrinsic molecular classifications have been further refined and standardized, most notably through the PAM50 gene expression assay, as well as through integrative genomic and transcriptomic analyses (18, 21, 32-35).

Luminal tumors, defined by ER expression, are generally less aggressive; luminal A tumors display low proliferative activity and are highly hormone-dependent, whereas luminal B tumors exhibit higher proliferation rates (elevated Ki-67), and often co-express *HER2* or *EGFR*. Luminal BCs are driven by ER-dependent transcriptional programs that support tumor cell growth, survival, and differentiation, including the increased expression of genes such as *CCND1* and *BCL2*. In luminal B tumors, additional activation arises from interactions with growth factor receptor signaling and the frequent presence of *PIK3CA* mutations which stimulate pathways such as PI3K/AKT/mTOR and RAS/MAPK. This enhanced signaling leads to greater proliferative activity and contributes to therapeutic resistance, making these tumors more difficult to manage (21, 24).

HER2-enriched BCs lack significant ER and PR expression and are characterized by the amplification or overexpression of *ERBB2/HER2*, a gene that encodes the tyrosine kinase receptor HER2. Constitutive HER2 activation through ligand-independent homo- or heterodimerization of receptors, including interactions with EGFR or HER3, triggers downstream PI3K/AKT/mTOR and RAS/MAPK signaling. Activation of these pathways

promotes cell cycle progression, survival, and angiogenesis via key effectors such as CCND1, BCL2, and VEGF, underpinning the more aggressive behavior of this subtype compared to luminal tumors. Dysregulation of the PI3K pathway, including *PIK3CA* mutations and the loss of *PTEN*, are frequent in this subtype as well, additionally amplifying oncogenic signaling and contributing to tumor aggressiveness (21, 24).

Basal-like tumors, which do not express ER, PR, and HER2, are clinically classified as TNBC. This subtype is defined by the expression of basal cytokeratins, elevated proliferative signaling, frequent alterations in DNA repair pathways, and pronounced genomic instability (21, 24).

Although molecular profiling techniques, such as gene expression assays and genomic analyses, can provide additional prognostic and biological insights, their use is currently limited to selected clinical scenarios and does not replace routine pathological evaluation. Immunohistochemical assessment of ER, PR, HER2, and Ki67 therefore remains the standard for BC subtype classification and guides most treatment decisions.

1.1.4. Treatment strategies in breast cancer

BC treatment strategies are guided by tumor biology and clinical behavior, with subtype, stage, patient characteristics, and genetic alterations playing important roles in therapeutic decision-making (19).

At the time of BC diagnosis, more than 90% of patients do not have metastatic disease, and treatment is therefore focused on tumor removal and recurrence prevention. Local management involves surgical excision, with radiotherapy considered following breast-conserving surgery. Despite this, most patients need some form of additional systemic therapy. Systemic treatment strategies in EBC are administered preoperatively (neoadjuvant), postoperatively (adjuvant), or both, and are guided by tumor size, lymph node involvement, subtype, and other molecular and clinical parameters. Patients with HR+ disease are primarily treated with endocrine therapy (ET), with chemotherapy dependent on the clinical and molecular risk features. In HER2+ BC, treatment involves HER2-targeted agents, including monoclonal antibodies and small-molecule inhibitors, usually given alongside chemotherapy, and/or immunotherapy and targeted inhibitors of poly(adenosine diphosphate-ribose) polymerase inhibitors (PARPi) in appropriate high-risk or *BRCA*-mutated cases (14, 36).

In contrast, as MBC cannot be cured, the main goals are prolongation of survival, symptomatic relief and maintenance and improvement of the quality of life (QoL) (14, 36). The treatment remains subtype-specific systemic therapy, including ET, chemotherapy, and targeted therapy, while surgical and radiotherapeutic interventions are typically limited to cases with complications such as bleeding, pain, or skin ulceration (10, 36).

Same as in the early-stage setting, for patients with HER2+ MBC it is important to continue blocking the HER2 pathway. These patients are treated with *HER2*-targeted agents, such as monoclonal antibodies trastuzumab and pertuzumab, and the antibody-drug conjugates (ADC) trastuzumab deruxtecan (T-DXd) and trastuzumab emtansine (T-DM1), alongside chemotherapy (14, 19).

For metastatic TNBC, cytotoxic chemotherapy has for a long time been the only available therapeutic option (19, 36). However, this has changed with the introduction of immunotherapy for patients with PD-L1–positive tumors, as well as PARPi for those with *BRCA1/2* mutations. In addition, the ADC sacituzumab govitecan (SG) has been approved for pretreated metastatic TNBC, while additional ADCs, such as datopotamab deruxtecan (Dato-DXd), continue to be investigated (14, 19, 37, 38).

Throughout the years, ET has emerged as a cornerstone of treatment for advanced-stage HR+ BC, due to the high hormone expression (9, 19, 31). With this approach, the aim is to inhibit estrogen-dependent intracellular signaling pathways that control the expression of genes required for cell survival and proliferation, while minimizing the toxic effects associated with chemotherapy. Different approved therapies for the management of HR+ BC affect ER-dependent signaling in different ways: tamoxifen is a commonly used selective estrogen receptor modulator (SERM) that binds to the ER and acts as an anti-estrogen in breast tissue, inhibiting transcription and suppressing tumor growth; letrozole, anastrozole and exemestane are aromatase inhibitors (AIs) that suppress estrogen synthesis by preventing the conversion of androgens, minimizing ER signaling; fulvestrant is the first selective estrogen receptor degrader (SERD) approved for the management of advanced-stage, endocrine-sensitive BC, and it suppresses ER signaling by binding to the ER and preventing its nuclear translocation, as well as promoting its degradation; at present, oral ER-targeting degraders/antagonists approved for ER+ MBC harboring *ESR1* mutations include elacestrant and imlunestrant (20, 31, 39, 40) (**Figure 5**).

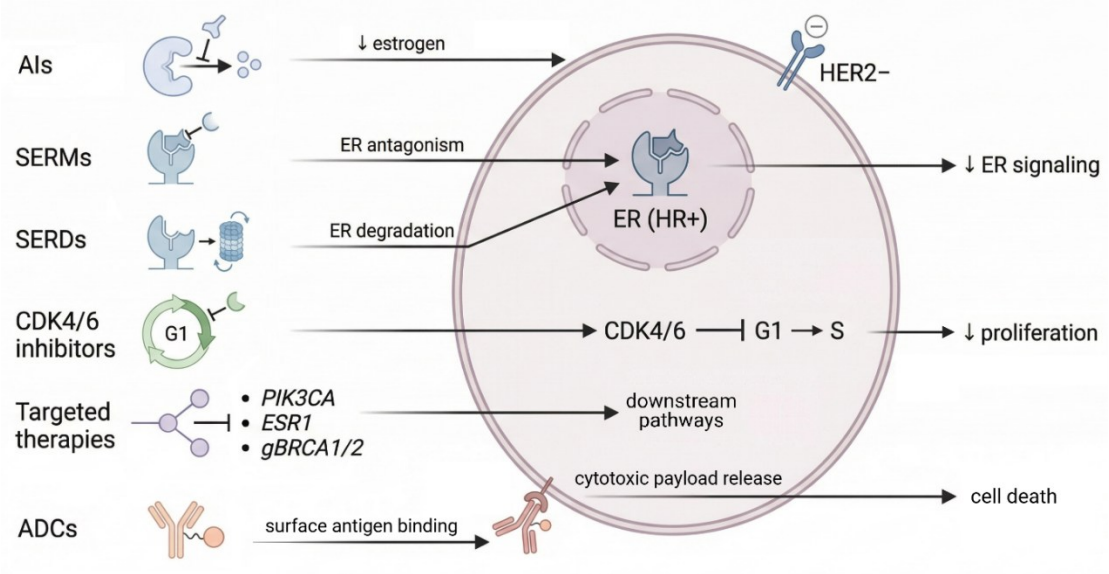

Figure 5. Main therapeutic strategies in HR+/HER2- ABC. ETs target ER signaling through multiple mechanisms: AIs reduce estrogen synthesis, SERMs act as ER antagonists, and SERDs promote ER degradation. CDK4/6 inhibitors inhibit cell cycle progression at the G1–S checkpoint, reducing cell proliferation. Targeted therapies directed against specific molecular alterations, including *PIK3CA* mutations, *ESR1* mutations, and g*BRCA1/2* mutations, further affect downstream signaling pathways. ADCs bind to antigens expressed on the surface of tumor cells and deliver cytotoxic payload into the tumor cell, leading to its destruction. Collectively, these therapeutic strategies inhibit ER signaling, suppress proliferation, and induce cancer cell death. HR+ hormone receptor-positive, HER2- HER2-negative, ABC advanced breast cancer, ET endocrine therapy, ER estrogen receptor, AI aromatase inhibitor, SERM selective estrogen receptor modulator, SERD selective estrogen receptor degrader, CDK4/6 cyclin-dependent kinase 4/6, ADC antibody-drug conjugate. Created with BioRender.com

The introduction of cyclin-dependent kinase 4 and 6 inhibitors marked a major milestone in the management of HR+/HER2- BC. CDK4 and CDK6, through their interaction with cyclin D, regulate the progression from G1 to S phase of the cell cycle via phosphorylation of the retinoblastoma protein. In HR+ tumors, ER signaling promotes cyclin D expression, leading to CDK4/6 activation and subsequent phosphorylation of Rb. Once phosphorylated, Rb becomes inactivated and releases E2F transcription factors, thereby driving cell-cycle progression and cell proliferation (20). When combined with ET, CDK4/6 inhibitors such as palbociclib, ribociclib, and abemaciclib demonstrated consistent improvements in progression-free survival (PFS) in patients with advanced disease, while overall survival (OS) benefit has been demonstrated for ribociclib (31, 41, 42). These agents have therefore become an integral component of the standard of care for ABC, fundamentally reshaping the therapeutic landscape. In clinical practice, CDK4/6 inhibitors are most commonly administered in combination with AIs as first-line therapy, or with fulvestrant in the endocrine-resistant setting.

However, despite these therapeutic advances, the development of resistance is inevitable and a significant proportion of patients still experience disease progression. For patients with HR+/HER2- metastatic BC, treatment with ET in combination with CDK4/6 inhibitors typically provides clinical benefit for a median of approximately two years, and PFS with systemic therapies given after progression on CDK4/6 inhibitors was as low as four months, highlighting the need for more effective interventions (42-45).

More recently, targeted therapies are increasingly being incorporated into ABC treatment. These approaches selectively target specific molecular alterations within tumor cells, thereby reducing off-target effects on healthy tissue and improving clinical outcomes (19). For example, tumors harboring *PIK3CA* mutations may be treated with alpelisib—a PI3Kα-specific inhibitor—which is approved by the US Food and Drug Administration (FDA) and the European Medicines Agency (EMA) for patients with ER+/HER2- ABC. As mentioned above, patients carrying germline *BRCA1/2* mutations derive clinical benefit from PARPi, including olaparib and talazoparib. Furthermore, the presence of *ESR1* mutations has prompted the development of next-generation SERDs, particularly oral SERDs such as elacestrant, imlunestrant or camizestrant, which have shown promising efficacy in overcoming endocrine resistance compared to earlier agents (20, 40, 46). These agents exhibit improved pharmacokinetic properties, including oral bioavailability and more consistent systemic exposure, thus enabling more effective ER degradation. Nevertheless, therapeutic strategies that target a single signaling pathway frequently encounter adaptive resistance mechanisms. Tumor cells can activate alternative pathways to maintain proliferative signaling, thereby attenuating treatment efficacy and promoting drug resistance. Although numerous oncogenic signaling cascades have been characterized, accurately predicting how an individual patient will respond to a specific agent remains a significant challenge. Further progress will require improved predictive biomarkers with greater sensitivity and specificity, allowing dynamic tracking of pathway activity and simultaneous assessment of multiple signaling networks (20).

ADCs are emerging as another promising therapeutic class, gaining a prominent role in treating all ABC subtypes (47). ADCs represent a hybrid of chemotherapy and targeted therapy, and fundamentally consist of three parts: a monoclonal antibody that selectively targets antigens or proteins on tumor cells; a highly potent cytotoxic agent termed payload; and a linker that binds the two components. All three components, along with their conjugation method, are

determinants of the ADC's overall biophysical properties and physiological behavior. The antibody component reduces the off-target cytotoxic effects, and the linker ensures the complex remains stable until it reaches the target cell, where the payload is safely and selectively delivered to exert its cytotoxic effect, maximizing antitumor activity while sparing normal cells. The linkers can be cleavable (responsive to the cell or tumor microenvironment, such as low pH) or non-cleavable (require lysosomal degradation of the antibody to facilitate linker cleavage and payload liberation). Depending on the properties of the linker and payload, ADCs may additionally induce a bystander effect, where the released payload diffuses into the tumor microenvironment to kill adjacent, non-targeted tumor cells. This mechanism is crucial as it overcomes tumor heterogeneity in antigen expression. This construct altogether has positioned ADCs as a key focus of research in the treatment of solid tumors, including BC (47, 48). The efficacy and the toxicity of an ADC depend, among others, on the design of the linker (which regulates the rate of payload delivery) and the drug-to-antibody ratio (the average number of payload molecules attached to each antibody, typically two to eight molecules per antibody). A higher drug-to-antibody ratio generally improves the efficacy, even with lower antigen expression. These criteria have driven the evolution of ADCs from earlier generations, such as T-DM1, which was limited to HER2+ BC, to subsequent generations that demonstrate broader application and greater bystander activity (47). To date, three ADCs have received FDA approval for the treatment of HR+/HER2– ABC: T-DXd, SG and datopotamab deruxtecan (Dato-DXd) (49-51). For SG and Dato-DXd, the therapeutic target is trophoblast cell surface antigen 2 (TROP2), a single-pass transmembrane protein whose high expression is common in epithelial cancers and serves as a strong biomarker for poor prognosis (52). The application of both agents showed improvement in PFS in previously treated patients with HR+/HER2– ABC (51, 53). In T-DXd, a humanized anti-HER2 monoclonal antibody trastuzumab is joined to a potent membrane-permeable topoisomerase I inhibitor payload deruxtecan (one trastuzumab conjugated to eight molecules of deruxtecan, drug-to-antibody ratio 8:1) via a cleavable linker (29, 47). Treatment with T-DXd resulted in more favorable PFS and OS in patients with HR+/HER2– MBC that had a low expression of HER2 (54).

1.1.5. HR+/HER2-low: a potential new subtype

HER2, encoded by the *HER2* (also known as *ERBB2*) oncogene on the long arm of chromosome 17, is a transmembrane receptor tyrosine kinase with a molecular weight of approximately 185 kDa. It belongs to the human epidermal growth factor receptor family (14, 55). Although no HER2-specific ligand has been identified, HER2 becomes activated primarily through homo- or heterodimerization—most commonly with other ligand-activated ErbB family members (*EGFR, ERBB3* and *ERBB4*)—thereby triggering downstream signaling that promotes proliferation, survival, adhesion, and metastasis (56).

In clinical practice, HER2 status is routinely determined using molecular techniques such as immunohistochemistry (IHC), which evaluates protein expression, and in situ hybridization (ISH), which assesses gene amplification. According to the criteria established by the American Society of Clinical Oncology (ASCO) and the College of American Pathologists (CAP) (57), IHC results are initially categorized as 0, 1+, 2+, or 3+, with IHC 2+ considered equivocal and requiring further evaluation by ISH. Final classification is determined by integrating the results of both IHC and ISH, with tumors considered as HER2+ if they exhibit an IHC score of 3+ or 2+ with confirmed gene amplification, and HER2- if they show IHC scores of 0 or 1+, or 2+ without gene amplification. Approximately 10−20% of breast tumors are considered to be HER2+, whereas the remaining 80–90% are classified as HER2-. However, HER2- tumors do not necessarily lack the HER2 protein entirely, and recent evidence indicates that these patients with low expression of the HER2 protein and no detectable amplification of the *HER2* gene (IHC 1+ or IHC 2+ / ISH-negative) represent a new targetable category of BC, termed “HER2-low” (29, 58, 59).

Namely, for a long period, the therapeutic efficacy of HER2-targeted agents was believed to require HER2 overexpression or gene amplification. However, more recent evidence has demonstrated that the ADC T-DXd confers a clinically meaningful improvement in survival among patients with HER2-low MBC (58). After binding to the HER2 receptor, the cytotoxic payload of T-DXd is delivered not only to target cells but also to adjacent cells, irrespective of their level of HER2 expression, due to the bystander effect (**Figure 6**). This mechanism likely explains the therapeutic activity of T-DXd even in tumors with low HER2 expression (29, 60, 61).

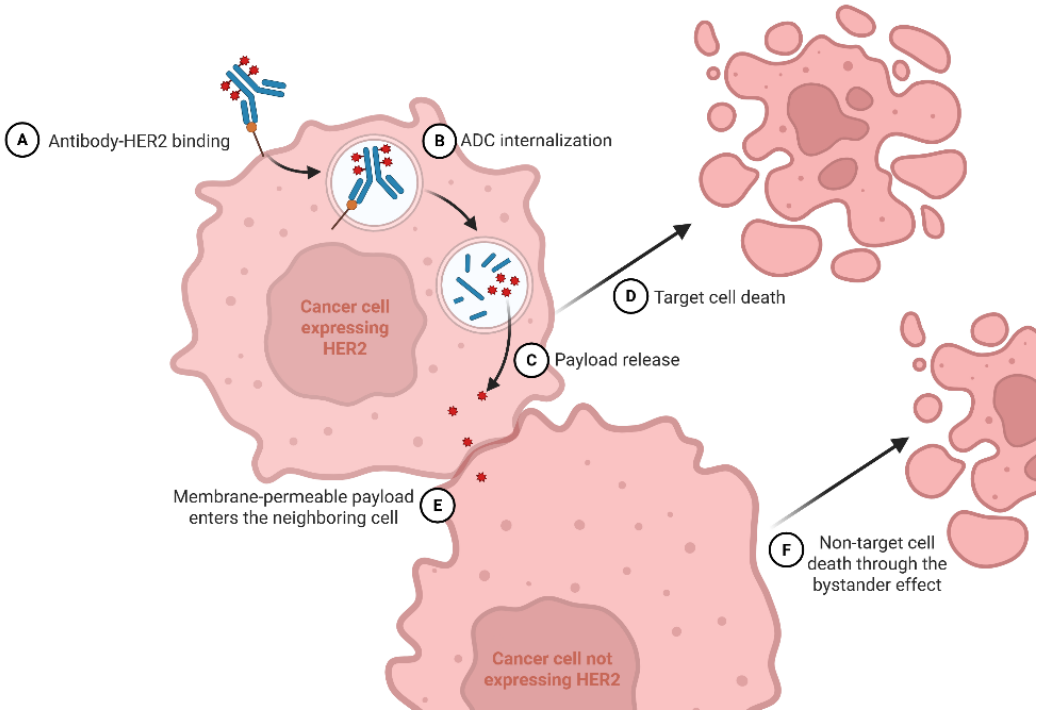

Figure 6. T-DXd mechanism of action in HER2-low BC. Following HER2 binding and internalization, the cytotoxic payload is released intracellularly, leading to the target cell death. Due to its membrane permeability, the payload is able to diffuse into adjacent cells, resulting in additional tumor cell killing through a bystander effect, including cells with absent HER2 expression. T-DXd trastuzumab deruxtecan, BC breast cancer. Created with BioRender.com

The clinical benefit of T-DXd in heavily pretreated HER2-low ABC was confirmed in the phase III DESTINY-Breast04 trial, where treatment with T-DXd resulted in a significantly lower risk of disease progression or death compared with chemotherapy of the physician's choice (48, 54, 58). Within tumors previously classified as HER2- (IHC score 0), a spectrum of HER2 expression may still exist. While some tumors show a complete absence of HER2 staining, others exhibit very faint, incomplete membrane staining in ≤ 10% of tumor cells. This latter group has recently been referred to as "HER2-ultralow". The clinical relevance of this category has begun to emerge after the publication of the phase III DESTINY-Breast06 trial (62), but is not yet incorporated into current clinical guidelines (57, 63).

The development of additional HER2-targeted strategies, including HER2 vaccines and bispecific antibodies, has further stimulated discussion regarding whether HER2-low disease represents a distinct biological entity. However, evidence supporting its classification as a clinically relevant subtype of BC remains limited, and the criteria that should define HER2-low tumors as a separate category are still not clearly established. Therefore, further investigation

of the molecular and genetic characteristics of HER2-low tumors appears necessary to better understand their biological behavior and to identify patients who may benefit from emerging targeted therapies such as T-DXd (59, 61, 64). In this context, minimally invasive approaches such as liquid biopsy analysis may provide valuable insights into the genomic landscape of these tumors.

1.2. Liquid biopsy and circulating tumor DNA

1.2.1. The concept of liquid biopsy

Ongoing advances in experimental methodologies and sequencing technologies have substantially improved tumor detection and diagnostic capabilities. In particular, combining liquid biopsy approaches with high-throughput sequencing has come up as a promising alternative to, and complement for, conventional tissue-based diagnostics in oncology (18, 65).

The term liquid biopsy refers to the use of bodily fluids, most commonly peripheral blood, for the analysis of tumor-derived material, thus obtaining molecular information about a tumor without the need for invasive tissue sampling (65-67). A traditional solid biopsy provides a single time-point representation of one tumor region and is limited by its invasive nature, procedural risks, and practical constraints that often hinder repeated sampling over the course of disease. In addition, technical factors such as variable tumor cellularity (i.e., the proportion of tumor cells within the sample), limited tissue yield, and DNA degradation associated with formalin-fixed paraffin-embedded (FFPE) specimens can restrict the scope and reliability of molecular analyses. Most importantly, tissue biopsies fail to adequately capture intratumoral and intermetastatic heterogeneity, as sampling from a single lesion may overlook clinically relevant subclonal populations. In contrast, liquid biopsy enables minimally invasive, longitudinal sampling and has the potential to capture tumor-derived signals released from multiple tumor sites and subclones, thereby facilitating a more comprehensive and dynamic assessment of tumor biology (68-70). Liquid biopsies encompass various circulating analytes, such as circulating tumor cells (CTCs), extracellular vesicles (EVs), and cell-free DNA and RNA, as well as proteins, lipids, and metabolites. These analytes can be isolated from peripheral blood, but also other bodily fluids, such as urine or cerebrospinal fluid, depending on the tumor type and clinical context. The analysis of these circulating components enables molecular

profiling without repeated invasive procedures and has therefore gained increasing importance in both clinical and research settings (65, 67).

Clinically, liquid biopsy has been investigated for a range of applications, including early cancer detection, identification of actionable molecular alterations, detection of MRD, monitoring of treatment response, and early identification of relapse (70). Despite their considerable promise, liquid biopsy approaches face technical and biological challenges, including limited sensitivity in early-stage disease, pre-analytical variability, and background signals originating from non-malignant tissues. Nevertheless, continuous improvements in assay sensitivity, sequencing depth, and bioinformatic analyses are steadily enhancing the robustness of liquid biopsy technologies, reinforcing their role as an important component of precision oncology.

1.2.2. Circulating cell-free DNA

Circulating cell-free DNA (cfDNA) represents DNA fragments that are shed into blood and other bodily fluids as a result of cellular turnover. In healthy individuals, cfDNA largely originates from hematopoietic cells and is present in plasma at relatively low concentrations, typically in the range of 1–10 ng/mL. cfDNA fragments are believed to be predominantly generated through the processes of apoptosis and necrosis, with NETosis and active secretion being suggested as well. This results in a fragment size distribution characterized by a peak at approximately 166 base pairs (bp), which aligns with the length of nucleosome-protected DNA, consisting of DNA bound to nucleosome and linker DNA associated with histone H1. cfDNA is eliminated via nuclease-mediated degradation and renal excretion, and is additionally hypothesized to be cleared by macrophage degradation in the liver and spleen (**Figure 7**). The short half-life of cfDNA in the circulation, generally ranging from minutes to hours, allows its concentration and composition to rapidly reflect changes in physiological or pathological states, making it well-suited for a biomarker (71, 72).

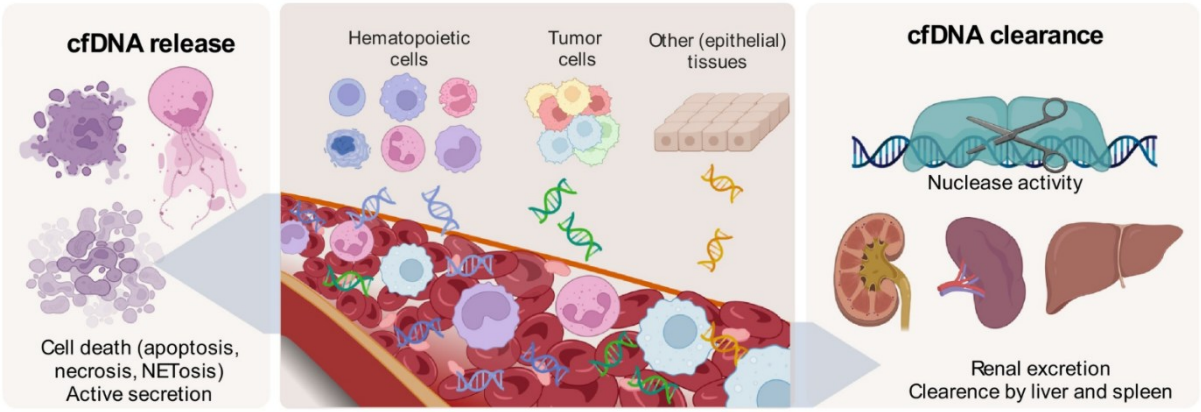

Figure 7. Biological processes contributing to the release and clearance of cfDNA. The cfDNA pool comprises small DNA fragments that originate predominantly from hematopoietic cells with a smaller contribution from solid tissues. In the context of cancer, tumor cells provide an additional source of cfDNA in the circulation. The overall concentration of cfDNA is governed by the dynamic balance between its release into the bloodstream and its clearance through processes such as nuclease-mediated degradation, renal excretion, and uptake by organs including the liver and spleen. cf DNA, cell-free DNA Figure and legend adapted from Moser et al. (72), under the terms of the Creative Commons CC BY 4.0 license, https://creativecommons.org/licenses/by/4.0/. The figure was created with BioRender.com

The presence of cfDNA in human plasma was first reported in 1948 (73), but the investigation into its nature and sources emerged only gradually, with relatively limited research activity in the following decades (68, 74). However, these early observations established that extracellular DNA circulates in plasma under physiological conditions and provided the foundation for subsequent studies exploring its biological significance and clinical relevance. In the late 1970s, elevated cfDNA concentrations were first observed in serum samples from patients with cancer (75); by the late 1980s, it became evident that cfDNA is not exclusively derived from normal tissues, with studies demonstrating that a proportion of cfDNA in patients with cancer is derived from tumor cells (76, 77). In the following years, tumor-specific genetic alterations were detected in other biological specimens, including *TP53* mutations in urinary sediments from patients with bladder cancer and *KRAS* mutations in stool or sputum samples from individuals with colorectal, pancreatic, and lung cancers (71, 78-81). In 1994, tumor-specific *KRAS* mutations were identified in the plasma cfDNA from patients with pancreatic cancer, and were shown to be identical to those present in the corresponding tumor tissue, conclusively demonstrating that mutant cfDNA fragments in plasma can be of tumor origin (71, 82).

The clinical relevance of cfDNA became particularly evident following the discovery of fetal DNA circulating in maternal plasma in 1997 (83). This discovery demonstrated that cfDNA originating from a genetically distinct tissue could be reliably detected in the circulation,

leading to important cfDNA-based applications in prenatal medicine, such as fetal sex and Rhesus factor determination (84, 85), the detection of monogenic disorders (86), and the development of non-invasive prenatal testing (NIPT) for fetal aneuploidies such as trisomy 13, 18 and 21 (71, 87-90). Other studies demonstrated that increased cfDNA levels may also be observed in a variety of other physiological and clinical contexts, including physical exercise (91), acute trauma (92), organ transplantation (93), and infection (70, 94). Together, these findings established that cfDNA represents a heterogeneous pool comprised of both non-malignant and malignant DNA fragments arising from multiple tissues due to different biological processes (72).

1.2.3. Circulating tumor DNA

Circulating tumor DNA (ctDNA) is defined as the subset of cfDNA that originates from malignant cells and carries somatic changes that reflect the tumor genome, including point mutations, copy-number alterations (CNAs), and structural rearrangements (70, 95). This uniqueness to the tumor distinguishes ctDNA from background cfDNA and underpins its value as a cancer-specific biomarker.

The proportion of ctDNA within the total cfDNA pool spans a broad range, from less than 0.01% to more than 90%, and is influenced by tumor type, disease stage, intrinsic tumor characteristics, treatment status and physiological factors (68, 70, 72). In advanced or metastatic disease, ctDNA often represents a relatively large fraction of circulating cfDNA, whereas in early-stage disease or following effective therapy, ctDNA levels may be extremely low. In addition to tumor-related determinants, biological variability—including reported day-to-day fluctuations in cfDNA levels of approximately 25%—may further influence measurable ctDNA concentrations, underscoring the dynamic nature of circulating tumor-derived DNA (70).

Analytical strategies for ctDNA assessment broadly encompass targeted and genome-wide approaches. Targeted methods focus on predefined somatic alterations, often identified from tumor tissue or recurrently mutated genomic loci, and include techniques such as allele-specific polymerase chain reaction (PCR), digital PCR (dPCR), beads, emulsion, amplification, and magnetics (BEAMing), and targeted next-generation sequencing (NGS) panels. These approaches enable highly sensitive ctDNA detection and quantification, often reaching very low variant allele frequencies (VAFs). Such approaches are particularly well-suited for

monitoring known driver mutations, assessing treatment response, and detecting MRD, but are inherently limited in genomic breadth and typically rely on prior knowledge of tumor-associated variants. In contrast, genome-wide approaches interrogate larger portions of the genome without requiring predefined mutation targets. These include whole-exome sequencing (WES), and whole-genome sequencing (WGS), which facilitate the discovery of novel mutations, CNAs, and structural rearrangements. Advances in NGS technologies, including molecular barcoding and other error-suppression strategies, have substantially improved the sensitivity and specificity of ctDNA detection in such analyses. Nevertheless, the performance of genome-wide approaches remains strongly influenced by tumor fraction (TFx) and sequencing depth. Consequently, targeted and genome-wide methodologies represent complementary strategies, with the choice of approach determined by the clinical context and the balance between analytical sensitivity and genomic coverage (68, 69, 71).

Beyond mutation-based profiling, ctDNA analyses are increasingly incorporating non-genetic genome-wide features that reflect tumor-associated chromatin organization and DNA fragmentation processes (71, 72). Compared with cfDNA that stems from non-malignant cells, ctDNA fragments are typically shorter and display distinct fragmentation patterns, including characteristic end motifs, nucleosome positioning signals, and regional coverage oscillations across the genome. These fragmentomic features are thought to arise from differences in chromatin structure and cell-of-origin–specific nucleosomal organization and can be leveraged to enhance tumor signal detection, particularly in samples with low TFx. Integrating genomic alterations with these non-genetic features has therefore emerged as a way to improve analytical sensitivity and biological interpretability of ctDNA assays (65, 72).

Taken together, the biological characteristics and analytical adaptability of ctDNA position it as a versatile biomarker for cancer research and clinical management. ctDNA burden can be quantified using several metrics, including VAF, estimated TFx, or absolute ctDNA concentration in plasma. Measuring ctDNA at a single time point may provide information on tumor burden and prognosis, while genomic profiling can inform therapeutic decision-making. Serial ctDNA analyses further enable dynamic assessment of treatment response and clonal evolution through minimally invasive longitudinal sampling (71). The relevance of ctDNA is particularly pronounced in advanced malignancies, where sufficient ctDNA levels enable robust molecular characterization and repeated assessment over time.

1.3. Circulating tumor DNA in HR+/HER2- advanced breast cancer

HR+/HER2− ABC is characterized by prolonged disease trajectories and sequential lines of endocrine and targeted therapies, during which tumor evolution under therapeutic pressure is common. While activating mutations in genes such as *PIK3CA* often represent early clonal driver events with therapeutic implications, additional alterations—most notably *ESR1* mutations—frequently emerge under ET pressure and contribute to acquired resistance. Given the spatial heterogeneity of metastatic disease and the difficulty of repeated tumor tissue sampling, ctDNA has emerged as a particularly attractive tool in this subtype, enabling non-invasive, real-time molecular characterization throughout the course of treatment (**Figure 8**).

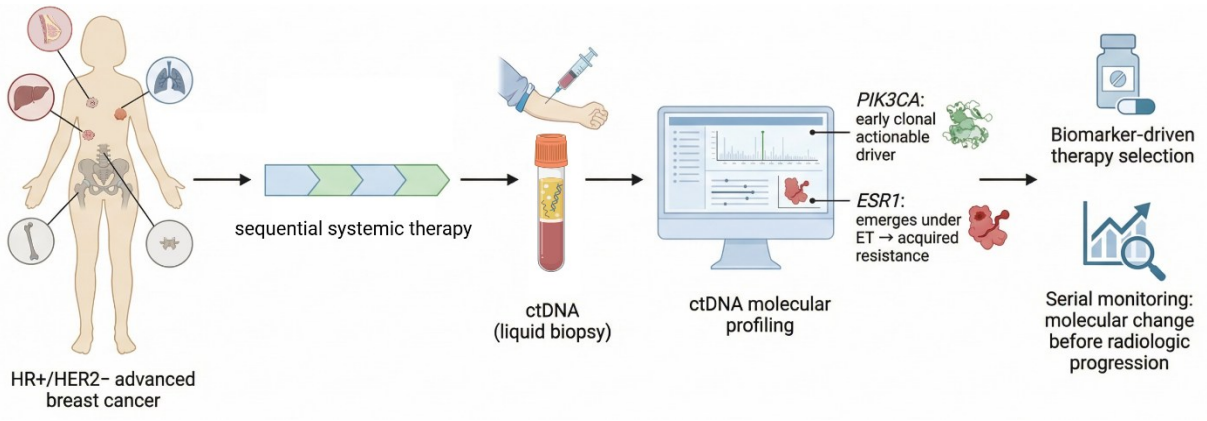

Figure 8. Clinical utility of ctDNA in HR+/HER2− ABC. Multiple metastatic sites contribute their DNA to the ctDNA pool, reflecting spatial tumor heterogeneity. Tumor evolution under therapeutic pressure leads to the emergence of clinically relevant alterations, which can be detected through ctDNA analyses using liquid biopsy. This enables real-time molecular profiling, supports biomarker-driven therapy selection, and allows longitudinal monitoring of disease dynamics. ABC advanced breast cancer, ctDNA circulating tumor DNA. Created with BioRender.com

Several biological and clinical features make HR+/HER2− ABC particularly well-suited for ctDNA-guided management. First, the genomic landscape of this subtype is relatively well-characterized and often involves recurrent, targetable alterations, such as mentioned mutations in *ESR1* or components of the PI3K pathway, which can be detected in ctDNA (96, 97). Second, the advanced disease setting is typically associated with higher tumor burden and increased ctDNA shedding, supporting more reliable detection of tumor-derived alterations in plasma. Third, the often-prolonged clinical course of HR+/HER2− disease allows for serial monitoring and the detection of molecular changes prior to overt radiological progression (71, 98). Collectively, these characteristics provide a strong rationale for the use of ctDNA analysis to guide molecular profiling and disease monitoring in HR+/HER2− ABC.

These considerations have been translated into clinical practice through several landmark trials. The SOLAR-1 trial demonstrated the predictive relevance of *PIK3CA* mutations for treatment with the PI3Kα inhibitor alpelisib and showed that ctDNA genotyping could reliably identify patients eligible for targeted therapy (99). Similarly, the PlasmaMATCH trial demonstrated that plasma-based molecular screening could successfully stratify patients to genotype-matched treatment arms, with objective responses observed across genomic cohorts (100). These studies confirmed that ctDNA-based profiling is feasible and clinically actionable in metastatic HR+/HER2− disease.

Beyond baseline genotyping, subsequent trials have explored ctDNA as a dynamic biomarker for early detection of acquired resistance. The PADA-1 trial pioneered a proactive monitoring strategy in patients receiving AIs combined with CDK4/6 inhibition. Routine ctDNA surveillance enabled early detection of *ESR1* mutations preceding radiological progression and switching ET upon molecular progression significantly improved PFS (101). The phase III SERENA-6 trial further validated this concept by using ctDNA-detected *ESR1* mutations to guide early transition from AI therapy to the oral SERD camizestrant, resulting in a clinically meaningful PFS benefit compared to standard care (46).

Additional trials support the utility of ctDNA for tracking response and resistance in endocrine-resistant HR+/HER2− ABC. In the EMERALD trial, patients with *ESR1*-mutant tumors identified via ctDNA derived a significant PFS benefit from the oral SERD elacestrant compared with standard ET (39). Similarly, the phase III EMBER-3 trial reported improved PFS with imlunestrant-based therapy in patients harboring *ESR1* mutations detected in plasma (40). Together, these studies establish *ESR1* mutation status assessed by ctDNA as both a marker of acquired resistance and a predictive biomarker guiding the selection of new therapies.

These trials demonstrate the transition of ctDNA analysis from a predominantly investigational tool towards its increasing integration into the clinical management of HR+/HER2− ABC. In this setting, ctDNA enables molecularly informed treatment selection, early identification of resistance, and dynamic adaptation of therapy based on tumor evolution.

1.4. Aim of the dissertation

Despite the substantial and continuous advances in the treatment of HR+/HER2− ABC, accurately identifying patients with an unfavorable prognosis at the initiation of therapy remains a challenge. While recent clinical trials have established the predictive role of ctDNA for guiding targeted treatment decisions, accumulating evidence suggests that ctDNA may also reflect disease aggressiveness. In particular, higher baseline TFx, increased VAFs, and a greater burden of detectable somatic alterations in plasma have been associated with inferior PFS and OS in patients with advanced disease (102-105).

However, most available findings stem from retrospective cohort analyses, exploratory biomarker assessments within randomized trials, or tumor-informed strategies that require prior sequencing of tumor tissue. While these studies provide valuable insights and/or high analytical sensitivity, their implementation in routine clinical practice may be limited. Moreover, many studies have evaluated individual genomic alterations or single ctDNA-derived parameters in isolation (106-109), which may not fully capture the biological complexity and heterogeneity characteristic of metastatic HR+/HER2− BC.

Therefore, in this thesis we prospectively investigated the prognostic relevance of ctDNA for patients with HR+/HER2− ABC undergoing early lines of systemic therapy in a real-world setting. Using a tumor-agnostic approach, we analyzed plasma-derived genomic alterations and quantitative tumor metrics at baseline and early progression to determine whether integrating these features could improve patient stratification. In addition, given the emerging clinical relevance of HER2-low disease—particularly following the development of ADCs such as T-DXd—we explored whether ctDNA characteristics differed between HER2-low and HER2-0 tumors within this cohort.

Accordingly, this thesis had three main objectives: (i) characterization of the ctDNA-derived genomic landscape in early-line HR+/HER2− ABC; (ii) evaluation of ctDNA-derived tumor metrics for improved risk stratification; and (iii) exploratory assessment of ctDNA characteristics according to the HER2 expression status.

At the same time, while the development and approval of therapies targeting resistance-associated alterations has created new treatment opportunities in HR+/HER2− ABC, it has also emphasized the need for reliable liquid biopsy-based testing to identify eligible patients.

To address this emerging clinical need and extend the clinical applicability of ctDNA-based analyses, we implemented a national real-world initiative to offer and evaluate plasma-based *ESR1* mutation testing in patients with HR+/HER2− ABC, aiming to assess its feasibility for identifying candidates for elacestrant. This analysis further aimed to characterize the molecular heterogeneity of this heterogenous patient population in a clinically driven setting.

2. MATERIAL AND METHODS

The data presented in this thesis were generated from two distinct but related research projects, both centered on the clinical and translational application of ctDNA in HR+/HER2− ABC. Accordingly, separate patient cohorts were analyzed, each with independent study protocols and ethics approvals. While several methodological approaches overlapped between the two cohorts, including plasma processing and mutational profiling, the study designs and specific analyses were not identical, reflecting their different clinical objectives.

For clarity and ease of reading, in the following sections these cohorts/studies will be referred to as the primary (early-line) cohort/study and the ESR1 testing cohort/study. The general overview of the sample collection and analysis workflow for both projects is shown in **Figure 9**.

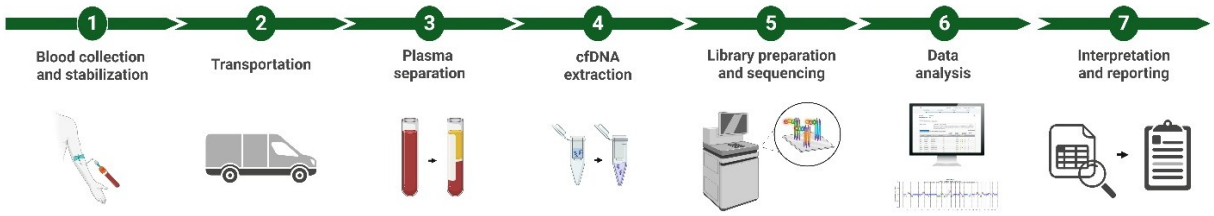

Figure 9. Sample collection and ctDNA analysis workflow. Blood samples were collected at the participating institutions. Genomic profiling of ctDNA and interpretation of results were performed at the Medical University of Graz. Created in BioRender.com

2.1. Ethics statements

Both studies were approved by the lead ethics committee of Medical University of Graz. The primary study had the approval numbers 32–415 ex 19/20 for the lead Medical University of Graz, 1495/2023 for the Medical University of Vienna, and 1164/2022 for the Medical University of Innsbruck. Analyses performed for the ESR1 testing study were approved under the number 1425/2025.

All participants provided informed consent. The study was conducted in compliance with the Declaration of Helsinki and the institutional guidelines for good scientific practice of the Medical University of Graz.

2.2. Patient cohorts

The primary cohort included patients with locally advanced BC or MBC recruited at the Medical University of Graz, Medical University of Vienna, and Medical University of Innsbruck during routine clinical practice. Eligible patients were diagnosed with HR+/HER2− ABC and underwent blood sample collection prior to the initiation of a line of systemic therapy for advanced disease. While patients receiving later lines of therapy were also enrolled, the majority of analyses presented in this thesis focused on patients undergoing first- or second-line treatment. All patients expressed ER, only some expressed PR, and all had either a 0 or 1+ score at IHC evaluation, or as a 2+ IHC score without amplification based on ISH. Samples with a 1+ IHC score or having a score of 2+ without amplification, were further classified as HER2-low. Diagnosis and histological evaluation were based on the most recent tissue sample obtained from either the primary tumor or a metastatic lesion.

The ESR1 testing cohort was comprised of patients with HR+/HER2- ABC as well. However, patients were included irrespective of treatment line, reflecting routine clinical practice. The analyses were performed within the framework of the Molecular Tumor Board (MTB) of the University Comprehensive Cancer Center Graz, where plasma samples were referred to from multiple centers across Austria. Clinical data for this cohort are still being collected; therefore, the present analysis is limited to the descriptive evaluation of the mutational landscape and its association with TFx. Assessment of prognostic and predictive value will be possible once the dataset is complete.

The REDCap electronic data capture platform at the Medical University of Graz was used for the systematic collection and management of patient data (110).

2.3. Blood collection and plasma separation

Blood samples from the primary cohort were collected at the timepoint of ABC diagnosis (baseline, before the start of treatment for metastatic disease) or at the time of progression on an early line of therapy (before starting a new line). For the ESR1 testing cohort, the timing of blood collection was determined by the treating physicians based on clinical indications, rather than a predefined study timepoint.

Whole blood was collected in PAXgene Blood ccfDNA Tubes (Qiagen, Hilden, Germany) at the participating centers and transported to Graz at room temperature conditions. For the primary project, we collected two tubes containing 10-30 mL of blood from each patient, while for the ESR1 testing project we collected three tubes with approximately 20-30 mL of blood.

Blood was centrifuged at 1900 x g for 10 minutes, and the supernatant and the buffy coat containing the white blood cells were collected separately. The supernatant was then centrifuged again at 1900 x g for 10 minutes, making sure that the plasma was separated from any remaining cells containing high molecular weight DNA. Both the plasma and the white blood cells were aliquoted into 2 mL tubes and stored in a freezer at -80°C until further processing.

2.4. cfDNA extraction

The QIAamp Circulating Nucleic Acid Kit (Qiagen, Hilden, Germany) or the QIASymphony PAXgene Blood ccfDNA Kit (Qiagen, Hilden, Germany) were used for the cfDNA extraction in the primary project, starting from 1-4 mL of plasma. cfDNA extraction in the ESR1 testing project was performed solely using the QIAamp Circulating Nucleic Acid Kit, starting from 4 mL of plasma. The extraction was performed according to the manufacturer's instructions. All samples were eluted in 50 µL of PCR-grade, nuclease-free water. Isolated DNA was quantified using the Qubit 1X dsDNA High Sensitivity Assay Kit (Thermo Fisher Scientific, Vienna, Austria) on a Qubit 4 Fluorometer (Thermo Fisher Scientific, Waltham, MA, USA; RRID: SCR_026883), and either processed right away or stored at -20°C, until further processing.

2.5. Library preparation and panel sequencing

Molecular profiling was performed using the AVENIO ctDNA Expanded Kit (Roche, Basel, Switzerland), a hybridization capture-based NGS assay designed to target 77 clinically relevant cancer-associated genes, including those referenced in the U.S. National Comprehensive Cancer Network (NCCN) Guidelines and additional emerging cancer biomarkers (**Table 6**). Library preparation was performed following the manufacturer's protocol, starting from an input of 10-50 ng of cfDNA. Both the final enriched libraries and intermediate whole-genome libraries were prepared and preserved. The enriched libraries were quantified using the Qubit 1X dsDNA HS Assay Kit on the Qubit 4 Fluorometer, and their quality and size distribution were assessed on an Agilent Bioanalyzer (Agilent Technologies, Santa Clara, CA, USA; RRID:

SCR_018043) or a 4200 TapeStation System (Agilent, Santa Clara, USA; RRID: SCR_018435). 4 to 16 libraries were pooled equimolarly, quantified using qPCR (Applied Biosystems, Thermo Fisher Scientific, Waltham, MA, USA; RRID: SCR_023455), and sequenced in paired-end runs on an Illumina NextSeq 550 System (Mid or High Output kit) (Illumina, San Diego, CA, USA; RRID: SCR_016381) or a NovaSeq 6000 Sequencing System (SP flowcell, XP workflow) (Illumina, San Diego, CA, USA; RRID: SCR_016387), generating 2 x 150 bp reads. Sequencing for the ESR1 testing project was performed using only the NovaSeq 6000 Sequencing System (SP flowcell, XP workflow).

As a result, a mean of 38 million (range: 13–82 million) read pairs was produced per sample in the primary cohort, with an average unique depth of 3399× (range: 943–8557×), and an average fragment length of 176 bp (range: 159–355 bp). In the ESR1 testing cohort, an average of 48 million (range: 27–68 million) read pairs were produced per sample, with an average unique depth across samples of 4578× (range: 899–9884×), and an average fragment length of 171 bp (range: 157–191 bp).

2.6. Variant calling and filtering

Following the library preparation and sequencing, variant calling was done using the AVENIO Oncology Analysis Software (version 2.1.0, Roche, Basel, Switzerland). Custom filtering parameters were implemented, with variants showing a VAF ≥ 1% in the ExAC (version 1.0) or 1000 Genomes (phase_3_v5b) databases, or annotated as common SNPs in dbSNP150, being automatically excluded by the analysis software. Variants passing these filters with fewer than 10 mutated reads or a VAF below the predefined limit of detection (LOD) were manually excluded, alongside copy-number variations (CNVs) called by the software, additional likely germline variants (VAF ~ 50 % but low tumor content) and sequencing or assay artifacts (recurrent low-level variants detected in multiple patients), in an effort to have a variant call set of high confidence. The variants that passed these filters – presumed somatic, tumor-specific variants – were annotated for pathogenicity using Golden Helix VarSeq (Golden Helix, Bozeman, MT, USA; RRID: SCR_001285, v2.2.0) and the OncoKB database (111). For each sample, the variant with the highest VAF (hVAF) was identified and considered to represent the dominant (clonal) population. Variants with a VAF less than 20% of the corresponding hVAF were classified as subclonal.

For the primary study, we applied a conservative detection threshold (VAF ≥ 0.5%) for variant calling. This cutoff was chosen to prioritize analytical confidence rather than maximal sensitivity, in order to minimize false-positive calls arising from the hematopoietic background. To evaluate the influence of low-frequency variants on the overall genomic landscape, secondary analyses were performed using a lower LOD of 0.1% VAF. In contrast, for the ESR1 testing study, all variants detected at VAF ≥ 0.1% were reported to maximize sensitivity for clinically relevant *ESR1* alterations, which may emerge at low VAFs as early subclonal events during treatment. Variants below 0.5% VAF were therefore interpreted in the context of this increased sensitivity and a repeated measurement was recommended.

2.7. Shallow whole-genome sequencing

In the ESR1 testing cohort, shallow whole-genome sequencing (sWGS) was performed systematically for all samples to enable consistent assessment of TFx. To this end, whole-genome libraries prepared using the AVENIO ctDNA Expanded Kit were sequenced to a target coverage of approximately 0.1×. In the primary cohort, however, sWGS was performed only for a subset of samples, reflecting differences in study design, as TFx was estimated using alternative approaches. For these samples, whole-genome libraries were prepared using either the AVENIO ctDNA Expanded Kit or the TruSeq Nano DNA LT Sample Preparation Kit (Illumina, San Diego, CA, USA), as previously described (112).

After library preparation, all libraries were quantified using the Qubit 1X dsDNA HS Assay Kit on the Qubit 4 Fluorometer, and quality-checked on an Agilent Bioanalyzer or a 4200 TapeStation System. They were then pooled equimolarly, quantified using qPCR and sequenced single- or paired-end on an Illumina MiSeq, NextSeq (Mid or High Output kit) or NovaSeq 6000 platform in the case of the primary study, or only paired-end on the NovaSeq 6000 platform (SP flowcell, XP workflow) in the case of the ESR1 testing study.

2.8. Estimation of tumor burden

Plasma tumor burden in these projects was estimated using three different approaches: untargeted aneuploidy profiling with mFAST-SeqS, the hVAF identified using the AVENIO ctDNA Expanded assay, and the ichorCNA algorithm.

mFAST-SeqS and hVAF were used in the primary study as complementary approaches for the estimation of tumor burden in plasma. In this study, when sWGS data were available, TFx was additionally estimated using ichorCNA as an exploratory comparative measure. In contrast, for the ESR1 testing cohort, ichorCNA was the only method used to assess the TFx, and was therefore done for all samples.

2.8.1. mFAST-SeqS

The modified Fast Aneuploidy Screening Test-Sequencing System (mFAST-SeqS) assay is an untargeted and cost-efficient approach for estimating TFx based on genome-wide aneuploidy. This assay quantifies chromosomal CNAs by sequencing long interspersed nuclear element-1 (LINE-1) regions and evaluating deviations in read counts relative to a normal reference. Library preparation was performed as previously described (113).

In brief, LINE-1 amplicon libraries were prepared from 1 ng of cfDNA, followed by quantification on the Qubit 4 Fluorometer, and quality control using either an Agilent Bioanalyzer or a 4200 TapeStation system. Libraries were then pooled equimolarly and sequenced on the Illumina MiSeq or NextSeq platform. Due to the low sequence complexity of LINE-1 amplicons, a higher-diversity library was included in each sequencing run to improve base-calling accuracy. Sequencing was performed using either 150 bp single-end or 76 bp paired-end reads, aiming for a minimum of 100,000 reads per sample. FASTQ files were aligned to the hg19/GRCh37 reference genome using an in-house pipeline based on the Burrows–Wheeler Aligner (bwa-mem, version 0.7.4). Reads with a mapping quality above 15 were counted for each chromosome arm. Chromosomal over- and underrepresentation was assessed using z-score statistics, and a genome-wide z-score (z-score) was derived as a surrogate measure of TFx, reflecting overall aneuploidy.

Although mFAST-SeqS was initially established using a z-score threshold of 5 (113), our group has shown that absolute z-scores of ≥ 3 already yield informative estimates of TFx, capturing underlying copy-number gains and losses (114). Accordingly, in this study, a z-score cutoff of 3 was applied to define elevated TFx.

2.8.2. AVENIO-based tumor burden

In the primary study, in parallel with mFAST-SeqS, tumor burden was evaluated using a mutation-based approach derived from VAFs detected with the AVENIO ctDNA Expanded Kit. This targeted strategy was applied to complement the aneuploidy-based TFx assessment and enhance associations with clinical outcomes. Mutation-based TFx was estimated using the hVAF observed among all detected somatic variants within a sample.

Based on the analytical LODs of both mFAST-SeqS and the AVENIO assay, ctDNA positivity was defined as the detection of at least one somatic variant reaching a z-score ≥ 3 or a VAF ≥ 0.5%. As shown in our previous work (115), the combination of aneuploidy-derived TFx and mutation-based hVAF at a 1% VAF threshold increases the reliability of negative liquid biopsy results and contributes to clinical decision-making. Accordingly, we defined elevated ctDNA levels as a sample having either an hVAF ≥ 1% or a z-score ≥ 3.

Therefore, to evaluate the prognostic impact of ctDNA, apart from single ctDNA measures (z-scores, hVAF), we employed these two binary composite variables: ctDNA positivity (≥ 1 somatic variant or z-score ≥ 3) and elevated ctDNA (z-score ≥ 3 or hVAF ≥ 1%). In addition, we assessed the impact of a three-tier composite variable, which stratified patients into three tumor burden categories: low (z-score < 3 and hVAF < 1%), intermediate (either z-score ≥ 3 or hVAF ≥ 1%), and high (both z-score ≥ 3 and hVAF ≥ 1%).

2.8.3. ichorCNA

In both studies, TFx was inferred from sWGS data using ichorCNA (RRID: SCR_024768), a widely adopted and current state-of-the-art method for analyzing of ultra–low-coverage sequencing of cfDNA (116, 117). ichorCNA leverages genome-wide read depth information to detect large-scale somatic CNAs and estimate the proportion of tumor-derived DNA within a background of normal cfDNA.

In brief, sequencing reads are aggregated into fixed-width genomic bins and normalized to correct for technical biases such as GC content and mappability. ichorCNA then employs a Hidden Markov Model (HMM) to segment the genome into regions of distinct copy-number states, while simultaneously modeling TFx and ploidy (116, 118). The method is designed to be robust to the low signal-to-noise ratio characteristic of shallow sequencing data by enforcing

spatial continuity of copy-number states across adjacent genomic bins and limiting over-segmentation driven by local noise.

In the primary study, we applied this method on samples with available sWGS data, as an exploratory comparative method that provides a more refined estimation of TFx. In the ESR1 testing study, ichorCNA was the sole method used for TFx estimation. The pipeline was run using default parameters, the bin size set to 1 Mb, and the lower LOD set to 3% TFx, a threshold previously shown to reliably distinguish ctDNA-positive from ctDNA-negative samples (116, 118).

2.9. Copy-number analysis

Low-pass WGS data available for a subset of samples from the primary study were additionally analyzed using GISTIC 2.0 (Genomic Identification of Significant Targets in Cancer, version 2.0.23), an algorithm developed to detect genomic regions that show significant and recurrent amplification or deletion across a cohort (119). GISTIC identifies regions likely to harbor driver CNAs from background noise by integrating both the amplitude and frequency of events across samples.

Segmented copy-number profiles derived from sWGS data were used as input. The algorithm assigned a G-score to each genomic region, reflecting the magnitude and recurrence of copy-number changes, and estimated statistical significance using permutation-based testing with false discovery rate (FDR) correction.

Analyses were performed using default parameters, including a focal length cutoff of 0.50 Mb to distinguish focal from broad events, a q-value threshold of 0.25 to define statistical significance, and a confidence level of 0.90 for peak region identification. All analyses were conducted with respect to the hg19/GRCh37 reference genome. Significantly amplified and deleted regions identified by GISTIC were further explored and visualized in R (version 4.3.1) using the maftools package (120), enabling cohort-level representation of recurrent CNAs.

2.10. Statistical analyses

Statistical analyses were carried out using GraphPad Prism (RRID:SCR_002798; version 10.5.0), Stata (RRID:SCR_012763; version 19.5), and R Project for Statistical Computing (RRID:SCR_001905; version 4.3.1). Descriptive statistics were used to summarize patient and

tumor characteristics, with medians and ranges reported for continuous variables and counts and percentages for categorical variables. As some patients had repeated measurements, we used linear mixed-effects models with patient-level random intercepts to account for within-patient correlation in the case of continuous outcomes, and logistic regression models with cluster-robust standard errors in the case of binary outcomes. Count data were analyzed using mixed-effects negative binomial regression to estimate incidence rate ratios (IRRs). For comparisons between HER2 expression subgroups, the earliest available sample per patient was used in the primary analysis to preserve independence of observations, while mixed-effects models including all available samples were performed as sensitivity analyses. Discordant mutation patterns between paired samples were examined using McNemar's test for paired data.

The co-occurrence and mutual exclusivity relationships between pairs of somatic alterations were evaluated using the somaticInteractions function in the maftools R package (RRID: SCR_024519) (120). Co-occurrence frequencies are reported as percentages, and statistical significance was assessed using Fisher's exact test. Odds ratios were not emphasized due to instability of effect size estimates in the presence of sparse data.

PFS was determined as the time from blood sampling to either disease progression or death from any cause. As this study reflects real-world clinical practice, PFS was determined on the basis of imaging results and clinical evaluation, rather than standardized RECIST criteria. OS was defined as the time from blood draw to death from any cause. Patients who had not experienced an event by the last follow-up were censored. The median follow-up time was estimated using the reverse Kaplan–Meier method (121). Survival differences were evaluated using the log-rank test and visualized with Kaplan–Meier curves.

Univariable and multivariable Cox proportional hazards models incorporating clinically relevant covariates were used for survival analyses. Schoenfeld residuals were used to evaluate the proportional hazards assumption. Hazard ratios are presented with corresponding 95% confidence intervals (CIs). Model performance was assessed using Uno's concordance index (C-index) based on 5,000 bootstrap resamples (122), and model fit was evaluated using the Akaike Information Criterion (AIC) (123). All statistical tests were two-sided, with p-values <0.05 considered as statistically significant.

3. RESULTS

The results are presented according to the two independent cohorts described above. For clarity, the findings from the primary cohort are presented first, followed by the results from the ESR1 testing cohort.

3.1. Patient characteristics of the primary cohort

A total of 225 blood samples were obtained from 184 patients with HR+/HER2- ABC. Of them, 128 samples were collected before starting first-line (1L) therapy, 76 before starting second-line (2L) therapy, 19 before starting third-line (3L), and 2 before starting fourth-line (4L) therapy. Forty patients contributed with paired samples, of which 39 patients had two and one had three blood samples taken. For 32 patients, blood was drawn prior to 1L and 2L treatment specifically. An overview of the patients and the study design is presented in **Figure 10.** Sample collection is depicted in more detail in **Figure 11**. Each sample was collected before the start of the specified treatment line.

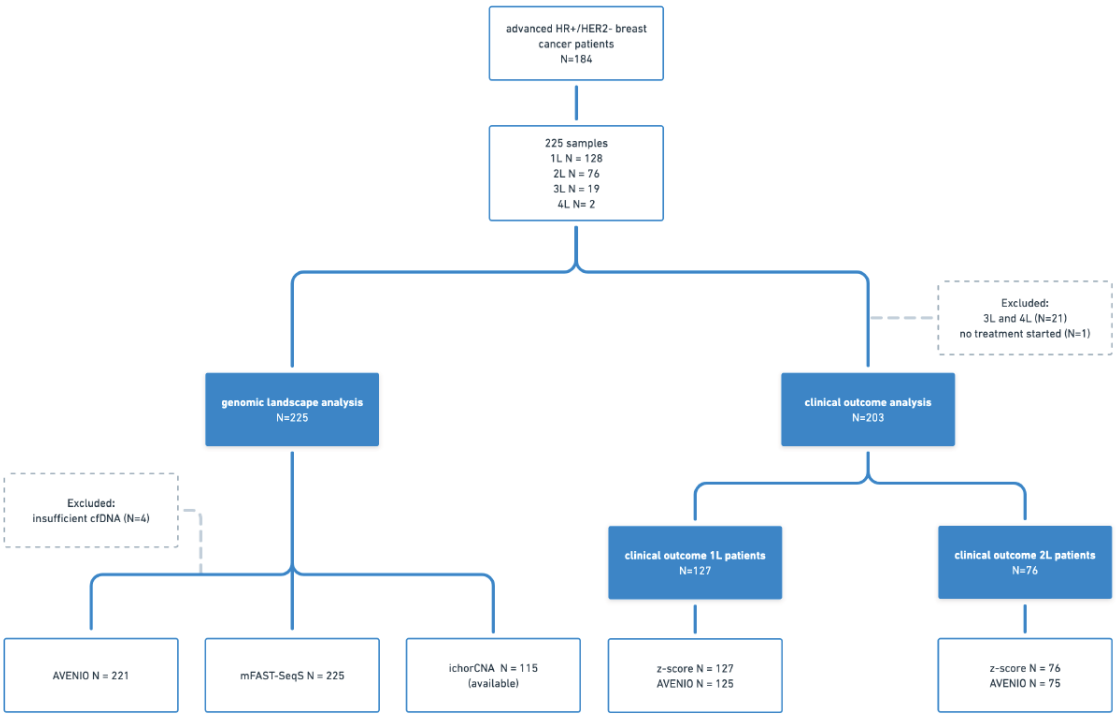

Figure 10. Consort diagram showing the selection of samples for genomic and survival analyses. A total of 225 plasma samples from 184 HR+/HER2- patients were collected and analyzed. 1L first-line, 2L second-line, 3L third-line, 4L fourth-line. Figure and legend adapted from Dobrić et al. (124), under the terms of the Creative Commons CC BY-NC-ND 4.0 license, https://creativecommons.org/licenses/by-nc-nd/4.0/.

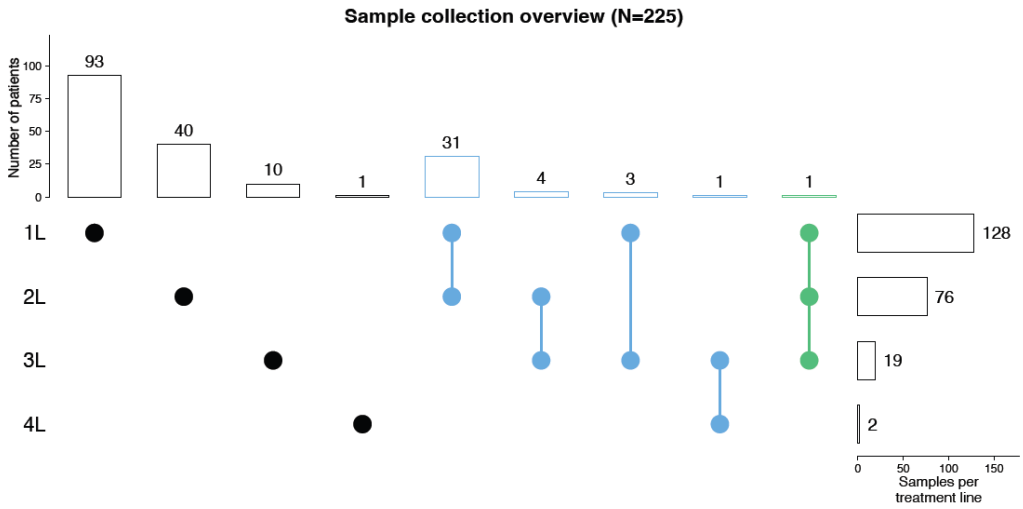

Figure 11. Representation of the sample collection timepoints. Each sample was collected before the initiation of the respective treatment. Colors represent the number of samples patients contributed with: one (black), two (blue), or three (green). 1L first-line, 2L second-line, 3L third-line, 4L fourth-line. Figure and legend adapted from Dobrić et al. (124). Reproduced with permission from the original authors, under the terms of the Creative Commons CC BY-NC-ND 4.0 license, https://creativecommons.org/licenses/by-nc-nd/4.0/.

The median patient age at the time of blood sample collection was 66.1 years (range 28.8–93.3 years), and the majority of the patients were female (96.7%). The histological subtype observed most frequently was NST (71.2%), followed by ILC (18.5%) and mixed types (5.4%). Information regarding the HER2 status was available for 181/184 patients, of which 64.1% were classified as HER2-low, and 34.3% as HER2-0. At the timepoint of advanced disease diagnosis, 39.7% of patients had de novo metastatic disease, 56.5% had recurrent metastatic disease, and 3.8% presented with locally advanced disease. Liver metastases were detected in 19.2% of metastatic patients, while 32.8% of patients had visceral metastases that did not include liver. Additionally, 15.2% of metastatic patients had non-visceral metastases, and 30.5% had metastatic disease confined to bone. More than 90% of patients had metastases in one to three organs. An overview of the clinicopathological characteristics of the patients is presented in **Table 1**. When multiple blood samples were available from a single patient, only the status at the first timepoint was included in the description.

Table 1. Patient and tumor characteristics of the study cohort at the time of enrollment. Adapted from Dobrić et al. (124), under the terms of the Creative Commons CC BY-NC-ND 4.0 license, https://creativecommons.org/licenses/by-nc-nd/4.0/.

	***N* = 184 *n* (%)**
Age at blood sample collection, years (range)	66.1 (28.8-93.3)
Sex	
Female	178 (96.7)
Male	6 (3.3)
Histological type	
NST	131 (71.2)
ILC	34 (18.5)
Mixed	10 (5.4)
Unknown/other	9 (4.9)
HER2 subtype	
HER2-0[a]	63 (34.3)
HER2-low[b]	118 (64.1)
Unknown	3 (1.6)
Disease setting at diagnosis of advanced disease	
De novo metastatic	73 (39.7)
Metastatic recurrent	104 (56.5)
Locally advanced	7 (3.8)
Metastases localization	
Liver[c]	34 (19.2)
Visceral (nonliver)[d]	58 (32.8)
Nonvisceral[e]	27 (15.2)
Bone only	54 (30.5)
Other[f]	4 (2.3)
Number of metastatic organs	
0	7 (3.8)
1	81 (44.0)
2	55 (29.9)
3	31 (16.9)
≥4	10 (5.4)
Time from initial diagnosis to first metastases	
≤24 months	7 (6.7)
>24 months	97 (93.3)
Number of previous palliative lines	
0	128 (69.6)
1	44 (23.9)
2	11 (6)
3	1 (0.5)

[a]HER2-0: samples with an IHC 0 score.
[b]HER2-low: samples with either an IHC 1+ score, or 2+ without amplification based on ISH.
[c]Liver: alone or with other metastases.
[d]Visceral (non-liver): lung/pleura, peritoneal cavity; if any of the locations were visceral, the patient was counted as visceral.
[e]Non-visceral: bone (with others), brain/CNS, lymph nodes.
[f]Other: breast, soft tissue, ovary.

Table 2 summarizes the treatment landscape in the 1L and 2L settings. The large majority of patients received ET combined with a CDK4/6 inhibitor, representative of the time when the study was performed, but in line with real world data. Namely, at the time the study was conducted, alpelisib was the only approved targeted therapy in Austria for patients with *PIK3CA*-mutated disease; accordingly, a subset of patients received alpelisib in the 2L setting. Other targeted agents, including inavolisib, elacestrant, and capivasertib, were not yet approved during the study period.

Table 2. Systemic therapies received by patients in 1L and second-line 2L settings. 1L first-line, 2L second-line. Reproduced from Dobrić et al. (124), under the terms of the Creative Commons CC BY-NC-ND 4.0 license, https://creativecommons.org/licenses/by-nc-nd/4.0/.

	1L (%)	**2L (%)**
ET alone (AI or SERD)	6 (4.7)	8 (10.5)
AI + CDK 4/6i (+-OFS)	94 (73.4)	10 (13.2)
SERD + CDK4/6i (+-OFS)	26 (20.3)	11 (14.5)
Chemotherapy	1 (0.8)	19 (25)
ET + Alpelisib (+-OFS)	/	12 (15.8)
ET + mTORi	/	8 (10.5)
ET + other targeted treatment	/	3 (3.9)
Other	1 (0.8)	5 (6.6)

ET endocrine treatment
AI aromatase inhibitor
CDK4/6i cyclin-dependent kinase 4/6 inhibitor
OFS ovarian function suppression
SERD selective estrogen receptor degrader
mTORi mTOR inhibitor

3.2. Genomic landscape in advanced HR+/HER2- breast cancer

Of 225 samples, 221 were successfully sequenced and analyzed using the AVENIO assay, while four had to be excluded because of insufficient material. Across all 221 analyzed samples, looking at all timepoints, one or more mutations were observed in 68/77 genes covered by the AVENIO panel. In total, 529 somatic variants were detected in 160/221 (72.4%) samples. Across the 160 samples with somatic variants, the median variant count per sample was 2 (range 1–28). Of these, a median of 2 variants per sample (range 1–14) were classified as clonal, whereas a median of zero (range 0–23) were subclonal. The median hVAF was 4.7% (range 0.5%–75.4%).

3.2.1. Mutational profiles at baseline and progression

Given the clinical importance of therapeutic decision-making in early treatment phases, we first assessed the mutational landscapes of samples collected before 1L (N=126) and 2L (N=75) treatment. In the 1L cohort, we identified somatic variants in 82 patients (65.1%), and in 62 cases (49.2%) these variants were pathogenic or likely pathogenic (P/LP). In the 2L cohort, 61 patients (81.3%) had detected somatic variants, and in 52 of them (69.3%) the variants were P/LP. Using a mixed-effects negative binomial model, even after adjusting for elevated TFx (z-score ≥ 3), 2L samples were shown to have a significantly higher number of somatic variants compared with 1L samples, corresponding to an 80% increase in variant counts (IRR = 1.80, 95% CI: 1.36–2.38; $p < 0.001$).

In both 1L and 2L patients, the most frequently mutated genes were *PIK3CA*, *TP53*, and *ESR1*. Among 126 successfully analyzed 1L patients, 41 (32.5%) carried *PIK3CA* mutations, with H1047R being the most common alteration (15.6%), followed by E545K (7.0%) and E542K (3.1%). *ESR1* variants were detected in 12 1L patients (9.5%), D538G being the most common alteration (2.3%). Among 75 successfully analyzed 2L patients, 30 (40.0%) carried *PIK3CA* mutations. H1047R was again the most frequent alteration (17.1%), followed by E545K (9.2%) and E542K (6.6%). As expected, *ESR1* alterations were more frequent in the 2L cohort, being detected in 21 patients (28.0%). The most common *ESR1* variants were D538G and Y537S, each observed in 7.8% of 2L patients. *TP53* variants were detected in 21 (16.7%) 1L and 19 (25.3%) 2L patients and were primarily located within the DNA-binding domain, although their positional distribution was heterogeneous.

Although the full mutational spectrum was assessed, only P/LP variants were included in downstream analyses and visualizations. This approach was adopted to focus on alterations with established or putative relevance for disease pathogenesis. P/LP mutations detected prior to 1L and 2L treatment are shown in **Figure 12**.

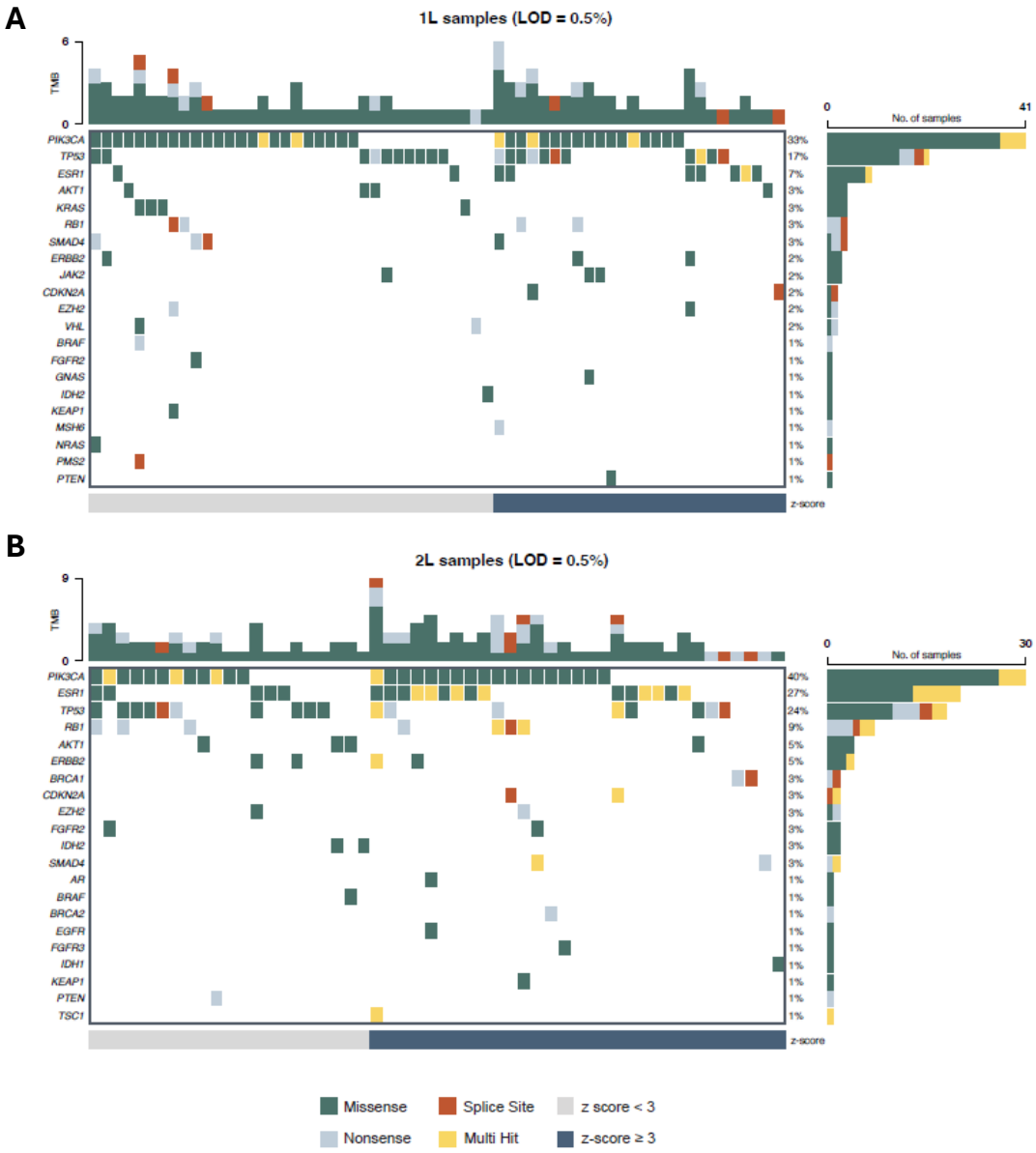

Figure 12. Landscape of P/LP somatic alterations detected in liquid biopsy samples taken before (A) 1L (N=62/126) and (B) 2L (N=52/75) treatment for HR+/HER2- ABC, using a LOD of 0.5%. The upper bars illustrate the number of alterations per sample, while the bars on the right show the frequency of alterations detected in each gene. Colors represent the mutation type: missense (green), nonsense (gray), splice-site (red), and multi-hit (yellow). The bar below the oncoprints illustrates the TFx of the samples, defined as a z-score < 3 (light gray) or ≥ 3 (dark gray). P/LP pathogenic/likely pathogenic, 1L first-line, 2L second-line, ABC advanced breast cancer, TFx tumor fraction, LOD limit of detection. Reproduced from Dobrić et al. (124), under the terms of the Creative Commons CC BY-NC-ND 4.0 license, https://creativecommons.org/licenses/by-nc-nd/4.0/.

All detected *PIK3CA*, and the majority of detected *TP53* and *ESR1* variants, were classified as P/LP; their distribution within these genes is illustrated in **Figure 13**.

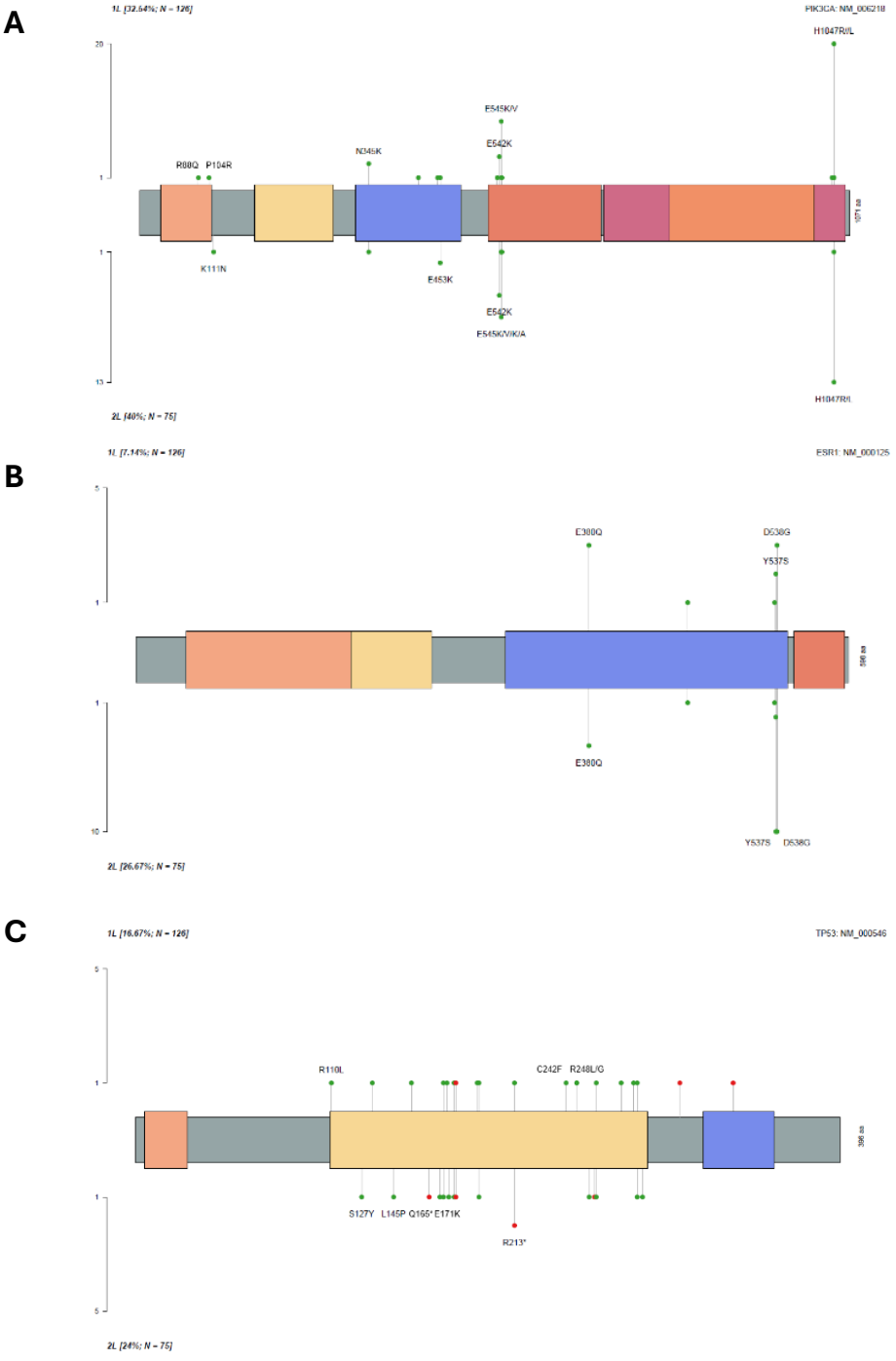

Figure 13. P/LP alterations detected in (A) *PIK3CA*, (B) *ESR1* and (C) *TP53*, mapped at the protein level and positioned according to their respective protein domains. Variants are mapped at the protein level and positioned according to the respective protein domains. Mutations detected at baseline are shown above the protein schematics, whereas mutations detected at progression are shown below. Missense mutations are indicated in green and nonsense mutations in red. 1L first-line, 2L second-line.

P/LP alterations in genes within the PI3K pathway (*PIK3CA*, *AKT1*, and/or *PTEN*) were identified in 34.9% of 1L and 44.0% of 2L samples. At progression, an increase in clonal complexity was observed. Among *ESR1*-mutated samples, polyclonality was observed in 11% (1/9) of 1L samples compared with 35% (7/20) of 2L samples. Similarly, the presence of multiple concurrent mutations in *PIK3CA*, *TP53*, and *RB1* was more frequently observed in 2L samples (**Figure 14**).

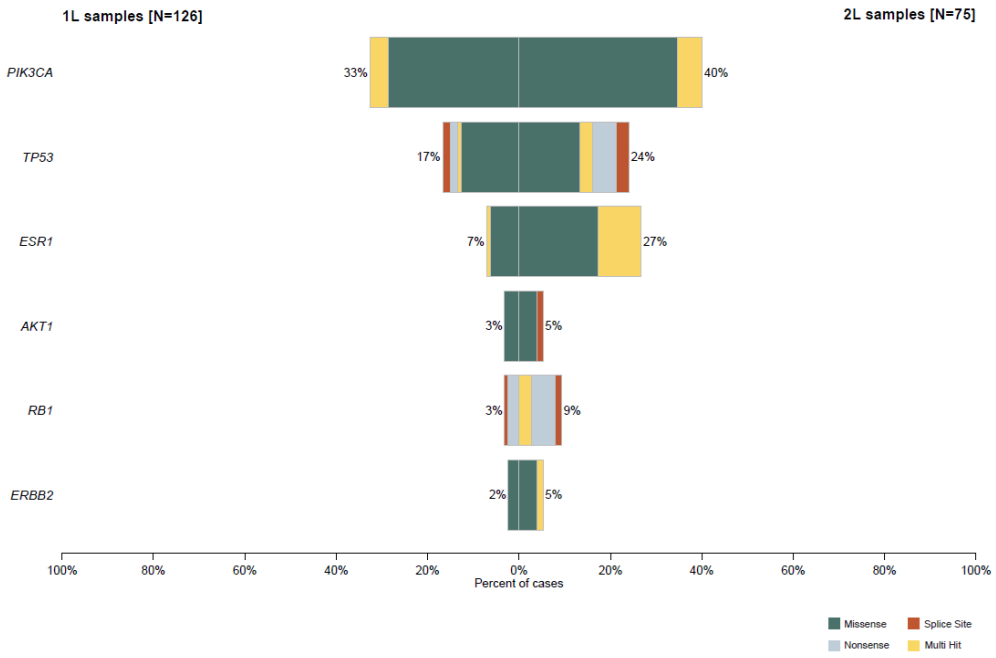

Figure 14. Comparative representation of the most frequently mutated genes detected in samples collected before 1L and 2L treatment, using an LOD of 0.5%. Mutation types are color-coded as follows: missense (green), nonsense (gray), and splice-site (red); the presence of multiple mutations within a single gene is indicated in yellow. Compared with baseline samples, progression samples showed a higher mutation frequency and increased clonal complexity. 1L first-line, 2L second-line, LOD limit of detection.

Using cluster-robust logistic regression to account for intra-patient correlation, we demonstrated that P/LP *ESR1* alterations were significantly more frequent in 2L compared to 1L samples (OR = 4.7, 95% CI 2.2–10.0, $p < 0.001$). Consistently, when we analyzed the subset of 31 patients with paired 1L and 2L samples, *ESR1* mutations presented as the most frequently acquired alteration (25.8%, McNemar test, $p = 0.005$). Although mutations in *RB1*, *PIK3CA*, and *TP53* were numerically more common in 2L samples, these differences were not statistically significant. **Figure 15** provides a graphical representation of the paired analysis results.

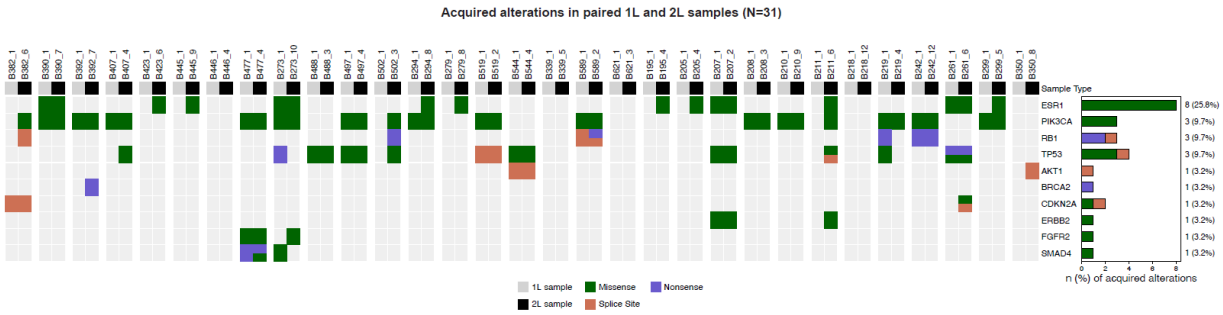

Figure 15. Acquired P/LP somatic alterations detected in a subset of 31 patients with paired samples taken before 1L (gray) and 2L (black) treatment. Bars on the right represent the number of acquired alterations detected in each gene. Colors represent the mutation type: missense (green), nonsense (purple), and splice-site (red). ABC advanced breast cancer, P/LP pathogenic/likely pathogenic, 1L first-line, 2L second-line. Reproduced from Dobrić et al. (124), under the terms of the Creative Commons CC BY-NC-ND 4.0 license, https://creativecommons.org/licenses/by-nc-nd/4.0/.

3.2.2. Sensitivity analysis at a lower detection threshold

Although the AVENIO ctDNA Expanded Kit can detect variants down to a VAF of 0.1%, a prespecified cutoff of 0.5% was used for the primary analyses to ensure high analytical confidence. At this threshold, the assay achieves a reported sensitivity of 99% and a positive predictive value (PPV) of 95%, as specified by the manufacturer (Roche). Given the increased uncertainty associated with low-frequency calls, variants between 0.1% and 0.5% VAF were evaluated in a secondary exploratory analysis to assess their potential contribution without influencing the primary results.

As expected, lowering the detection threshold increased the number of samples harboring somatic variants. With the LOD set to 0.1% VAF, we identified 864 somatic variants in 87.3% of all analyzed samples, compared to the above-reported 529 somatic alterations detected in 72.4% samples using the LOD of 0.5% VAF. The median variant count per sample was three (range 1–34), of which a median of two variants per sample (range 1–14) were classified as clonal, and a median of one (range 0–23) were subclonal.

Looking at early treatment lines, somatic variants were identified in 84.9% of 1L samples and 90.7% of 2L samples. Consistent with the primary analysis, the overall distribution of recurrent alterations remained largely unchanged. *PIK3CA* alterations were found in 47 baseline samples (36.7%); the most common H1047R mutation was observed in 18.0% samples, and E545K and E542K were detected in 7.0% and 3.9% of samples, respectively. Seventeen 1L (13.3%)

samples harbored *ESR1* variants, and D538G was the most frequent alteration, detected in 3.1% of patients. In 2L, 32 samples (42.1%) carried *PIK3CA* variants, while 25 (32.9%) had *ESR1* alterations. The most frequent *PIK3CA* variant in 2L was H1047R, detected in 18.4% patients, followed by E545K and E542K (both found in 9.2% of samples). The most common *ESR1* variant in 2L when using the LOD of 0.1% was Y537S; it was detected in 17.1% of samples, while D538G was identified in 14.5% of samples. *TP53* variants were detected in 28 (22.2%) 1L and 21 (28.0%) 2L patients.

P/LP variants were detected in 64.3% of baseline and 70.7% of progression samples. As shown in **Figure 16**, the mutational landscape at the lower threshold closely resembles the one obtained with the higher detection threshold. *PIK3CA*, *TP53*, and *ESR1* continued to represent the most frequently mutated genes in both 1L and 2L samples, with comparable relative frequencies.

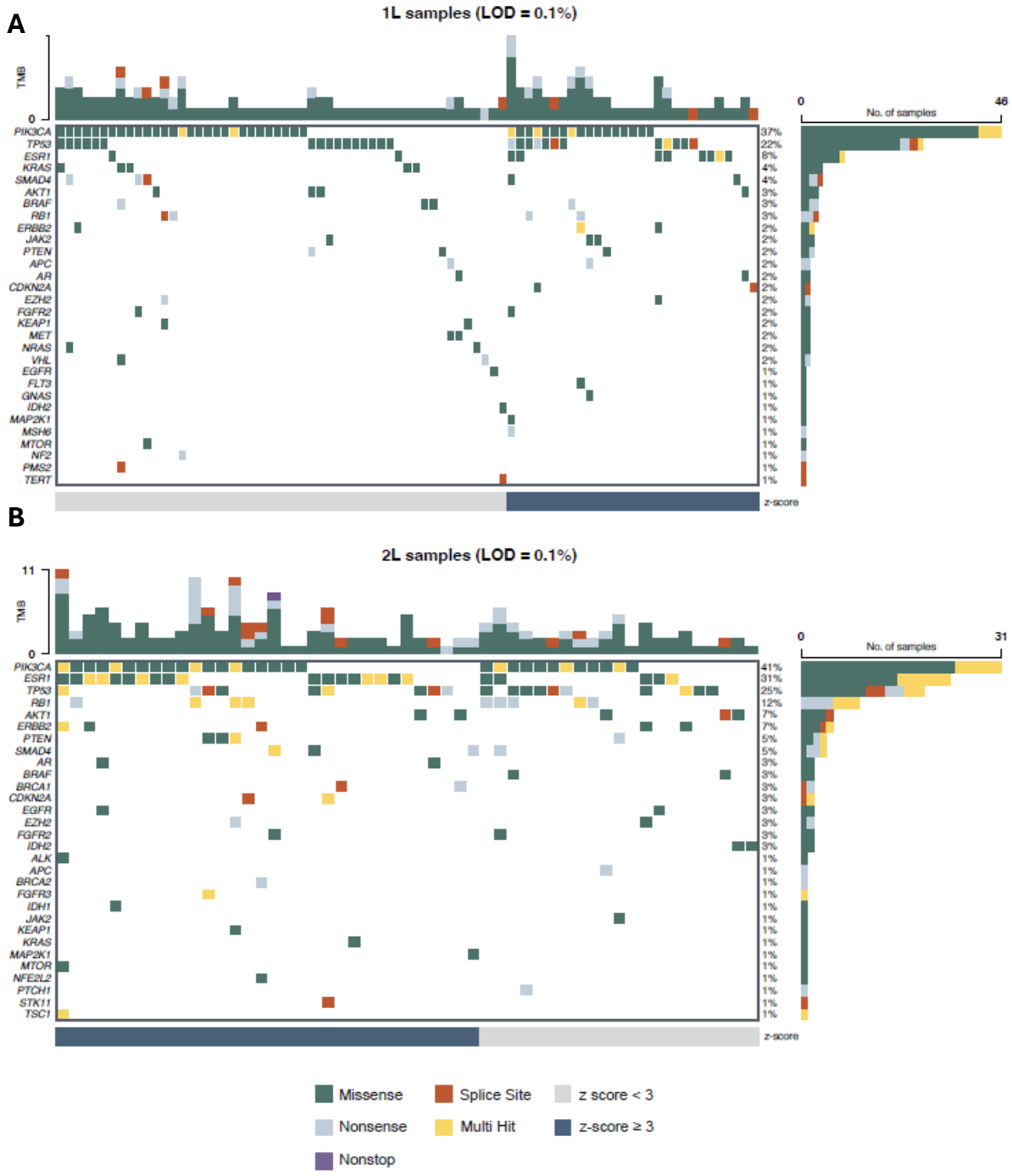

Figure 16. Landscape of P/LP somatic alterations detected in liquid biopsy samples taken before (A) 1L (N=81/126) and (B) 2L (N=53/75) treatment for HR+/HER2- ABC, using a LOD of 0.1%. The upper bars illustrate the number of alterations per sample, while the bars on the right show the frequency of alterations detected in each gene. Colors represent the mutation type: missense (green), nonsense (gray), nonstop (purple), splice-site (red), and multi-hit (yellow). The bar below the oncoprints illustrates the TFx of the samples, defined as a z-score < 3 (light gray) or ≥ 3 (dark gray). P/LP pathogenic/likely pathogenic, 1L first-line, 2L second-line, ABC advanced breast cancer, TFx tumor fraction, LOD limit of detection. Reproduced from Dobrić et al. (124), under the terms of the Creative Commons CC BY-NC-ND 4.0 license, https://creativecommons.org/licenses/by-nc-nd/4.0/.

Similarly, alterations observed within the PI3K pathway were found at slightly higher rates (41.4% in 1L and 52.6% in 2L), reflecting the increased sensitivity of variant detection at the lower threshold.

Patterns of clonal architecture were also largely preserved. The proportion of polyclonal *ESR1*-mutated samples remained low in 1L (10%) and higher in 2L (35%), consistent with the primary findings. Likewise, 2L samples more frequently exhibited multiple simultaneous mutations in *PIK3CA*, *TP53*, and *RB1* (**Figure 17**), supporting the observation of increased genomic complexity at progression.

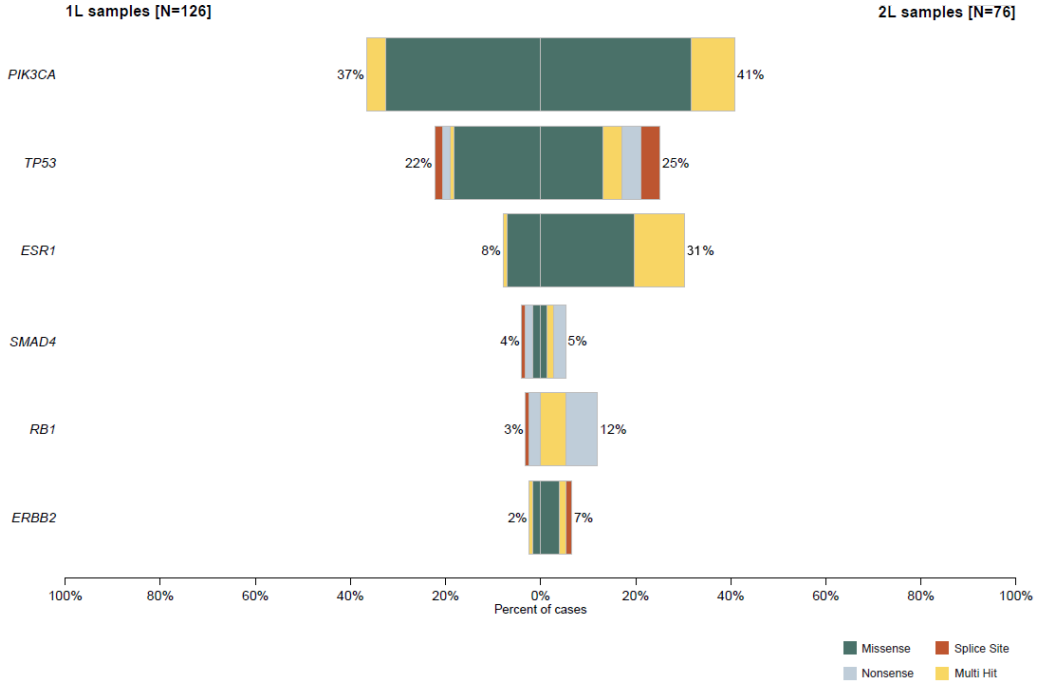

Figure 17. Comparative representation of the most frequently mutated genes detected in samples collected before 1L and 2L treatment, using an LOD of 0.1%. Mutation types are color-coded as follows: missense (green), nonsense (gray), and splice-site (red); the presence of multiple mutations within a single gene is indicated in yellow. Compared with baseline samples, progression samples showed a higher mutation frequency and increased clonal complexity. 1L first-line, 2L second-line, LOD limit of detection.

Analysis of the paired 1L–2L subset at the 0.1% threshold reproduced the primary findings. *ESR1* continued to emerge as the most frequently acquired mutation, whereas increases in *RB1*, *PIK3CA*, and *TP53* mutations in 2L samples remained numerically apparent but statistically non-significant (**Figure 18**).

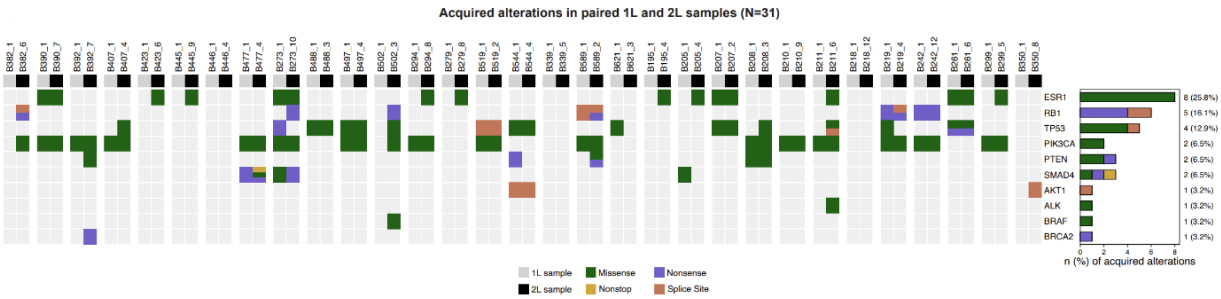

Figure 18. Acquired P/LP somatic alterations detected in the same subset of 31 patients with available and successfully analyzed paired samples, but with a lower LOD of 0.1%. Samples marked in gray were collected at baseline, and samples marked in black were collected at progression. Bars on the right correspond to the number of acquired alterations in each gene. Colors represent the mutation type: missense (green), nonsense (purple), and splice-site (red). 1L first-line, 2L second-line, P/LP pathogenic/likely pathogenic.

Taken together, lowering the detection threshold to 0.1% increased the overall variant detection and slightly shifted mutation frequencies, as expected. However, the relative distribution of recurrent alterations and the key patterns observed in the primary analysis were largely preserved. Given the modest increase in detection at 0.1% and the greater interpretative uncertainty associated with very low VAFs, the use of a 0.5% cutoff for the primary analyses was supported by the observed data.

3.2.3. Co-occurrence patterns at baseline and progression

To further characterize the genomic architecture at baseline and progression, we examined the patterns of co-occurring P/LP variants in our samples.

Co-mutation analysis performed with variants established using the 0.5% LOD revealed several significant co-occurrence patterns. *RB1* and *PIK3CA* mutations significantly co-occurred in both settings (1L: 3.1%, unadjusted p = 0.010; 2L: 9.3%, unadjusted p = 0.001), while a significant co-occurrence between *PIK3CA* and *SMAD4* mutations was observed only prior to 1L treatment (3.1%, unadjusted p = 0.010). Additionally, at baseline we found an interesting, statistically significant co-occurrence between *ESR1* and *TP53* mutations (3.1%, unadjusted p = 0.042). Borderline associations in the 1L setting included *RB1–ERBB2* (0.8%, unadjusted p = 0.093) and *ERBB2–TP53* (1.6%, unadjusted p = 0.072) co-occurrence (**Figure 19A**). In the 2L setting, significant co-occurrence was additionally observed between *ERBB2* and *TP53* (4.0%, unadjusted p = 0.041), while *ESR1–ERBB2* showed only a trend toward significance (4.0%, unadjusted p = 0.056) (**Figure 19B**). In addition to statistically significant associations,

clinically relevant targetable co-alterations involving *ESR1* and *PIK3CA* were also observed. Concurrent *ESR1* and *PIK3CA* alterations were detected in 3 patients (2.4%) in the 1L cohort and in 11 patients (14.7%) in the 2L cohort.

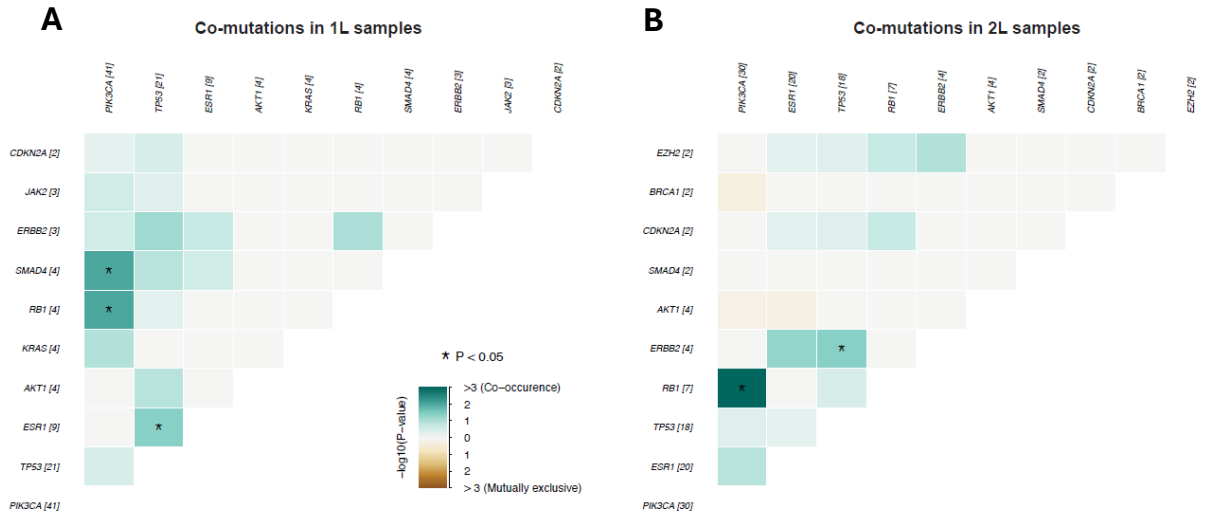

Figure 19. Co-occurrence plots of the top 10 mutated genes in (A) 1L and (B) 2L samples (pairwise Fisher's Exact test), with the variant detection threshold of 0.5% VAF. As samples in 1L and 2L groups come from different patients, the analysis was intended as exploratory and the two groups should not be compared. 1L first-line, 2L second-line, * statistically significant ($p < 0.05$). Adapted from Dobrić et al. (124), under the terms of the Creative Commons CC BY-NC-ND 4.0 license, https://creativecommons.org/licenses/by-nc-nd/4.0/.

When the LOD was lowered to 0.1%, the overall pattern was largely preserved, such as significant co-occurrence between *RB1* and *PIK3CA* mutations that remained evident in both settings (1L: 3.1%, unadjusted p = 0.016; 2L: 12.0%, unadjusted p < 0.001). However, the *PIK3CA–SMAD4* association at baseline lost statistical significance (3.1%, unadjusted p = 0.059), while *RB1–ERBB2* remained borderline significant (0.8%, unadjusted p = 0.093) (**Figure 20A**). In the 2L samples, a new significant co-occurrence emerged between *PIK3CA* and *PTEN* (5.3%, unadjusted p = 0.026), and the *TP53–ERBB2* association persisted as a borderline finding (4.0%, unadjusted p = 0.099) (**Figure 20B**). Concurrent *ESR1* and *PIK3CA* alterations were detected in 3 patients (2.4%) in the 1L cohort and in 12 patients (16.0%) in the 2L cohort.

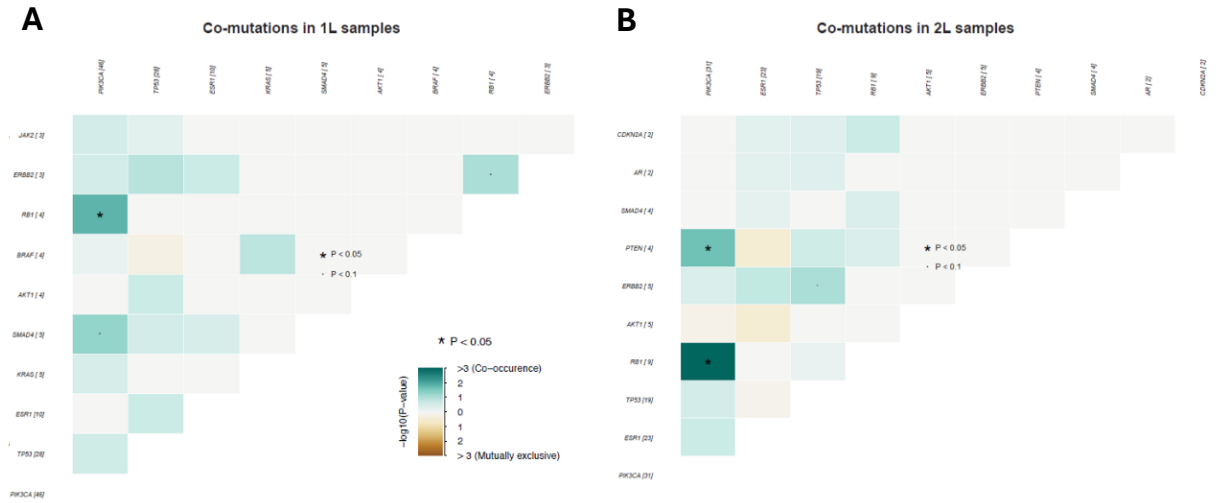

Figure 20. Co-occurrence patterns of the top 10 mutated genes in (A) 1L and (B) 2L samples (pairwise Fisher's Exact test), with the variant detection threshold set to 0.1% VAF. As samples in 1L and 2L groups come from different patients, the analysis was intended as exploratory and the two groups should not be compared. 1L first-line, 2L second-line, * statistically significant ($p < 0.05$).

Compared to single-gene mutation frequencies, the co-occurrence analyses appeared to be more sensitive to threshold selection, reflecting the greater statistical dependency of interaction testing on low-frequency variants. Accordingly, marginal associations may be influenced by the applied VAF cutoff and should therefore be interpreted cautiously.

3.2.4. Mutational profiles according to the HER2 expression status

In light of the emerging therapeutic relevance of the HER2-low phenotype, particularly following the clinical activity of antibody–drug conjugates such as T-DXd, we compared the mutational landscapes of HER2-low and HER2-0 tumors within our HR+/HER2− cohort to explore whether these groups exhibit distinct genomic characteristics.

118 patients with HER2-low ABC contributed to this study with 146 samples, and 63 patients with HER2-0 disease contributed with 76 samples. In total, somatic variants were detected in 129 out of the 218 (59.2%) successfully analyzed samples. P/LP somatic alterations were detected in 105 patients, of which 37 had a HR+/HER2-0 and 68 had a HR+/HER2-low status. The mutational profiles of the two patient groups are represented in **Figure 21.** As some patients participated in the analysis with more than one blood draw, P/LP variants detected in any of the samples were included in the representation, while mutations that appeared in both samples were counted only once. From a mutational aspect, HER2-0 and HER2-low patients did not show considerable differences, with the most frequently mutated genes—*PIK3CA*, *TP53* and

ESR1—presenting with a very similar frequency. HER2-0 patients had a higher proportion of *RB1* pathogenic alterations, including nonsense, splice-site and multi-hit variants, but the numbers were too small to assess significance. All detected splice-site mutations in *TP53* were found in HER2-low patients.

Overall, the mutational landscapes of HER2-low and HER2-0 tumors were largely similar, suggesting that the HER2-low phenotype in this cohort was not associated with a distinct pattern of recurrent genomic alterations.

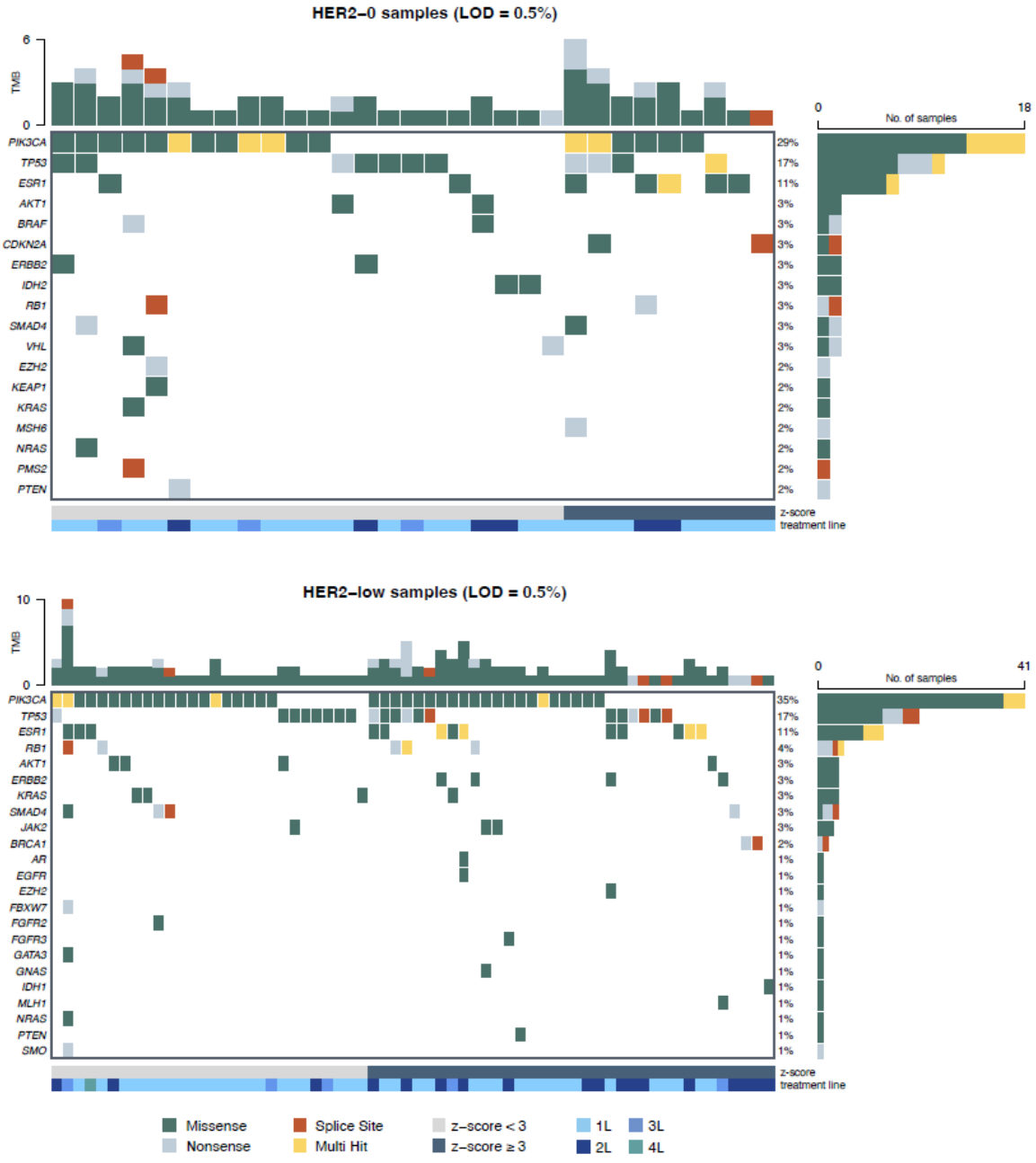

Figure 21. Landscape of P/LP somatic alterations detected in (A) HR+/HER2-0 (N=31/63) and (B) HR+/HER2-low (N=64/118) ABC patients, using the established LOD of 0.5%. The upper bars illustrate the number of alterations per sample, while the bars on the right show the frequency of alterations detected in each gene. Colors represent the mutation type: missense (green), nonsense (gray), splice-site (red), and multi-hit (yellow). The bars below the oncoprints illustrate the TFx of the samples (defined as a z-score) and the treatment line. For patients with repeated samples, only the first one was used for analysis. P/LP pathogenic/likely pathogenic, ABC advanced breast cancer, TFx tumor fraction, LOD limit of detection. Reproduced from Dobrić et al. (124), under the terms of the Creative Commons CC BY-NC-ND 4.0 license, https://creativecommons.org/licenses/by-nc-nd/4.0/.

3.3. Copy-number landscape

To complement the analysis of somatic mutations, we performed an exploratory assessment of CNAs in a subset of samples for which low-pass WGS data were available using GISTIC 2.0. Subsequent analyses examined copy-number patterns across treatment lines and according to the HER2 expression status.

3.3.1. Copy-number alterations across treatment lines

We first compared recurrent CNAs between samples obtained from 70 samples collected prior to 1L and 29 samples obtained prior to 2L treatment, to explore potential differences associated with treatment exposure. Across both treatment settings, recurrent copy-number gains were detected at chromosomal region 11q13.3 (includes *CCND1* and *FGF19*), as well as at 5q13.2, 8p23.1, and 9p11.2 (**Figure 22A**). Amplification peaks at 11q13.3 and 8p11.23 (encompass *FGFR1*, *ZNF703*, and *RAB11FIP1*) were more frequently identified in 1L samples, while a focal gain at 10q22.2 (*KAT6B*) was predominantly observed in the 2L cohort. Recurrent copy-number losses were observed at 1q21.1, 16p11.2, 4q35.2, and 10p11.1 in both groups (**Figure 22B**). Additional deletion peaks at 17p11.2 and 14q32.33 were present in the 1L samples. In summary, 1L samples demonstrated a broader distribution of recurrent CNAs, whereas 2L samples exhibited fewer recurrent events. Key recurrent CNAs highlighting shared and line-specific patterns were summarized, focusing on representative regions and genes with known or putative relevance in BC biology (**Table 3**).

Table 3. Selected recurrent copy-number alterations and associated genes. 1L first-line, 2L second-line, BC breast cancer.

Chromosomal region	Key gene(s)	Type	Seen in	Putative relevance in BC
11q13.3	*CCND1*, *FGF19*	Gain	Both	Cell cycle regulation / proliferation
8p11.23	*FGFR1*, *ZNF703*, *RAB11FIP1*	Gain	1L	Growth signaling and endocrine resistance
10q22.2	*KAT6B*	Gain	2L	Epigenetic regulation (histone modification)
1q21.1	—	Loss	Both	Recurrent genomic alteration; functional impact unclear
17p11.2	—	Loss	1L	Region containing tumor suppressor genes

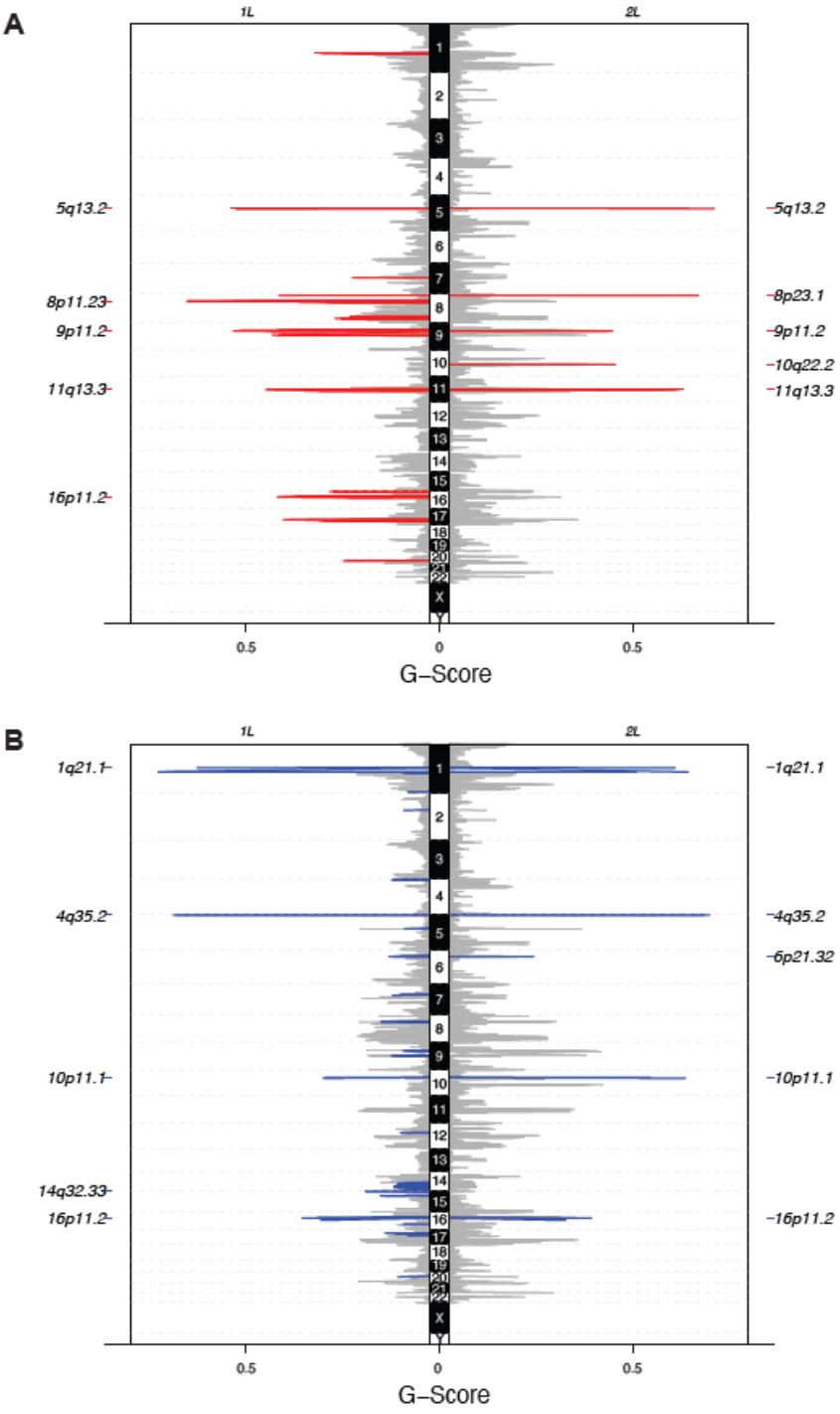

Figure 22. Copy-number alteration profiles in HR+/HER2- ABC generated with GISTIC 2.0. (A) Amplification and **(B)** deletion peaks are visualized for patients before 1L (left) and 2L (right) treatment. The G-score considers the amplitude of the aberration as well as the frequency of its occurrence across samples. 1L first-line, 2L second-line. Adapted from Dobrić et al. (124), under the terms of the Creative Commons CC BY-NC-ND 4.0 license, https://creativecommons.org/licenses/by-nc-nd/4.0/.

3.3.2.Copy-number alterations according to the HER2 expression status

We next compared the copy-number profiles between 65 patients with HER2-low and 40 patients with HER2-0 tumors, to explore potential CNA differences associated with the HER2 status. When multiple samples were available from a single patient, only the earliest sample was included in this analysis.

In both groups, recurrent amplifications were observed at 5q13.2, 8p23.1, and 9p11.2 (**Figure 23A**). The HER2-low group exhibited a broader range of focal and broad amplifications, including a peak at 8p11.23 (*FGFR1*, *ZNF703*, *RAB11FIP1*), as well as additional peaks at 11q13.3 (*CCND1*, *FGF19*) and 17q23.1 (*MIR21*). In contrast, the HER2-0 group demonstrated fewer focal amplification events, with several peaks located on the q-arm of chromosome 8, including 8q24.21 (*MYC*). Deletion patterns were largely comparable between groups, with recurrent losses at 1q21.1, 16p11.2, 4q35.2, and 10p11.1 observed in both cohorts (**Figure 23B**). Overall, HER2-low samples exhibited a somewhat broader amplification profile, while HER2-0 showed a quieter landscape dominated by shared alterations. Selected recurrent CNAs highlighting shared and subgroup-specific patterns were summarized, focusing on representative regions and genes with known or putative relevance in BC biology (**Table 4**).

Table 4. Selected recurrent copy-number alterations and associated genes. BC breast cancer.

Chromosomal region	Key gene(s)	Type	Seen in	Putative function in BC
11q13.3	*CCND1*, *FGF19*	Gain	HER2-low	Cell cycle regulation / proliferation
8p11.23	*FGFR1*, *ZNF703*, *RAB11FIP1*	Gain	HER2-low	Growth signaling and endocrine resistance
17q23.1	*MIR21*	Gain	HER2-low	Oncogenic signaling, proliferation, and survival
8q24.21	*MYC*	Gain	HER2-0	Transcriptional regulation, proliferation, and tumor progression
1q21.1	—	Loss	Both	Recurrent genomic alteration; functional impact unclear

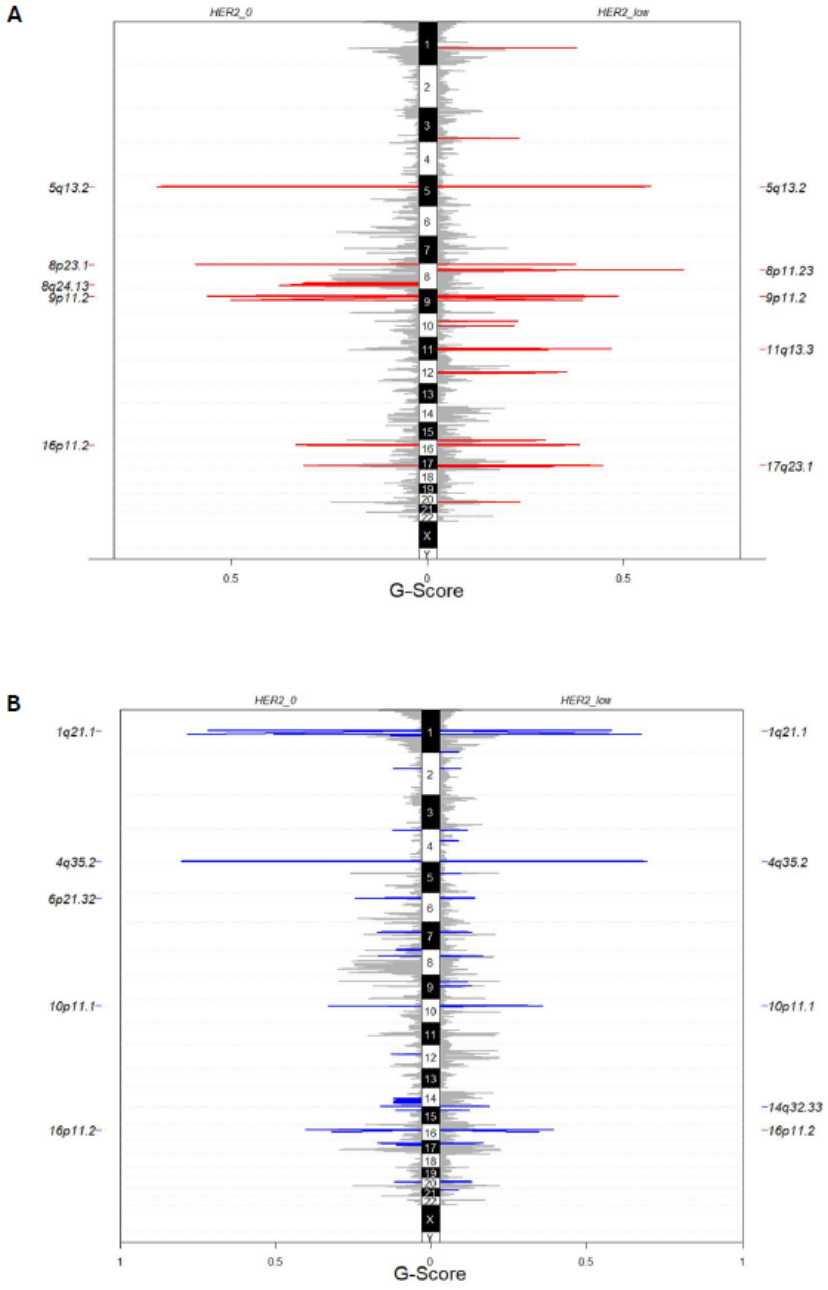

Figure 23. CNA profiles observed in HR+/HER2- ABC, generated with GISTIC 2.0. **(A)** Amplification and **(B)** deletion peaks are shown in parallel for HER2-0 (left) and HER2-low (right) samples. The G-score is a value that considers both the amplitude of the aberration and the frequency of its occurrence across samples. 1L first-line, 2L second-line, CNA copy-number alteration.

Taken together, these exploratory analyses identified recurrent CNAs across treatment lines and HER2 expression subgroups, including both shared alterations and subgroup-specific differences. As the analyses were restricted to a subset of samples with available sWGS data, these findings should primarily be regarded as descriptive patterns and warrant investigation in larger datasets.

3.4. Quantitative tumor burden assessment

Across 225 samples, mFAST-SeqS-based TFx estimates indicated generally low tumor DNA content within the cohort (median z-score 2.49; range −0.5 to 208.3). Applying a predefined threshold of z-score ≥ 3, elevated TFx was detected in 41.3% of samples. A significant positive correlation was observed between z-scores and hVAF derived from targeted sequencing (coefficient = 1.21; 95% CI, 1.05–1.37; p < 0.001; **Figure 24A**).

In the subset of 115 samples for which sWGS was performed, ichorCNA identified TFx ≥ 3% in 67.0% of samples, while 46.1% of samples had a z-score ≥ 3 estimated with mFAST-SeqS. As our group previously reported (114), TFx estimates made using ichorCNA and mFAST-SeqS showed significant correlation (coefficient = 0.78, 95% CI: 0.66-0.90; p < 0.001, **Figure 24B**). Expectedly, discordance was observed in samples with fewer chromosomal alterations.

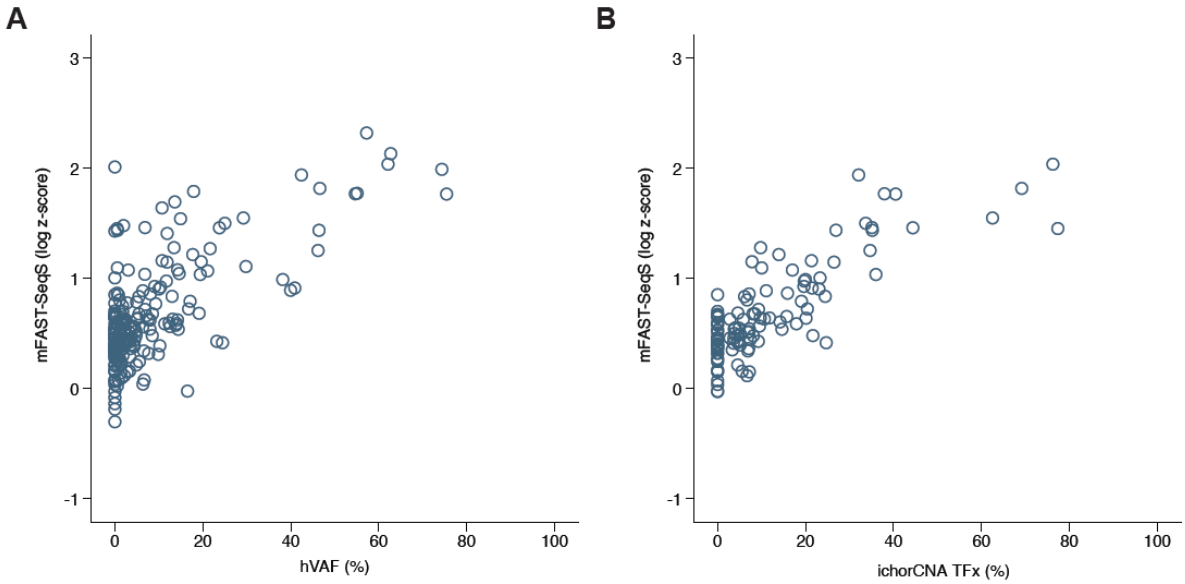

Figure 24. Correlation between mFAST-SeqS-based z-scores and (A) AVENIO-based hVAF, (B) ichorCNA-determined TFx. TFx tumor fraction, hVAF highest variant allele frequency. Reproduced from Dobrić et al. (124), under the terms of the Creative Commons CC BY-NC-ND 4.0 license, https://creativecommons.org/licenses/by-nc-nd/4.0/.

3.4.1. Concordance and complementarity of ctDNA metrics

Due to individual ctDNA metrics capturing different aspects of tumor-derived signal in plasma, we used two distinct metrics to approximate tumor burden: mFAST-SeqS–derived z-scores and the hVAF obtained from the AVENIO assay. Although these approaches demonstrated partially overlapping detection patterns, our findings highlight their complementary analytical performance. Of the 221 samples that could be evaluated by both approaches, elevated ctDNA was detected in 71 cases (32.1%). In contrast, 65 samples (29.4%) were positive exclusively based on hVAF ≥ 1%, whereas 20 samples (9.0%) met the criterion of z-score ≥ 3 only. These results reflect the distinct biological dimensions captured by each metric: mFAST-SeqS quantifies genome-wide copy-number imbalance, while hVAF derived from targeted sequencing reflects the presence of high-frequency somatic mutations.

To leverage these complementary properties, we introduced a composite metric to define elevated ctDNA in a sample: either a z-score ≥ 3 or a hVAF ≥ 1%. This combined approach increased the overall detection rate to 70.6%, including 62.7% of samples obtained prior to 1L treatment and 81.3% prior to 2L treatment. The improvement in detection was most evident in samples with lower tumor burden. Concordance between assays is depicted in **Figure 25A**, and the detection gain achieved by the combined metric is shown in **Figure 25B**.

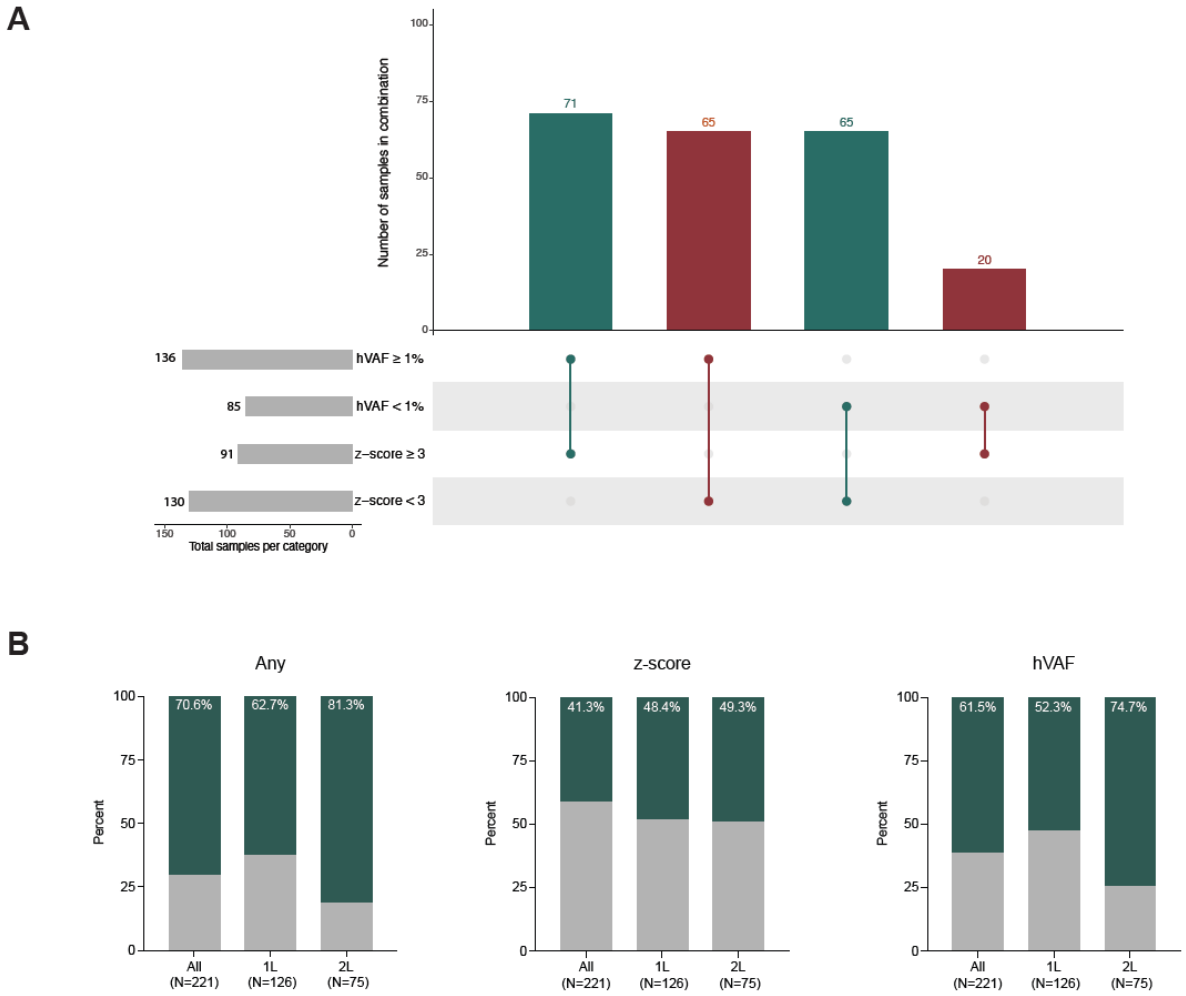

Figure 25. Complementary analytical sensitivity of mFAST-SeqS-derived z-scores and the AVENIO-derived hVAF in 221 samples. (A) Assay concordance shown as the number of samples with elevated ctDNA by one or both metrics. Green bars represent concordant samples and red bars represent discordant samples. **(B)** The increase in the number of samples with elevated ctDNA (green) detected using the combined metric (z-score ≥ 3 or hVAF ≥ 1%) compared to z-scores and hVAF alone, shown in all samples, as well as in 1L and 2L separately. hVAF highest variant allele frequency, 1L first-line, 2L second-line. Reproduced from Dobrić et al. (124), under the terms of the Creative Commons CC BY-NC-ND 4.0 license, https://creativecommons.org/licenses/by-nc-nd/4.0/.

3.4.2. Tumor burden characteristics at baseline and progression

To explore the potential differences in ctDNA-derived tumor burden between baseline and progression, we compared z-scores and hVAF between 1L and 2L samples. Consistent with expected increased tumor-derived DNA signal in plasma at later treatment stages, both metrics were numerically higher in 2L compared to 1L samples. This difference reached statistical significance for hVAF (adjusted mean difference = 4.74; 95% CI, 1.28–8.20; p = 0.007), but not for z-scores (adjusted mean difference = 6.33; 95% CI, −0.2 to 12.9; p = 0.058). After adjustment for elevated TFx based on mFAST-SeqS (z-score ≥ 3), the association between treatment line and hVAF remained significant (adjusted mean difference = 3.49; 95% CI, 0.49–6.49; p = 0.023). When TFx estimated using ichorCNA was compared between 70 1L samples and 29 2L samples with available sWGS data, no significant difference was observed (adjusted mean difference = -0.003, 95%CI: -0.06-0.07; p = 0.925).

Taken together, these findings suggest that mutation-based ctDNA metrics may capture changes in tumor-derived signal between treatment lines that are not fully reflected by copy-number–based TFx estimates. The observation that hVAF increased in later treatment lines while copy-number–derived TFx estimates remained similar may reflect therapy-driven clonal selection, where dominant resistant clones expand without necessarily increasing the overall tumor DNA fraction in plasma.

3.4.3. Tumor burden characteristics in HER2-low versus HER2-0 disease

We next evaluated whether ctDNA-derived tumor burden metrics differed between HER2-low and HER2-0 tumors. Because multiple samples were available for a proportion of patients in both HER2 expression groups, comparisons were performed using the earliest available sample per patient to preserve independence of observations. To assess the robustness of these findings, mixed-effects models including all available samples and accounting for repeated measures were additionally applied.

The z-scores in the HER2-low group ranged from –0.35 to 208.3, compared to –0.5 to 108 in the HER2-0 group. When comparing TFx using the earliest available sample from each patient, significantly higher values were observed in HER2-low compared to HER2-0 patients (median 2.88 vs. 1.85, respectively; p = 0.007). However, in the mixed-effects model including all

available samples, the difference between groups was attenuated and no longer statistically significant (p = 0.365).

We next compared the hVAF, as well as the number of detected variants (overall, clonal, and subclonal), between HER2-low and HER2-0 patients using the earliest available sample per patient. The median hVAF was 5.51% (range 0.57%–74.35%) in the HER2-low group and was significantly higher than the median of 3.39% (range 0.5%–46.61%) in the HER2-0 group (p = 0.043). Regarding mutation burden, HER2-low patients had a median of 2 detected somatic variants in total (range 1–28), compared with a median of 3 (range 1–15) in HER2-0 patients. Both groups had a median of 2 clonal variants (ranges 1–10 and 1–14, respectively) and 0 subclonal variants (ranges 0–23 and 0–5, respectively). The corresponding p-values for differences in total, clonal, and subclonal variant counts were 0.726, 0.307, and 0.539.

When these parameters were re-evaluated using mixed-effects models that incorporated all available samples and accounted for repeated measures, no statistically significant differences were observed between HER2-low and HER2-0 patients for either VAF metrics or somatic variant burden.

The attenuation of TFx associations in the mixed-effects analysis may reflect the biological and technical variability inherent to plasma cfDNA measurements across longitudinal samples. Metrics based on specific tumor-derived variants, such as hVAF, may provide a more stable representation of tumor-derived signal in plasma.

3.5. Prognostic implications of ctDNA-derived metrics

To evaluate the clinical relevance of ctDNA-derived tumor metrics, we examined their association with survival. PFS and OS were assessed in 127 patients initiating 1L and 76 patients initiating 2L therapy. The median follow-up duration was 35.8 months (25th–75th percentile: 17.1–54.4) for the 1L cohort and 25.5 months (25th–75th percentile: 22.1–52.2) for the 2L cohort. Throughout the follow-up period, 64 PFS events and 47 OS events were recorded among 1L patients, whereas 65 PFS events and 52 OS events occurred in the 2L group. Median PFS was 29.2 months (95% CI, 19.1–37.2) in the 1L cohort compared with 6.0 months (95% CI, 5.1–7.3) in the 2L cohort, with corresponding median OS of 57.3 months (95% CI, 35.3–not reached) and 16.1 months (95% CI, 12.6–19.8) (**Figure 26**).

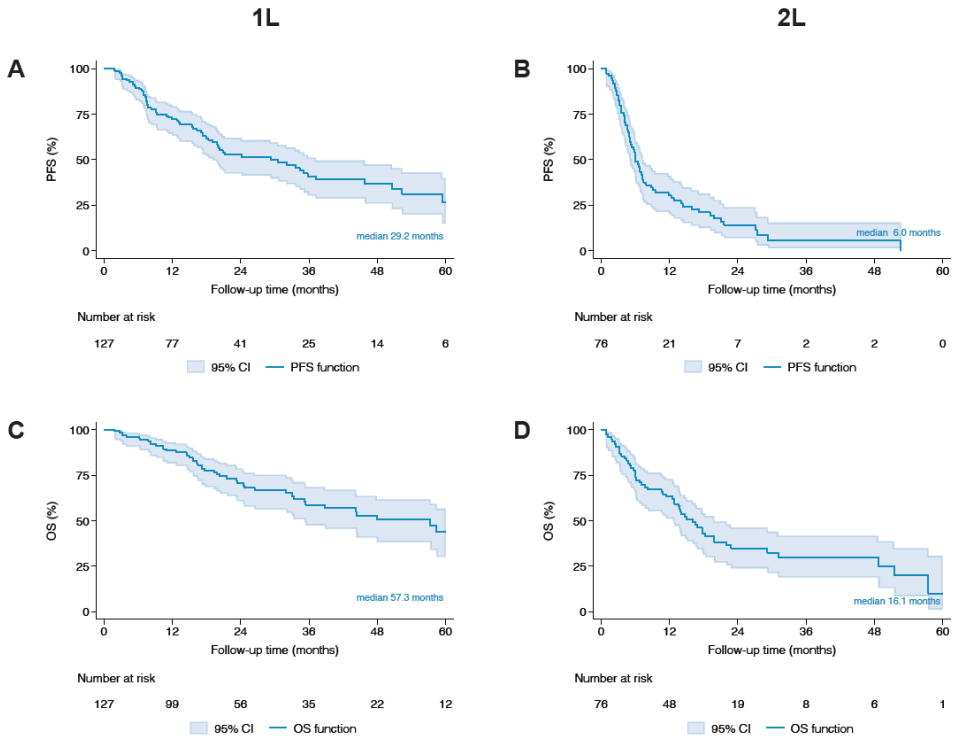

Figure 26. Kaplan-Meier curves representing (A-B) PFS (C-D) OS of patients before 1L and 2L treatment. PFS progression-free survival, OS overall survival, 1L first-line, 2L second-line. Reproduced from Dobrić et al. (124), under the terms of the Creative Commons CC BY-NC-ND 4.0 license, https://creativecommons.org/licenses/by-nc-nd/4.0/.

We evaluated a range of ctDNA-based metrics, encompassing mFAST-SeqS–derived z-scores (z-score ≥ 3), AVENIO-based hVAF (hVAF ≥ 1%), and composite measures. We included two binary composite metrics: ctDNA positivity (detection ≥ 1 somatic variant or z-score ≥ 3) and elevated ctDNA levels (≥ 3 or hVAF ≥ 1%), as well as a three-level composite variable, that stratified patients into low (z-score < 3 and hVAF < 1%), intermediate (either z-score ≥ 3 or hVAF ≥ 1%), and high (both z-score ≥ 3 and hVAF ≥ 1%) plasma tumor burden groups. In addition, we evaluated the three most frequently mutated genes (*PIK3CA*, *TP53* and *ESR1*) and the number of detected somatic variants.

Among patients initiating 1L therapy, univariable Cox regression analyses showed that nearly all ctDNA-derived metrics were significantly associated with both PFS (**Figure 27A**) and OS (**Figure 28A**). The only exception was *PIK3CA* mutations, which were not significantly associated with PFS. Of the evaluated measures, the three-level composite ctDNA variable demonstrated the strongest prognostic performance for both outcomes, as indicated by the highest Uno's C-index. Kaplan–Meier analyses further illustrated a progressive decline in PFS and OS with increasing ctDNA burden (**Figure 27B-G**, **Figure 28B-G**).

Variable	N	HR (95% CI)	P-value	Uno's C (95% CI)
z-score ≥ 3	48/127	2.48 (1.51-4.08)	<0.001	0.610 (0.544-0.676)
hVAF ≥ 1%	65/125	2.57 (1.53-4.34)	<0.001	0.617 (0.550-0.683)
ctDNA+	90/125	2.34 (1.22-4.49)	0.011	0.579 (0.511-0.648)
z-score ≥ 3 or hVAF ≥ 1%	78/125	3.15 (1.73-5.73)	<0.001	0.632 (0.565-0.699)
ctDNA intermediate (Ref.low)	45/125	2.41 (1.24-4.66)	0.009	0.663 (0.599-0.728)
ctDNA high (Ref.low)	33/125	4.66 (2.38-9.12)	<0.001	
No. of somatic variants	125/125	1.14 (1.06-1.22)	<0.001	0.630 (0.544-0.716)
PIK3CA mutant	41/125	1.25 (0.74-2.09)	0.407	0.524 (0.437-0.612)
TP53 mutant	21/125	2.51 (1.39-4.51)	0.002	0.560 (0.507-0.614)
ESR1 mutant	12/125	2.61 (1.32-5.17)	0.006	0.545 (0.507-0.584)

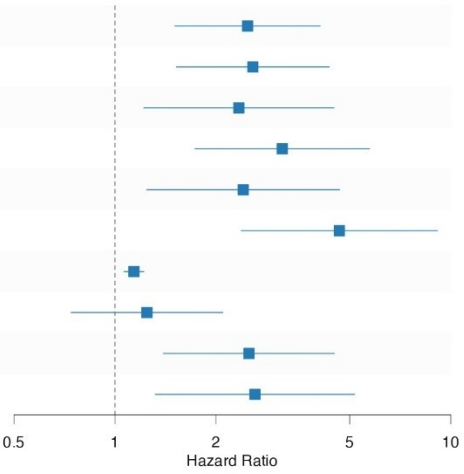

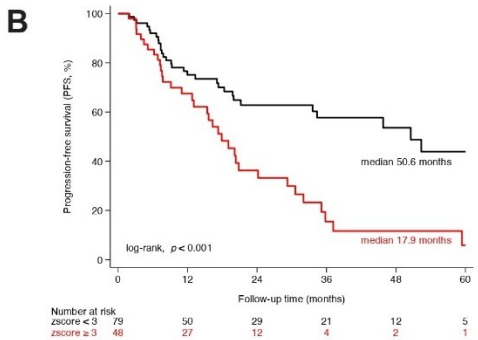

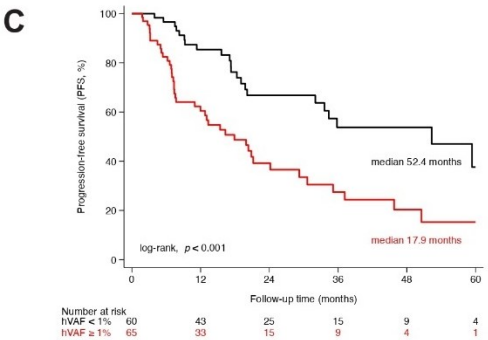

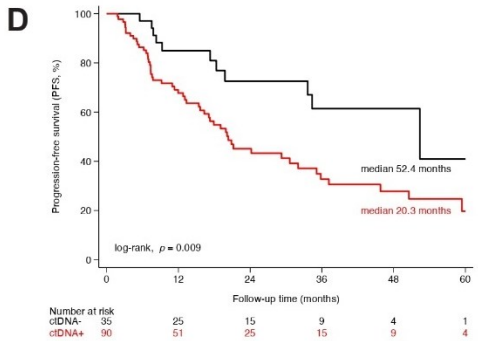

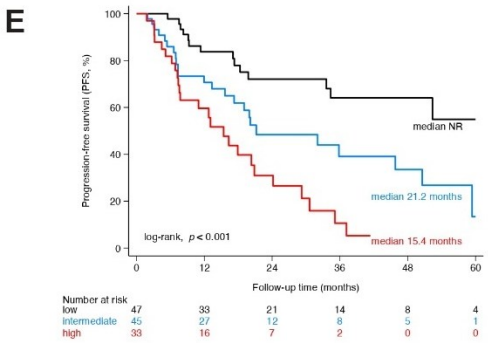

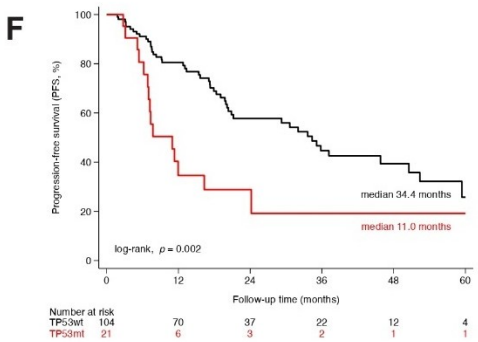

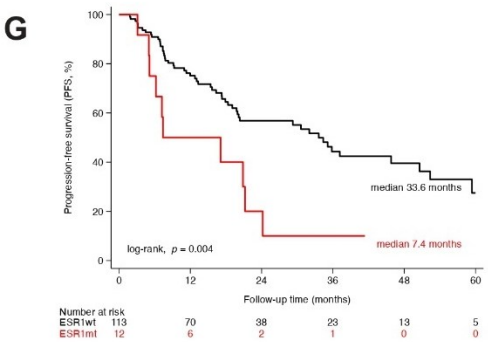

Figure 27. Association of ctDNA-based metrics with PFS of 1L patients. (A) Forest plot representing the performance of individual and composite ctDNA TFx metrics, the total somatic variant count and the most frequently mutated genes, based on univariable Cox regression, in relation to PFS. The prognostic discrimination was measured by Uno's C-index. **(B-C)** Kaplan-Meier curves distinguishing patients with high (red) and low (black) TFx estimated by mFAST-SeqS z-scores and AVENIO-based hVAF individually. **(D)** Kaplan-Meier curves distinguishing ctDNA+ (≥ 1 detected somatic variant or z-score ≥ 3, red) and ctDNA- (< 1 detected somatic variant and z-score < 1%, black) patients. **(E)** Kaplan-Meier curves illustrating the difference in PFS using a three-level composite variable stratifying patients into high (z-score ≥ 3 and hVAF ≥ 1%, red), intermediate (z-score ≥ 3 or hVAF ≥ 1%, blue) and low (z-score < 3 and hVAF < 1%, black) ctDNA burden. This variable achieved the highest prognostic discrimination. **(F-G)** Kaplan-Meier curves distinguishing patients with (mt, red) and without (wt, black) mutations in *TP53* and *ESR1*. PFS progression-free survival, 1L first-line, TFx tumor fraction, HR hazard ratio, CI confidence interval, Uno's C Uno's concordance index, hVAF highest variant allele frequency, mt mutated, wt wild-type. Reproduced from Dobrić et al. (124), under the terms of the Creative Commons CC BY-NC-ND 4.0 license, https://creativecommons.org/licenses/by-nc-nd/4.0/.

Variable	N	HR (95% CI)	P-value	Uno's C (95% CI)
z-score ≥ 3	48/127	2.42 (1.34-4.37)	0.003	0.607 (0.527-0.686)
hVAF ≥ 1%	65/125	4.09 (2.01-8.31)	<0.001	0.659 (0.584-0.734)
ctDNA+	90/125	2.71 (1.14-6.41)	0.023	0.575 (0.486-0.665)
z-score ≥ 3 or hVAF ≥ 1%	78/125	4.02 (1.79-9.04)	<0.001	0.638 (0.557-0.719)
ctDNA intermediate (Ref.low)	45/125	2.78 (1.14-6.76)	0.024	0.684 (0.605-0.763)
ctDNA high (Ref.low)	33/125	6.23 (2.63-14.76)	<0.001	
No. of somatic variants	125/125	1.12 (1.04-1.21)	0.003	0.642 (0.559-0.726)
PIK3CA mutant	41/125	2.01 (1.11-3.62)	0.021	0.575 (0.482-0.668)
TP53 mutant	21/125	2.25 (1.16-4.39)	0.017	0.559 (0.495-0.624)
ESR1 mutant	12/125	3.08 (1.41-6.73)	0.005	0.552 (0.506-0.598)

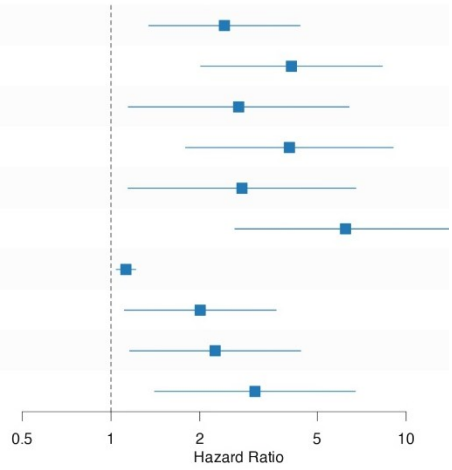

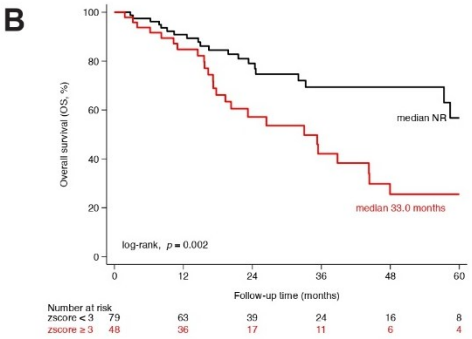

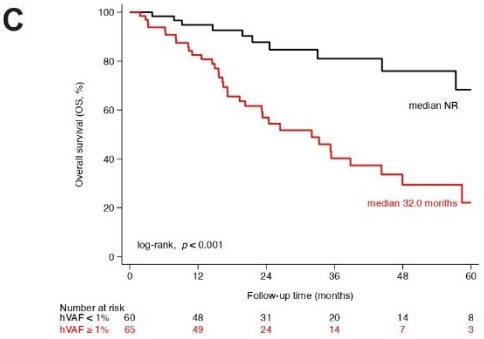

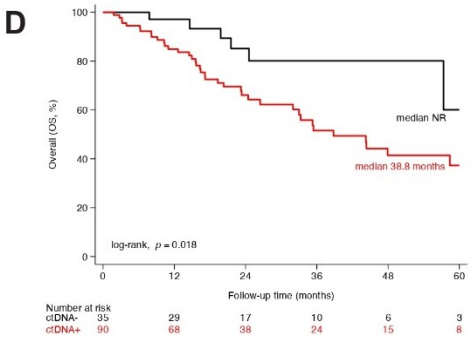

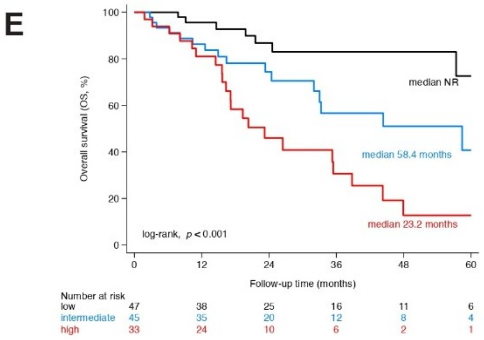

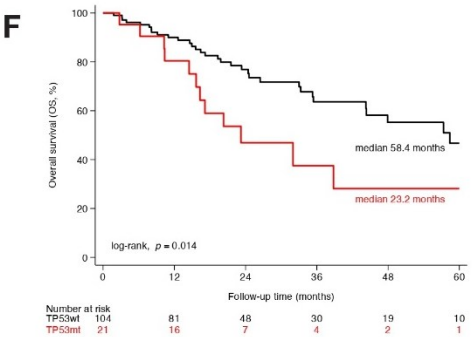

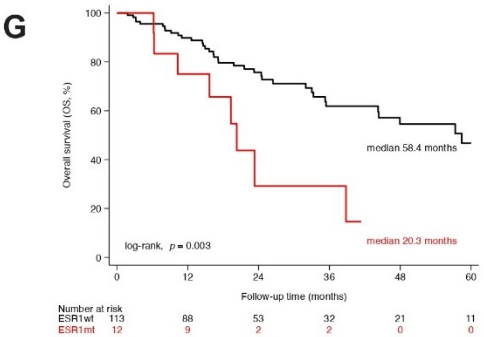

Figure 28. Association of ctDNA-based measures with OS of 1L patients. (A) Forest plot representing the performance of individual and composite ctDNA TFx metrics, the total somatic variant count and the most frequently mutated genes, based on univariable Cox regression, in relation to OS. The prognostic discrimination was measured by Uno's C-index. **(B-C)** Kaplan-Meier curves distinguishing patients with high (red) and low (black) TFx estimated by mFAST-SeqS z-scores and AVENIO-based hVAF individually. **(D)** Kaplan-Meier curves distinguishing ctDNA+ (≥ 1 detected somatic variant or z-score ≥ 3, red) and ctDNA- (< 1 detected somatic variant and z-score < 1%, black) patients. **(E)** Kaplan-Meier curves illustrating the difference in PFS using a three-level composite variable stratifying patients into high (z-score ≥ 3 and hVAF ≥ 1%, red), intermediate (z-score ≥ 3 or hVAF ≥ 1%, blue) and low (z-score < 3 and hVAF < 1%, black) ctDNA burden. This variable achieved the highest prognostic discrimination. **(F-G)** Kaplan-Meier curves distinguishing patients with (mt, red) and without (wt, black) mutations in *TP53* and *ESR1*. OS overall survival, 1L first-line, TFx tumor fraction, HR hazard ratio, CI confidence interval, Uno's C Uno's concordance index, hVAF highest variant allele frequency, mt mutated, wt wild-type. Reproduced from Dobrić et al. (124), under the terms of the Creative Commons CC BY-NC-ND 4.0 license, https://creativecommons.org/licenses/by-nc-nd/4.0/.

Comparable patterns were observed in 2L patients, where a significant association between ctDNA-based metrics and both PFS and OS persisted, with the three-level combined ctDNA variable showing the highest prognostic discriminatory power for both endpoints (**Figure 29**).

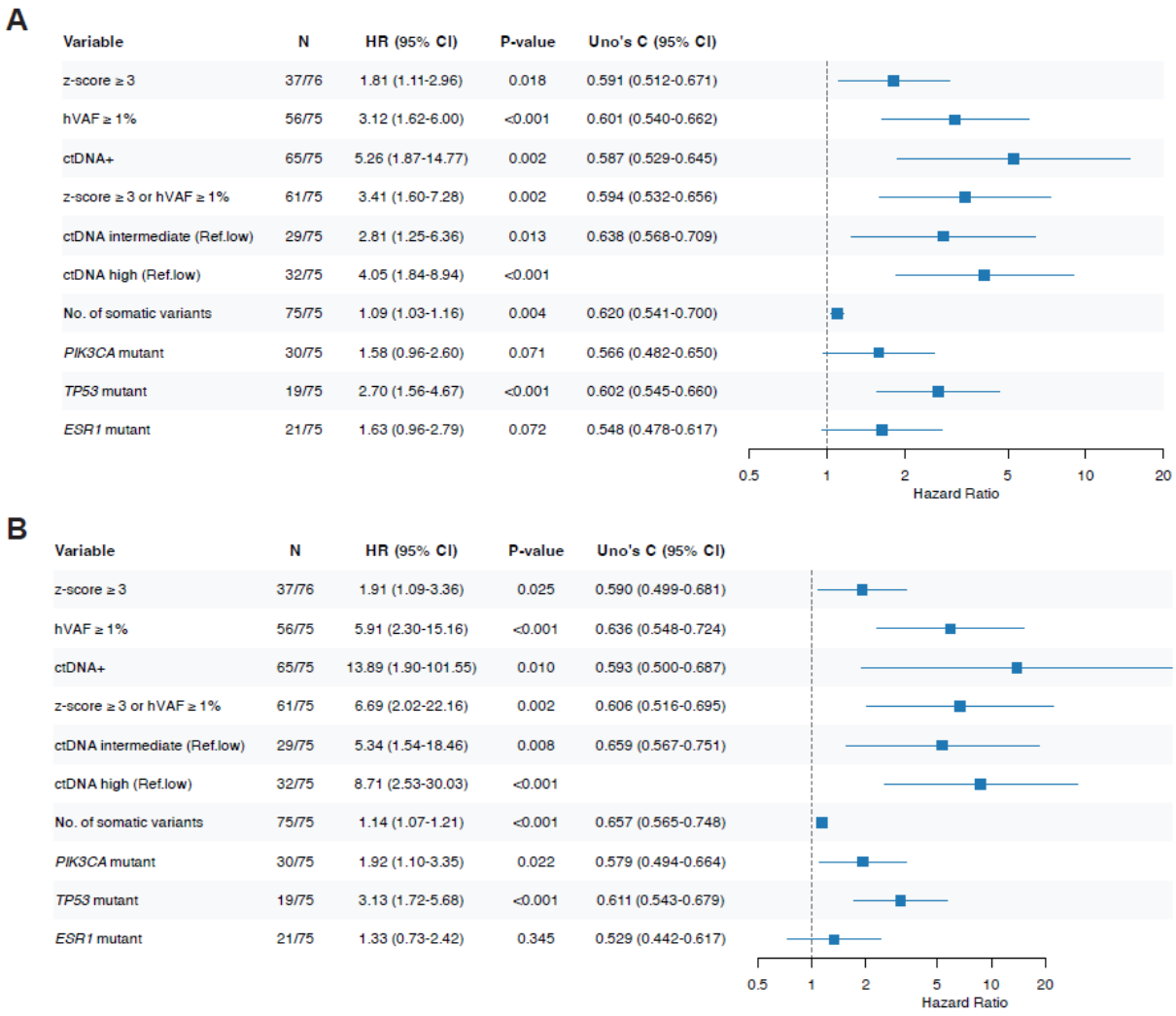

Figure 29. Forest plots representing the performance of individual and composite ctDNA TFx metrics, the total somatic variant count and the most frequently mutated genes in 2L patients, based on univariable Cox regression, in relation to (A) PFS (B) OS. The three-level composite ctDNA variable achieved the highest prognostic discrimination across both endpoints as measured by Uno's C-index. PFS progression-free survival, OS overall survival, 2L second-line, TFx tumor fraction, HR hazard ratio, CI confidence interval, Uno's C Uno's concordance index. Reproduced from Dobrić et al. (124), under the terms of the Creative Commons CC BY-NC-ND 4.0 license, https://creativecommons.org/licenses/by-nc-nd/4.0/.

To further assess these associations in a multivariable context, we developed a clinical model for patients initiating 1L therapy. The model included age, PR status, CDK4/6 inhibitor treatment, liver metastases, number of metastatic organs, and time to metastasis (categorized as de novo, ≤ 24 months, or > 24 months). Within this model, PR positivity (HR 0.47, 95% CI 0.27–0.82, p = 0.007) and treatment with a CDK4/6 inhibitor (HR 0.22, 95% CI 0.09–0.54, p < 0.001) were independently associated with longer PFS, whereas the presence of liver metastases (HR 2.03, 95% CI 1.04–3.98, p = 0.039) and a time to metastasis of ≤ 24 months (HR 14.02, 95% CI 4.47-44.00, p < 0.001) were linked to poorer PFS outcomes (**Figure 30A**). Similar relationships were observed in the corresponding multivariable model for OS (**Figure 31A**).

Incorporation of the three-level composite ctDNA metric to the clinical model resulted in an improvement in prognostic performance, with Uno's C-index for PFS increasing from 0.701 (95% CI: 0.631–0.772) to 0.758 (95% CI: 0.698–0.818) and a corresponding decrease in AIC (**Figure 30B**). After adjustment for clinical covariates, both intermediate (HR 2.11, 95% CI 1.06–4.22, p = 0.034) and high (HR 4.43, 95% CI 2.17–9.03, p < 0.001) ctDNA burden remained independently associated with poorer PFS. Comparable improvements in model discrimination were observed for OS when the ctDNA metric was added to the clinical model (**Figure 31B**).

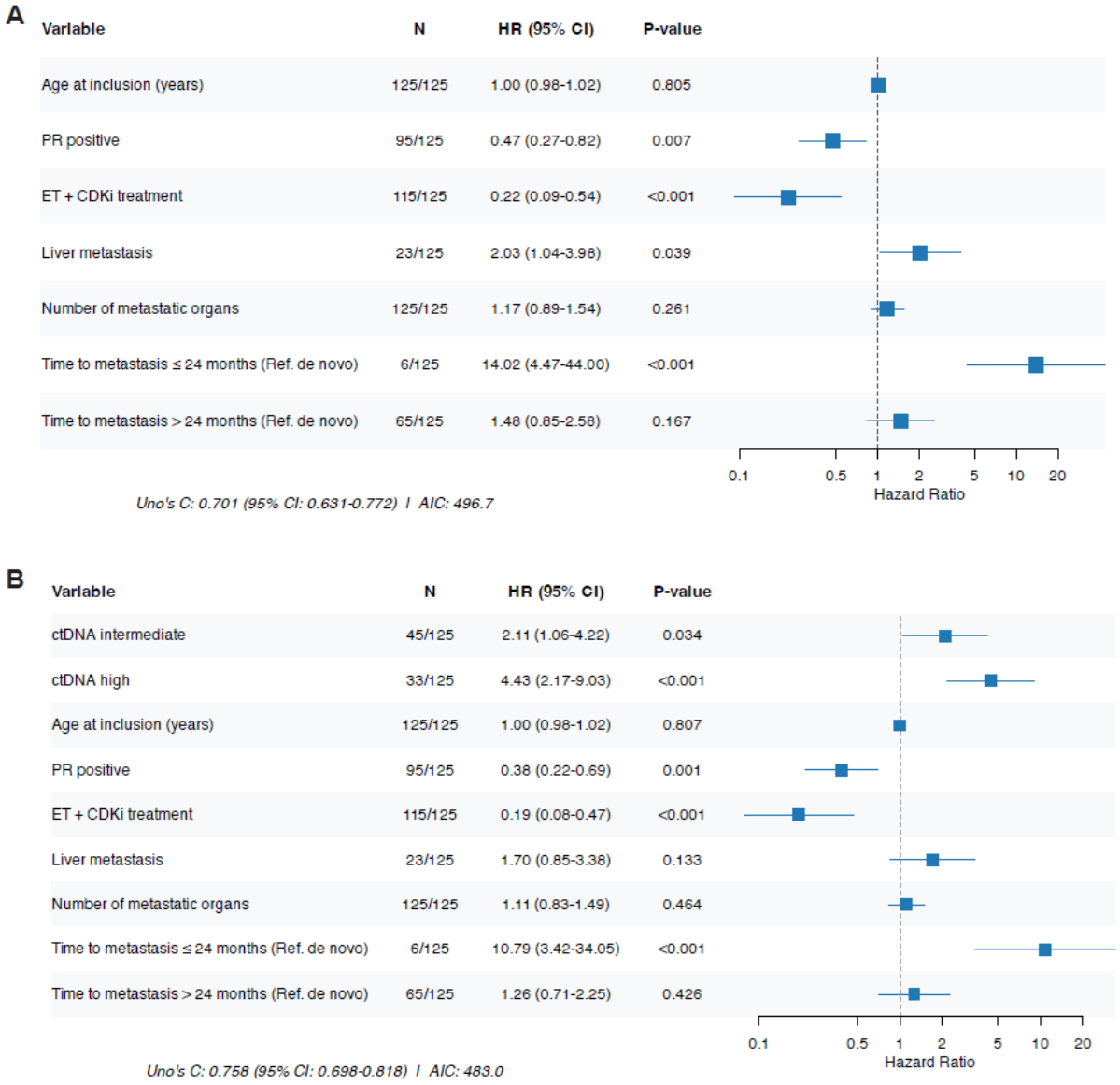

Figure 30. Multivariable PFS models of 1L patients. (A) Forest plot representing the clinical model including known clinically relevant variables. **(B)** Forest plot representing the clinical model incorporating the three-level composite ctDNA metric. Increased Uno's C-index and reduced AIC indicate a significantly improved prognostic performance of the extended model. PFS progression-free survival, 1L first-line, PR progesterone receptor, ET endocrine treatment, CDKi CDK 4/6 inhibitor, HR hazard ratio, CI confidence interval, Uno's C Uno's concordance index, AIC Akaike Information Criterion. Reproduced from Dobrić et al. (124), under the terms of the Creative Commons CC BY-NC-ND 4.0 license, https://creativecommons.org/licenses/by-nc-nd/4.0/.

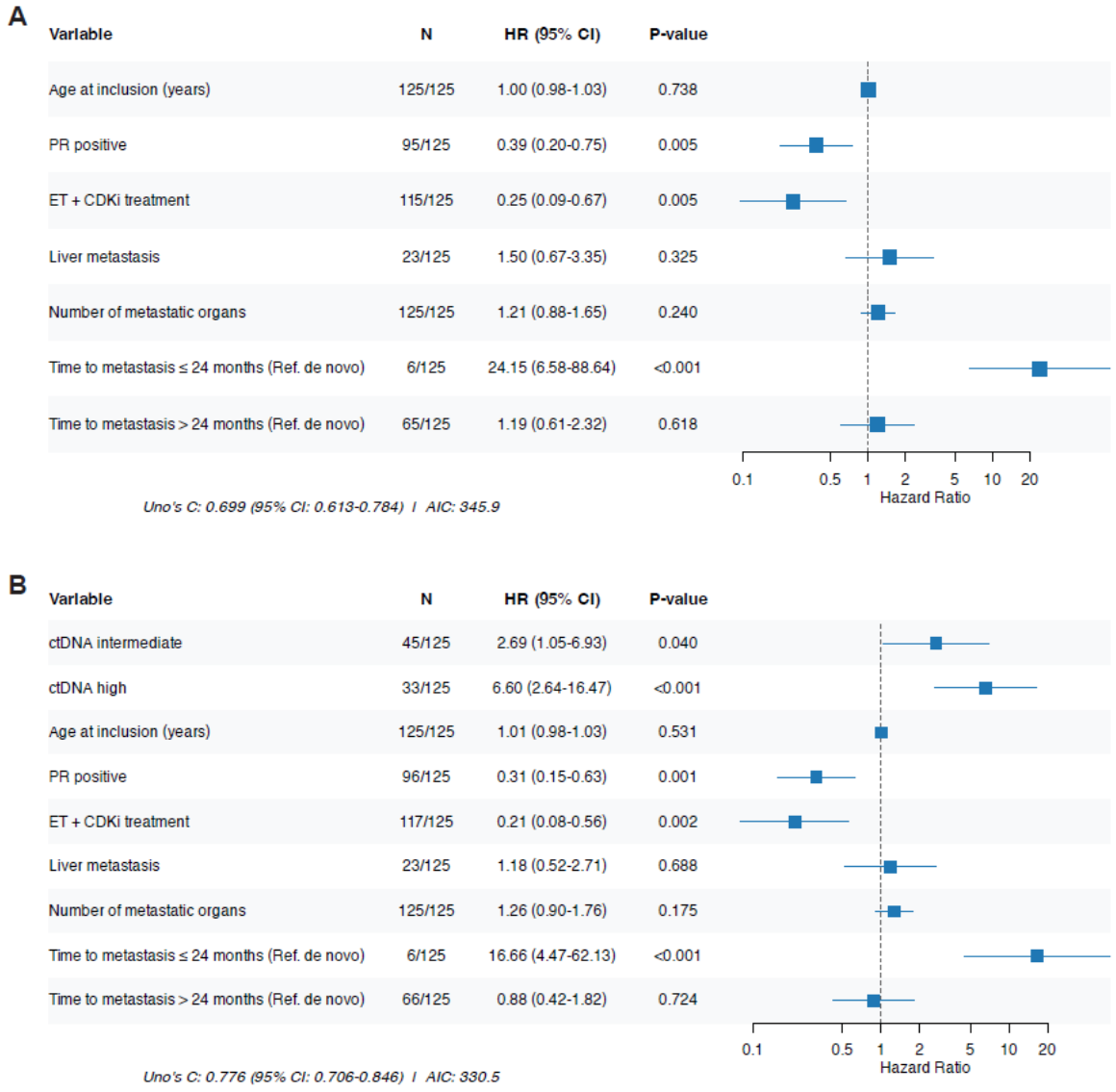

Figure 31. Multivariable OS models of 1L patients. (A) Forest plot representing the clinical model including known clinically relevant variables. **(B)** Forest plot representing the clinical model expanded by the three-level composite ctDNA metric. Increased Uno's C-index and reduced AIC indicate a significantly improved prognostic performance of the extended model. OS overall survival, 1L first-line, PR progesterone receptor, ET endocrine treatment, CDKi CDK 4/6 inhibitor, HR hazard ratio, CI confidence interval, Uno's C Uno's concordance index, AIC Akaike Information Criterion. Reproduced from Dobrić et al. (124), under the terms of the Creative Commons CC BY-NC-ND 4.0 license, https://creativecommons.org/licenses/by-nc-nd/4.0/.

3.6. Real-world *ESR1* mutation testing project

Between September 2023 and March 2025, a prospective study was conducted in Graz, Austria, following the approval of elacestrant for the treatment of *ESR1*-mutated patients. Given that *ESR1* mutations emerge over time, ctDNA-based methods were used to enable their timely detection. This setting provided an opportunity to characterize the mutational landscape and tumor burden features of an additional real-world patient cohort. As clinical data collection is ongoing, the present analysis is limited to descriptive evaluation of mutational and TFx characteristics.

3.6.1. Patient characteristics

A total of 150 samples from 135 patients referred by clinicians from 19 institutions were collected and analyzed. The patient population was heterogeneous with respect to clinical characteristics and treatment history. Patients had received up to 9 lines for metastatic disease, with a median of 2 treatment lines. Patient characteristics are summarized in **Table 5**.

Table 5. Patient and tumor characteristics of the study cohort at the time of referral.

Variable	N=135 (%)
Gender	
Female	133 (98.5)
Male	2 (1.5)
ER status	
Positive	134 (99.3)
Negative	1 (0.7)
PR status	
Positive	101 (74.8)
Negative	29 (21.5)
Unknown	5 (3.7)
HER2 status	
Low	71 (52.6)
Negative	64 (47.4)
Histology	
NST	113 (84.3)
ILC	16 (11.9)
Mixed	1 (0.7)
Unknown	4 (3)

3.6.2. Mutational spectrum and co-alterations

At initial testing, clinically relevant mutations in *ESR1* with a VAF ≥ 0.1% were detected in 50/135 patients (37%). More than one *ESR1* variant was found in 15 patients, while 20/50 *ESR1*-positive patients had only mutations below the LOD of 0.5%. Co-occurring *ESR1* and *PIK3CA* alterations were observed in 22 patients (16%), while in 2 patients we found *PTEN* alterations as well (**Figure 32**).

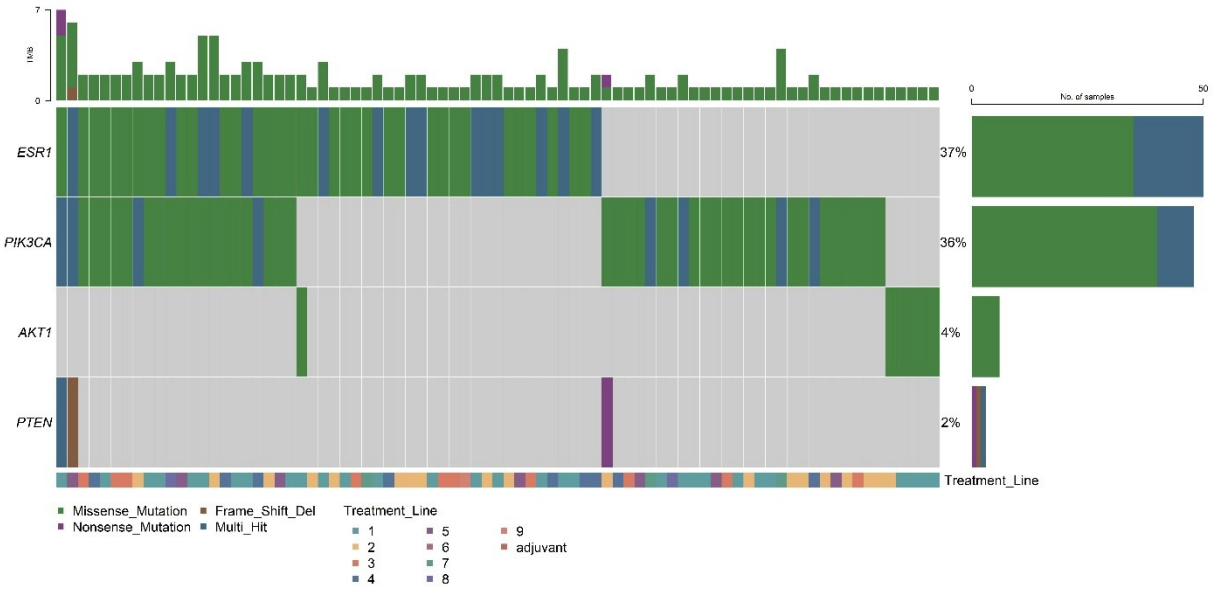

Figure 32. Oncoprint depicting somatic pathogenic alterations detected in *ESR1*, *PIK3CA*, *AKT1* and *PTEN* in 135 patients at the time of first blood draw. The upper bars illustrate the number of alterations per patient, while the right-side bars show the frequency of alterations for each gene. Colors represent the mutation type: missense (green), nonsense (purple), frameshift deletion (brown), and multi-hit (blue). The bar below the oncoprints illustrates the treatment line of each sample.

The median VAF of *ESR1* mutations was 0.4% (range 0.1-50.5%), of *PIK3CA* mutations 1.3% (range 0.1-75.4%), of *AKT1* 0.4% (range 0.1-45.1%), and of *PTEN* 0.3% (range 0.2-33.5%) (**Figure 33A**).

The most frequently detected *ESR1* mutations were D538G (35%) and Y537S (27%). They were followed by E380Q and Y537N (10% each), while other clinically relevant alterations were present in lower frequencies (**Figure 33B**).

3.6.3. *ESR1* detection in the context of tumor fraction

The average TFx at the first testing timepoint was 9.2% (range 0-82%). The observed prevalence of *ESR1*-positivity exhibited a direct, TFx-related increase, with detection rates rising from 22% in the minimal burden samples (TFx < 3%) to 55% in the high burden cohort (TFx > 10%) (**Figure 33C**). In samples with low tumor burden, most *ESR1* VAFs clustered near or below the LOD of 0.5% but were above 0.1% (**Figure 33D**). Reliable detection increased with higher TFx.

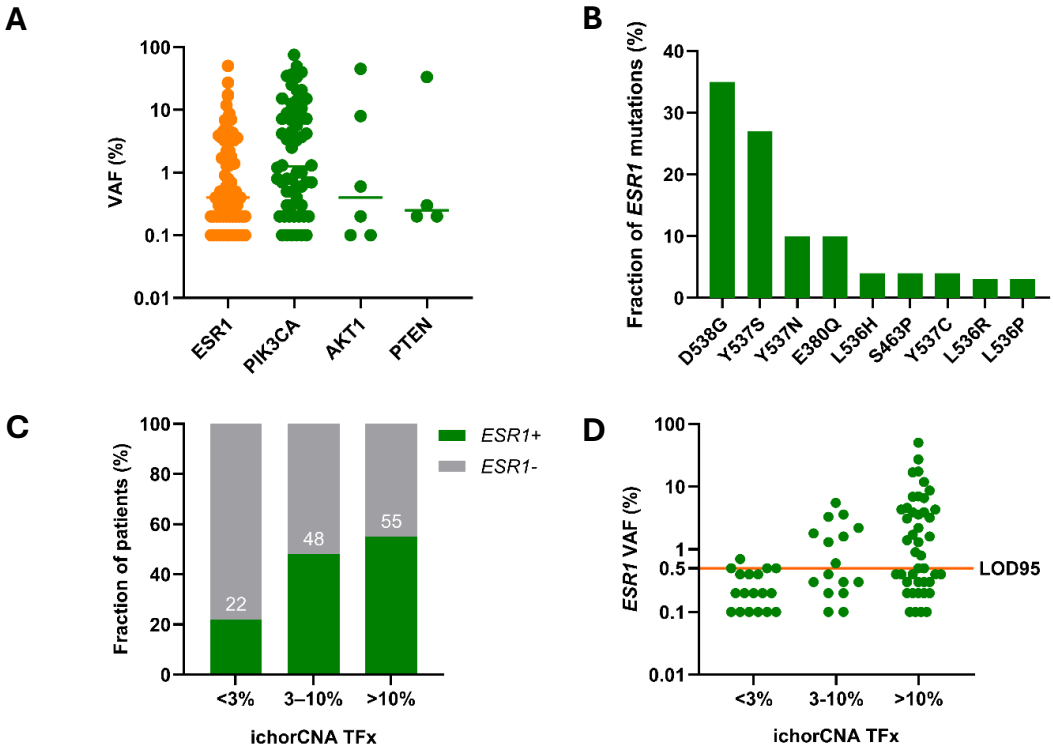

Figure 33. Mutational and tumor burden characteristics of the cohort. (A) VAF distribution in *ESR1*, *PIK3CA*, *AKT1*, and *PTEN*. **(B)** Most frequent *ESR1* mutation types. **(C)** Increasing prevalence of *ESR1* mutations with higher TFx. **(D)** Distribution of *ESR1* VAFs relative to ichorCNA-estimated TFx. VAF variant allele frequency, TFx tumor fraction, LOD limit of detection.

3.6.4. Emergence of *ESR1* mutations upon disease progression

Twelve patients who were *ESR1*-negative at initial testing or had a detected *ESR1* mutation below the LOD of 0.5% VAF were retested at subsequent disease progression. Retesting revealed four cases that developed an ESR1 mutation above the LOD (**Figure 34**).

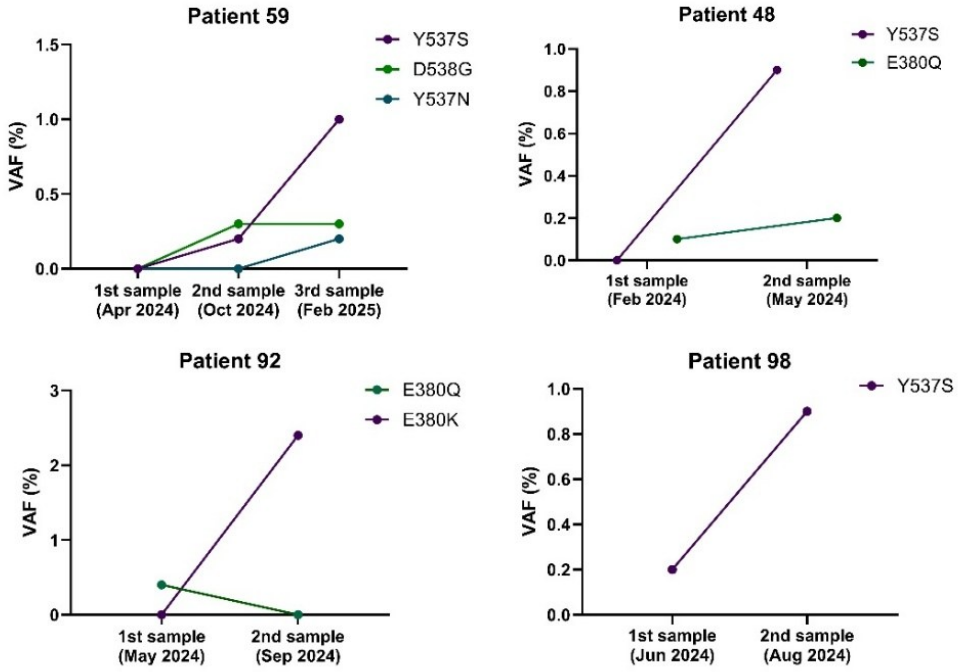

Figure 34. Evolution of VAF in 4 patients with acquired *ESR1* mutations after an initial negative result. VAF variant allele frequency.

4. DISCUSSION

The management of HR+/HER2− ABC has substantially evolved over the past decades, driven by advances in molecular biology, targeted therapies, and diagnostic technologies. Despite these developments, considerable heterogeneity persists, and survival outcomes vary markedly even among patients with comparable clinical characteristics at diagnosis. This variability highlights the need for more precise prognostic indicators capable of capturing the molecular complexity of ABC and improving individualized risk stratification.

Recently, an increasing number of studies have evaluated ctDNA as a biomarker in the early treatment phases of ABC, reflecting the ongoing efforts to refine therapeutic decision-making in this setting, and address the growing need for minimally invasive, liquid biopsy-based testing in this setting (102-104, 125). With the primary study reported in this thesis, we contribute to the field through a comprehensive analysis of baseline and early progression plasma samples from a clinically well-characterized, real-world, multicenter cohort of patients with HR+/HER2− ABC in Austria.

Accordingly, this study addressed two central questions: whether the real-world genomic landscape observed in this cohort aligns with established data in HR+/HER2− disease, and whether the integration of ctDNA-derived metrics enhances prognostic stratification beyond conventional clinical parameters. In addition, given the emerging therapeutic relevance of HER2-low disease, we explored potential differences in ctDNA characteristics between HER2-low and HER2-0 tumors within this cohort.

In a complementary, clinically driven analysis, a separate real-world cohort was evaluated to assess the feasibility of plasma-based *ESR1* mutation testing and to characterize the associated mutational and tumor burden features following the approval of elacestrant for the treatment of patients with HR+/HER2− ABC. This second cohort reflects a more advanced and heterogeneous clinical setting and provides additional insight into the molecular evolution of disease under treatment.

The following sections contextualize these findings within the existing literature and discuss their methodological and clinical implications.

4.1. Genomic landscape in early treatment lines

The genomic landscape observed in this cohort largely aligns with previously reported mutational profiles of HR+/HER2− ABC, with *PIK3CA*, *TP53*, and *ESR1* representing the most frequently altered genes (103, 126-128). This concordance supports the external validity of our cohort and reinforces the reliability of tumor-agnostic plasma-based profiling for capturing clinically relevant genomic alterations in early treatment lines.

The higher somatic variant burden observed in 2L samples may reflect the coexistence and expansion of multiple subclones under therapeutic pressure, consistent with models of branching clonal evolution in MBC (129, 130). In particular, the enrichment of alterations associated with ET resistance further supports the concept of adaptive tumor evolution in HR+/HER2− disease (31, 131). Although these observations are primarily based on cross-sectional comparisons, they suggest that ctDNA profiling can capture aspects of the evolving genomic landscape during early treatment lines, a pattern that was also reflected in the subset of patients with paired 1L and 2L samples.

4.1.1. *ESR1* mutations and endocrine resistance

Acquired mutations in *ESR1* are a well-described mechanism of resistance to ET, particularly in tumors previously exposed to AIs. Accordingly, their prevalence prior to the initiation of 1L treatment in our cohort was relatively low (7.1%) (126). Despite this low frequency, patients with *ESR1* mutations at baseline experienced significantly shorter PFS, indicating that these alterations may identify a subset of tumors with intrinsic resistance to endocrine-based therapies.

Importantly, treatment selection in this study was not guided by *ESR1* mutation status, as at the time of the first study oral SERDs were not yet approved in Austria, and the use of fulvestrant was determined by clinical considerations rather than ctDNA results. Therefore, the observed prognostic association likely reflects underlying tumor biology rather than a bias introduced by treatment selection. From a clinical perspective, these findings highlight the importance of therapeutic strategies capable of overcoming or delaying resistance in HR+/HER2− ABC. In particular, the development of novel endocrine agents with activity in *ESR1*-mutant disease, as well as upfront combination approaches, are important areas of ongoing research (46, 132).

ESR1 mutations were substantially more frequent in samples obtained prior to 2L therapy. This increase is in accordance with therapy-driven clonal selection under prior ET, particularly AI-based regimens combined with CDK4/6 inhibitors, which represented the most frequent 1L treatment in the cohort. Our findings are consistent with previously described patterns of genomic evolution in HR+/HER2− ABC (125, 133).

4.1.2. Impact of the detection threshold on the genomic landscape

To emphasize analytical specificity over maximal sensitivity, we applied a variant detection threshold of 0.5% VAF. In tumor-agnostic assays performed without matched white blood cell controls, low-VAF variants require cautious interpretation, as mutations arising from clonal hematopoiesis—the expansion of somatically mutated hematopoietic stem cell clones—cannot be reliably distinguished from true tumor-derived alterations (134). Given the increasing prevalence of hematopoietic mutations with age and prior treatment exposure, adopting a conservative threshold reduces the likelihood of falsely attributing these background variants to the tumor and enhances confidence in variant classification (135, 136).

To explore the impact of threshold selection, we additionally performed secondary analyses using a lower LOD of 0.1% VAF. As expected, this approach increased overall detection rates but also introduced greater uncertainty regarding the tumor specificity of low-frequency variants. For example, additional P/LP variants detected within the low-VAF range (0.1–0.5%) included alterations in *TP53*, a common driver gene in BC, but also a gene frequently affected by clonal hematopoiesis (134, 136). At reduced VAF thresholds, misclassification of hematopoietic variants is therefore more likely, potentially inflating the number of presumed tumor-derived alterations per patient. This may lead to an increased proportion of ctDNA-positive samples and artificially elevated VAF-derived TFx estimates, thereby influencing associations with clinical outcome and potentially overestimating the prognostic impact of ctDNA metrics. For these reasons, our primary analyses were anchored to the 0.5% threshold, while results obtained at 0.1% are presented as sensitivity analyses.

While the overall somatic variant detection rate at baseline increased from 83.3% to 87.3% when lowering the LOD, the principal genomic findings were largely preserved across VAF thresholds. The predominance of *ESR1* as an acquired alteration and the increased genomic complexity observed in 2L samples remained evident. Minor shifts in variant frequencies were

observed, but the overall biological interpretation was not substantially altered by the threshold selection.

4.1.3. Patterns of genomic co-occurrence

Although the overall mutational landscape largely reflected the established patterns of HR+/HER2- ABC, the analysis of co-occurring alterations revealed additional layers of genomic complexity. In contrast to single-gene mutation frequencies, which remained relatively stable across detection thresholds, co-occurrence patterns were more sensitive to the inclusion of low-VAF variants. As co-occurrence analyses depend on the joint presence of alterations within individual samples, even modest changes in variant inclusion can meaningfully influence the resulting associations.

The significant co-occurrence between *ESR1* and *TP53* mutations that we observed in samples obtained prior to 1L treatment represents a divergence from the previously reported patterns of mutual exclusivity between mutations in these genes (137, 138). Namely, Li et al. (137) analyzed six independent cohorts and reported mutual exclusivity between *ESR1* and *TP53* mutations in ER+ MBC, independent of histological subtype or metastatic site, suggesting that this pattern may broadly apply to ER+ disease. Discrepancies between their findings and ours may be attributable to differences in study design and treatment exposure, as prior investigations were predominantly retrospective and included heterogeneous patient populations with varying previous lines of therapy. This interpretation is further supported by the findings of Bielo et al. (139), who also reported mutual exclusivity in metastatic ER+ /HER2- tumors; however, their cohort consisted exclusively of patients previously treated with ET. In contrast, our study incorporated predefined sampling time points and focused specifically on ABC patients who were not previously treated for metastatic disease. The absence of prior therapeutic pressure may therefore permit the coexistence of *ESR1* and *TP53* mutations before clonal selection occurs. At the same time, our more restrictive inclusion criteria resulted in a comparatively smaller cohort, raising the possibility of selection bias and limiting generalizability. However, our use of liquid biopsy may have enabled the detection of spatially and temporally distinct clonal populations that would not have been captured in single-site tissue analyses used in other studies. Given these considerations, our findings should be regarded as exploratory. Larger,

prospective studies are required to clarify the biological and clinical implications of *ESR1–TP53* co-occurrence at baseline.

4.2. Integrating ctDNA-derived tumor metrics in risk stratification

Beyond qualitative genomic alterations, quantitative ctDNA-derived metrics may provide additional information on tumor burden and disease aggressiveness.

In our prior work, we used z-scores derived from mFAST-SeqS as a surrogate measure of TFx, setting a threshold of > |3| to define elevated TFx (114). However, z-score values primarily reflect the extent of chromosomal aneuploidy within a sample and may not fully capture the complexity of tumor-derived alterations. Increasingly, the ctDNA field has moved toward integrative strategies that leverage orthogonal biological signals to enhance detection sensitivity and interpretability. Multimodal liquid biopsy approaches incorporating genome-wide features such as fragmentation or copy-number profiling alongside mutation analysis illustrate the complementary utility of integrating distinct cfDNA signals (140, 141). Therefore, in the present study we combined aneuploidy-derived z-scores with mutation-based hVAF to obtain a more comprehensive estimate of TFx.

Differences between hVAF and mFAST-SeqS largely reflect their distinct biological readouts: hVAF is more sensitive in detecting low-level ctDNA and copy-number–quiet tumors through high-frequency focal mutations, whereas aneuploidy-based methods such as mFAST-SeqS rely on chromosomal imbalance and therefore typically require a higher TFx. However, aneuploidy-derived metrics provide mutation-independent estimates of TFx, enabling the detection of tumor DNA even in the absence of panel mutations, and helping contextual interpretation of variant clonality (65). Together, these complementary features explain the differences in detection rates achieved by these approaches and support their combined use.

In this context, we defined two binary composite ctDNA metrics, and a composite metric that stratified patients into three groups based on whether elevated ctDNA levels were detected through none, one or both of our main TFx assessment approaches. While nearly all ctDNA-based measures showed significant associations with survival, the three-level metric exhibited the highest prognostic discrimination in univariable analyses, supporting its selection for subsequent multivariable risk modelling. Incorporation of this metric into a clinical model

containing established clinicopathologic variables resulted in improved model performance, suggesting that ctDNA-based measures provide complementary prognostic information beyond conventional factors. These findings indicate that quantitative ctDNA assessment captures biologically relevant aspects of tumor burden and disease aggressiveness that are not fully reflected by standard clinical parameters. From a translational perspective, stratification based on ctDNA burden may enable more refined risk-adapted management, where patients with high ctDNA levels could be considered for intensified monitoring, earlier therapy escalation, or inclusion in clinical trials of novel agents, and patients with low ctDNA burden may represent candidates for more conservative strategies and treatment de-escalation. Collectively, these data support the clinical integration of structured ctDNA-based risk metrics as a step toward more individualized management of ABC.

4.3. Beyond single biomarkers: perspectives on serial ctDNA profiling

With the expanding array of early treatment options for HR+/HER2- ABC, combination strategies incorporating CDK4/6 inhibitors have become the predominant therapeutic approach. However, as treatment landscapes continue to become increasingly complex, efforts to individualize therapy have begun to incorporate molecularly guided strategies. The PADA-1 and SERENA-6 trials demonstrated the feasibility of adapting treatment based on emerging *ESR1* mutations, highlighting the clinical utility of serial ctDNA monitoring (46, 101). However, these approaches were restricted to a single resistance mechanism and did not account for additional genomic alterations that may influence resistance. The INAVO120 trial adopted a more integrative strategy, incorporating both clinical risk (e.g., early relapse) and molecular selection (*PIK3CA* mutation status) in treatment allocation (142). The SONIA trial underscored the ongoing uncertainty regarding the optimal sequencing of CDK4/6 inhibitors by demonstrating comparable OS (~48 months) irrespective of administration in the 1L or the 2L setting (143). Exploratory analyses from the SONIA investigators further suggested that ctDNA dynamics may help refine treatment selection and sequencing in HR+ ABC (104). Collectively, these studies illustrate the great potential to guide treatment in HR+/HER2− ABC based on ctDNA levels, potentially allowing for de-escalation strategies as shown with the SONIA analyses, and escalation strategies for selected patient populations as utilized in the INAVO120 study. While most approaches have largely focused on individual genomic alterations, the evolving and heterogeneous resistance landscape suggests that broader genomic

characterization through serial ctDNA profiling may be necessary to more comprehensively inform treatment strategies.

In this context, our present analysis, restricted to baseline ctDNA metrics, provides an initial prognostic framework and demonstrates the clinical relevance of quantitative ctDNA assessment in HR+/HER2− ABC. However, its full clinical potential would likely be enhanced by the integration of serial measurements. We hypothesize that early on-treatment ctDNA kinetics could further refine adaptive treatment strategies, potentially enabling more timely escalation or de-escalation decisions.

4.4. HER2-low: an ongoing discussion

HER2-low BC emerged as a clinically relevant subgroup within HER2- disease, particularly following the demonstrated benefit of HER2-targeting ADCs such as T-DXd. In this context, we explored whether HR+/HER2-low and HR+/HER2-0 tumors differed genomically within our cohort based on ctDNA-derived TFx and mutational profiles.

When analyzing the earliest available plasma sample per patient, HER2-low tumors exhibited significantly higher TFx compared with HER2-0 tumors. However, these associations did not persist in mixed-effects models incorporating serial samples, suggesting that intra-patient variability and subgroup size may have influenced these findings.

Overall, mutational landscapes between HER2-low and HER2-0 tumors were largely comparable. Consistent with prior reports, HER2-low cases showed a higher frequency of *PIK3CA* mutations (60, 64, 144). However, in contrast to some tissue-based analyses, the difference in *TP53* mutation frequency between HER2-0 and HER2-low tumors was not detected in our dataset. The broader amplification profile in HER2-low samples, alongside largely comparable deletion patterns between HER2-low and HER2-0 cohorts, suggests that differences between groups—if present—may be driven more by focal gains than by recurrent losses. However, these observations should be considered as exploratory only, and interpreted with caution.

Taken together, our findings suggest that HR+/HER2-low and HR+/HER2-0 tumors share largely overlapping genomic architectures at the ctDNA level. While subtle quantitative differences in TFx may exist, the absence of consistent, distinct mutational signatures supports

the notion that HER2-low status may represent only a therapeutic, rather than a biologically discrete entity. Given the exploratory nature of this analysis and limited subgroup sizes, these results should be considered suggestive rather than definitive and warrant validation in larger cohorts.

4.5. Real-world implementation of *ESR1* mutation testing

The clinical relevance of *ESR1* mutation testing in HR+/HER2− ABC has substantially increased with the emergence of biomarker-guided treatment strategies and the approval of novel ETs such as elacestrant (39). Building on evidence from recent trials demonstrating the feasibility of ctDNA-guided treatment adaptation (46, 101), plasma-based *ESR1* testing is starting to be incorporated into clinical practice to support therapeutic decision-making.

In this evolving landscape, *ESR1* mutation analysis is frequently performed in a clinically driven manner, particularly within multidisciplinary frameworks such as MTBs, where genomic findings are integrated with clinical parameters to guide treatment selection. In this setting, broader genomic profiling and TFx assessment may provide additional biological context beyond the primary clinical question. This shift from trial-based evaluation to real-world implementation underscores the need to better understand the performance and characteristics of ctDNA-based *ESR1* testing outside controlled study settings.

In this context, the present analysis of a referral-based, real-world cohort provides insight into the practical implementation of plasma-based *ESR1* mutation testing. By characterizing clinically actionable alterations and tumor burden features, it offers a clinically relevant perspective on ctDNA profiles in this setting. Nevertheless, given the descriptive nature of this cohort, the analyses remain primarily exploratory. As clinical data collection is ongoing and longitudinal outcome data are not yet fully available, assessment of prognostic and predictive value is currently not possible.

In our cohort, the observed frequency of *ESR1* mutations was lower than the prevalence of approximately 47–50% that was reported in the EMERALD trial (39). This difference likely reflects variations in patient selection and prior treatment exposure. In contrast to EMERALD, which enrolled a more uniform population of patients with disease progression on ET and prior CDK4/6 inhibitor treatment, our cohort was referral-based and included patients across heterogeneous treatment lines. Given that *ESR1* mutations accumulate under selective pressure

from ET, this difference in treatment history likely contributed to the lower observed prevalence.

In addition, technical factors related to ctDNA detection are likely to have influenced mutation rates in this setting. Variability in TFx affects the sensitivity of mutation detection, particularly for low-VAF variants. In samples with low tumor burden, *ESR1* mutations frequently clustered near or below the predefined LOD of 0.5% VAF, suggesting that the true prevalence of *ESR1* mutations in this cohort may be underestimated when applying conservative detection limits.

Despite these limitations, this analysis demonstrates the feasibility of implementing ctDNA-based *ESR1* testing in routine clinical practice. The detection of multiple *ESR1* mutations in individual patients and the emergence of new mutations upon disease progression highlight the dynamic nature of endocrine resistance and underscore the value of repeated liquid biopsy assessments. Furthermore, the frequent co-occurrence of *ESR1* mutations with alterations in genes such as *PIK3CA* and *PTEN* suggests potential opportunities for combination therapeutic strategies. Overall, these findings complement the primary analyses of this thesis by illustrating the translational relevance of ctDNA profiling for treatment-guiding decision-making in HR+/HER2- ABC.

4.6. Limitations

While the findings reported in this Dissertation provide valuable insights into the genomic and prognostic patterns in HR+/HER2- ABC, several limitations need to be acknowledged.

It is important to note that the primary study was designed to evaluate genomic and prognostic associations and was not powered to assess predictive effects or differential treatment benefit. Furthermore, the modest overall cohort size and unequal subgroup distributions (1L vs. 2L; HER2-low vs. HER2-0) may have limited the robustness of comparative analyses.

A major limitation of the primary study is the absence of standardized serial on-treatment plasma sampling. Although serial timepoints were prospectively attempted, consistent longitudinal sampling was not feasible in all patients. Furthermore, financial constraints inherent to research-funded testing limited the inclusion of a larger number of timepoints. As a result, the present analyses are restricted to baseline and progression samples, precluding comprehensive evaluation of ctDNA kinetics.

Methodological constraints related to the assay selection require consideration as well. The AVENIO platform represents a tumor-agnostic, broadly applicable approach that prioritizes scalability and feasibility over maximal analytical sensitivity. By design, this entails a trade-off, where sensitivity for variants at very low VAFs is reduced in exchange for ease of implementation without requiring prior tumor sequencing. Such tumor-agnostic assays are particularly valuable in the metastatic setting investigated in this study, where rapid turnaround, broader genomic coverage, and independence from archival tumor tissue offer important practical advantages. In contrast, although many tumor-informed assays report detection rates of approximately 90% or higher in metastatic HR+ disease (105, 106), they are primarily optimized for disease monitoring and MRD detection. These assays do not routinely screen for actionable alterations, which limits their utility for guiding targeted therapy selection in advanced disease, where newly acquired targetable genomic changes are common.

As we selected an LOD of 0.5% to ensure high specificity, ctDNA positivity may have been underestimated in patients with very low tumor burden, thereby reducing the number of patients eligible for downstream prognostic and longitudinal analyses. In addition, this approach may have led to the underrepresentation of tumors that shed low amounts of ctDNA. As matched white blood cell samples were unavailable for most patients, the low-VAF findings cannot be definitively assigned to a tumor or hematopoietic origin and should therefore be interpreted with caution.

Another limitation of the AVENIO ctDNA Expanded assay is that, although it targets 77 genes, indel calling is performed only on a subset of these targets. As a result, important BC–relevant tumor suppressor genes, such as *BRCA1* and *BRCA2*, were not comprehensively assessed for indels. In addition, the assay does not provide reliable copy-number calling for several clinically relevant genes associated with ET resistance (e.g. *CCND1*, *NF1*, or *FGFR1*) (145-147), which may further limit its capacity to identify the complete spectrum of clinically actionable genomic alterations.

Finally, the co-occurrence analyses were exploratory and utilized unadjusted p-values without correction for multiple testing, therefore requiring independent validation.

In addition, the analyses of the ESR1 testing cohort are subject to specific limitations. Given the referral-based design and the clinically driven nature of this cohort, clinical annotation and

longitudinal outcome data were not yet fully available. Consequently, the analyses were primarily descriptive and exploratory, and the prognostic and predictive relevance of the findings could not be assessed. Furthermore, patients were included across a wide range of treatment lines, resulting in a heterogeneous population with variable prior treatment exposure, which may have influenced the observed mutational patterns and tumor burden characteristics.

Taken together, these limitations should be considered when interpreting our results and in the design of future ctDNA-based studies.

5. CONCLUSION

This thesis investigated the clinical and biological relevance of ctDNA in two real-world cohorts of patients with HR+/HER2− ABC across different stages of the disease. Using a tumor-agnostic plasma sequencing approach, we characterized the ctDNA-derived genomic landscape, evaluated quantitative ctDNA-derived tumor metrics, and explored potential differences according to HER2 expression status.

Overall, the genomic alterations detected in plasma of patients in the primary cohort were consistent with the established mutational profile of HR+/HER2− disease, with recurrent alterations in genes such as *PIK3CA*, *TP53*, and *ESR1*. The complementary integration of genome-wide and mutation-based ctDNA metrics allowed a more comprehensive assessment of tumor-derived signals in plasma. In particular, the combination of mFAST-SeqS–derived aneuploidy estimates and mutation-based hVAF improved detection sensitivity and enabled a refined characterization of tumor burden and genomic complexity. In addition, the observed co-occurrence of *ESR1* and *TP53* mutations in treatment-naïve metastatic disease challenges previously reported assumptions of strict mutational exclusivity and highlights the potential influence of therapeutic pressure on clonal architecture.

Beyond genomic characterization, this work demonstrated that quantitative ctDNA-derived tumor metrics provide clinically meaningful information for patient risk stratification. Incorporating ctDNA-derived TFx estimates alongside established clinical variables enhanced prognostic stratification. In particular, a composite ctDNA variable combining quantitative ctDNA parameters demonstrated superior risk discrimination compared with conventional clinicopathological factors alone, underscoring that ctDNA captures biologically relevant aspects of the tumor and its aggressiveness.

Exploratory analyses comparing HER2-low and HER2-0 tumors revealed largely similar genomic and ctDNA profiles, supporting the concept that HER2-low disease may represent a biological continuum within HER2-negative breast cancer rather than a clearly distinct genomic subtype.

In a complementary, clinically driven analysis, the evaluation of a separate real-world cohort demonstrated the feasibility of implementing plasma-based *ESR1* mutation testing in a more advanced and heterogeneous clinical setting. This analysis highlighted the practical relevance

of ctDNA profiling for treatment-guided decision-making and provided additional insight into the molecular heterogeneity and evolution of disease under treatment, underscoring the importance of considering tumor burden and detection thresholds when interpreting liquid biopsy results in routine clinical practice.

Taken together, the findings of this thesis support the potential of ctDNA-based profiling as a practical tool for personalized management of HR+/HER2− ABC, encompassing both improved risk stratification in early treatment lines and clinically driven molecular testing to inform treatment selection. While further prospective validation is required to determine which ctDNA metrics—alone or in combination—are most robust for clinical implementation, our results highlight the value of integrating ctDNA-derived biomarkers into future clinical studies. In particular, the incorporation of both baseline and longitudinal ctDNA assessments into prospective trial designs will be crucial to evaluate whether dynamic ctDNA changes can provide additional predictive or response-adaptive value and thereby contribute to more personalized, biology-informed management of HR+/HER2− ABC.

6. BIBLIOGRAPHY

1. Sung H, Ferlay J, Siegel RL, Laversanne M, Soerjomataram I, Jemal A, et al. Global Cancer Statistics 2020: GLOBOCAN Estimates of Incidence and Mortality Worldwide for 36 Cancers in 185 Countries. CA: A Cancer Journal for Clinicians. 2021;71(3):209–49.

2. Arnold M, Morgan E, Rumgay H, Mafra A, Singh D, Laversanne M, et al. Current and future burden of breast cancer: Global statistics for 2020 and 2040. Breast. 2022;66:15–23.

3. Abdullah HMA, Chennapragada SS, Singh R, Zeidalkilani JMJ, Kesireddy M. Precision therapy in metastatic breast cancer: the current landscape of molecular alteration-based therapies. Transl Breast Cancer Res. 2025;6:24.

4. Łukasiewicz S, Czeczelewski M, Forma A, Baj J, Sitarz R, Stanisławek A. Breast Cancer-Epidemiology, Risk Factors, Classification, Prognostic Markers, and Current Treatment Strategies-An Updated Review. Cancers (Basel). 2021;13(17).

5. Sun YS, Zhao Z, Yang ZN, Xu F, Lu HJ, Zhu ZY, et al. Risk Factors and Preventions of Breast Cancer. Int J Biol Sci. 2017;13(11):1387–97.

6. Cardoso F, Kyriakides S, Ohno S, Penault-Llorca F, Poortmans P, Rubio IT, et al. Early breast cancer: ESMO Clinical Practice Guidelines for diagnosis, treatment and follow-up†. Annals of Oncology. 2019;30(8):1194–220.

7. Giaquinto AN, Sung H, Newman LA, Freedman RA, Smith RA, Star J, et al. Breast cancer statistics 2024. CA: A Cancer Journal for Clinicians. 2024;74(6):477–95.

8. Allemani C, Matsuda T, Di Carlo V, Harewood R, Matz M, Nikšić M, et al. Global surveillance of trends in cancer survival 2000–14 (CONCORD-3): analysis of individual records for 37 513 025 patients diagnosed with one of 18 cancers from 322 population-based registries in 71 countries. The Lancet. 2018;391(10125):1023–75.

9. Başaran GA, Twelves C, Diéras V, Cortés J, Awada A. Ongoing unmet needs in treating estrogen receptor-positive/HER2-negative metastatic breast cancer. Cancer Treat Rev. 2018;63:144–55.

10. Ning L, Liu Y, Hou Y, Wang M, Shi M, Liu Z, et al. Survival nomogram for patients with de novo metastatic breast cancer based on the SEER database and an external validation cohort. Cancer Pathog Ther. 2023;1(4):253–61.

11. McManaman JL, Neville MC. Mammary physiology and milk secretion. Advanced Drug Delivery Reviews. 2003;55(5):629–41.

12. Gudjonsson T, Adriance MC, Sternlicht MD, Petersen OW, Bissell MJ. Myoepithelial cells: their origin and function in breast morphogenesis and neoplasia. J Mammary Gland Biol Neoplasia. 2005;10(3):261–72.
13. Biswas SK, Banerjee S, Baker GW, Kuo C-Y, Chowdhury I. The Mammary Gland: Basic Structure and Molecular Signaling during Development. International Journal of Molecular Sciences. 2022;23(7):3883.
14. Harbeck N, Penault-Llorca F, Cortes J, Gnant M, Houssami N, Poortmans P, et al. Breast cancer. Nature Reviews Disease Primers. 2019;5(1):66.
15. Visvader JE, Stingl J. Mammary stem cells and the differentiation hierarchy: current status and perspectives. Genes Dev. 2014;28(11):1143–58.
16. Taurin S, Alkhalifa H. Breast cancers, mammary stem cells, and cancer stem cells, characteristics, and hypotheses. Neoplasia. 2020;22(12):663–78.
17. Stingl J, Caldas C. Molecular heterogeneity of breast carcinomas and the cancer stem cell hypothesis. Nature Reviews Cancer. 2007;7(10):791–9.
18. Xiong X, Zheng LW, Ding Y, Chen YF, Cai YW, Wang LP, et al. Breast cancer: pathogenesis and treatments. Signal Transduct Target Ther. 2025;10(1):49.
19. Sarhangi N, Hajjari S, Heydari SF, Ganjizadeh M, Rouhollah F, Hasanzad M. Breast cancer in the era of precision medicine. Molecular Biology Reports. 2022;49(10):10023–37.
20. Lei H, Fu J, Gu W, Qiao H, Guo H, Chen Z, et al. Breast Cancer: Molecular Pathogenesis, Targeted Therapy, Screening, and Prevention. MedComm (2020). 2026;7(1):e70560.
21. Clusan L, Ferrière F, Flouriot G, Pakdel F. A Basic Review on Estrogen Receptor Signaling Pathways in Breast Cancer. Int J Mol Sci. 2023;24(7).
22. Bombonati A, Sgroi DC. The molecular pathology of breast cancer progression. J Pathol. 2011;223(2):307–17.
23. Brooks MD, Burness ML, Wicha MS. Therapeutic Implications of Cellular Heterogeneity and Plasticity in Breast Cancer. Cell Stem Cell. 2015;17(3):260–71.
24. Laskar TT, Laskar HM, Mazumder JA, Bhattacharjee R, Husain MI, Das B, et al. Decoding breast cancer: insights into molecular pathways & therapeutic approaches. Discov Oncol. 2025;16(1):2103.
25. Panda VK, Mishra B, Mahapatra S, Swain B, Malhotra D, Saha S, et al. Molecular Insights on Signaling Cascades in Breast Cancer: A Comprehensive Review. Cancers (Basel). 2025;17(2).

26. Liang Y, Zhang H, Song X, Yang Q. Metastatic heterogeneity of breast cancer: Molecular mechanism and potential therapeutic targets. Seminars in Cancer Biology. 2020;60:14–27.
27. Riggio AI, Varley KE, Welm AL. The lingering mysteries of metastatic recurrence in breast cancer. Br J Cancer. 2021;124(1):13–26.
28. Koufopoulos NI, Boutas I, Pouliakis A, Samaras MG, Kotanidis C, Kontogeorgi A, et al. The "Forgotten" Subtypes of Breast Carcinoma: A Systematic Review of Selected Histological Variants Not Included or Not Recognized as Distinct Entities in the Current World Health Organization Classification of Breast Tumors. Int J Mol Sci. 2024;25(15).
29. Yang C, Brezden-Masley C, Joy AA, Sehdev S, Modi S, Simmons C, et al. Targeting HER2-low in metastatic breast cancer: an evolving treatment paradigm. Ther Adv Med Oncol. 2023;15:17588359231175440.
30. Sablin MP, Gestraud P, Jonas SF, Lamy C, Lacroix-Triki M, Bachelot T, et al. Copy number alterations in metastatic and early breast tumours: prognostic and acquired biomarkers of resistance to CDK4/6 inhibitors. Br J Cancer. 2024;131(6):1060–7.
31. Lloyd MR, Jhaveri K, Kalinsky K, Bardia A, Wander SA. Precision therapeutics and emerging strategies for HR-positive metastatic breast cancer. Nature Reviews Clinical Oncology. 2024;21(10):743–61.
32. Prat A, Pineda E, Adamo B, Galván P, Fernández A, Gaba L, et al. Clinical implications of the intrinsic molecular subtypes of breast cancer. The Breast. 2015;24:S26–S35.
33. Perou CM, Sørlie T, Eisen MB, van de Rijn M, Jeffrey SS, Rees CA, et al. Molecular portraits of human breast tumours. Nature. 2000;406(6797):747–52.
34. Sørlie T, Perou CM, Tibshirani R, Aas T, Geisler S, Johnsen H, et al. Gene expression patterns of breast carcinomas distinguish tumor subclasses with clinical implications. Proc Natl Acad Sci U S A. 2001;98(19):10869–74.
35. Parker JS, Mullins M, Cheang MC, Leung S, Voduc D, Vickery T, et al. Supervised risk predictor of breast cancer based on intrinsic subtypes. J Clin Oncol. 2009;27(8):1160–7.
36. Waks AG, Winer EP. Breast Cancer Treatment: A Review. JAMA. 2019;321(3):288–300.
37. Bardia A, Rugo HS, Tolaney SM, Loirat D, Punie K, Oliveira M, et al. Final Results From the Randomized Phase III ASCENT Clinical Trial in Metastatic Triple-Negative Breast Cancer and Association of Outcomes by Human Epidermal Growth Factor Receptor 2 and Trophoblast Cell Surface Antigen 2 Expression. Journal of Clinical Oncology. 2024;42(15):1738–44.

38. Dent R, Shao Z, Schmid P, Cortes J, Cescon DW, Saji S, et al. Datopotamab deruxtecan in patients with untreated, advanced triple-negative breast cancer (TROPION-Breast02): a randomised, open-label, international, phase III trial. Ann Oncol. 2026.
39. Bidard F-C, Kaklamani VG, Neven P, Streich G, Montero AJ, Forget F, et al. Elacestrant (oral selective estrogen receptor degrader) Versus Standard Endocrine Therapy for Estrogen Receptor–Positive, Human Epidermal Growth Factor Receptor 2–Negative Advanced Breast Cancer: Results From the Randomized Phase III EMERALD Trial. Journal of Clinical Oncology. 2022;40(28):3246–56.
40. Jhaveri KL, Neven P, Casalnuovo ML, Kim SB, Tokunaga E, Aftimos P, et al. Imlunestrant with or without Abemaciclib in Advanced Breast Cancer. N Engl J Med. 2025;392(12):1189–202.
41. Morrison L, Loibl S, Turner NC. The CDK4/6 inhibitor revolution - a game-changing era for breast cancer treatment. Nat Rev Clin Oncol. 2024;21(2):89–105.
42. Kindt CK, Alves CL, Ehmsen S, Kragh A, Reinert T, Vogsen M, et al. Genomic alterations associated with resistance and circulating tumor DNA dynamics for early detection of progression on CDK4/6 inhibitor in advanced breast cancer. Int J Cancer. 2024;155(12):2211–22.
43. Finn RS, Martin M, Rugo HS, Jones S, Im S-A, Gelmon K, et al. Palbociclib and Letrozole in Advanced Breast Cancer. New England Journal of Medicine. 2016;375(20):1925–36.
44. Tripathy D, Im SA, Colleoni M, Franke F, Bardia A, Harbeck N, et al. Ribociclib plus endocrine therapy for premenopausal women with hormone-receptor-positive, advanced breast cancer (MONALEESA-7): a randomised phase 3 trial. Lancet Oncol. 2018;19(7):904–15.
45. Mo H, Renna CE, Moore HCF, Abraham J, Kruse ML, Montero AJ, et al. Real-World Outcomes of Everolimus and Exemestane for the Treatment of Metastatic Hormone Receptor-Positive Breast Cancer in Patients Previously Treated With CDK4/6 Inhibitors. Clin Breast Cancer. 2022;22(2):143–8.
46. Bidard FC, Mayer EL, Park YH, Janni W, Ma C, Cristofanilli M, et al. First-Line Camizestrant for Emerging ESR1-Mutated Advanced Breast Cancer. N Engl J Med. 2025;393(6):569–80.
47. Torrisi R, Gerosa R, Miggiano C, Saltalamacchia G, Benvenuti C, Santoro A. Beyond failure of endocrine-based therapies in HR+/HER2 negative advanced breast cancer: What

before chemotherapy? A glimpse into the future. Critical Reviews in Oncology/Hematology. 2025;208:104634.

48. Buyukgolcigezli I, Tenekeci AK, Sahin IH. Opportunities and Challenges in Antibody-Drug Conjugates for Cancer Therapy: A New Era for Cancer Treatment. Cancers (Basel). 2025;17(6).

49. Dilawari A, Zhang H, Shah M, Gao X, Fiero M, Bhatnagar V, et al. US Food and Drug Administration Approval Summary: Trastuzumab Deruxtecan for the Treatment of Adult Patients With Hormone Receptor-Positive, Unresectable or Metastatic Human Epidermal Growth Factor Receptor 2-Low or Human Epidermal Growth Factor Receptor 2-Ultralow Breast Cancer. J Clin Oncol. 2025;43(26):2942–51.

50. Rugo HS, Schmid P, Tolaney SM, Dalenc F, Marmé F, Shi L, et al. Health-related quality of life with sacituzumab govitecan in HR+/HER2− metastatic breast cancer in the phase III TROPiCS-02 trial. The Oncologist. 2024;29(9):768–79.

51. Royce M, Shah M, Zhang L, Cheng J, Bonner MK, Pegues M, et al. FDA Approval Summary: Datopotamab Deruxtecan-dlnk for Treatment of Patients with Unresectable or Metastatic, HR-Positive, HER2-Negative Breast Cancer. Clin Cancer Res. 2025;31(21):4405–11.

52. Mobashir M, Tarique H, Ahmad S, Habib I, Inam A, Qamar I, et al. Datopotamab deruxtecan: a new era in targeted therapy for metastatic breast cancer. Ann Med Surg (Lond). 2025;87(11):6898–9.

53. Rugo HS, Bardia A, Marmé F, Cortes J, Schmid P, Loirat D, et al. Sacituzumab Govitecan in Hormone Receptor–Positive/Human Epidermal Growth Factor Receptor 2–Negative Metastatic Breast Cancer. Journal of Clinical Oncology. 2022;40(29):3365–76.

54. Modi S, Jacot W, Yamashita T, Sohn J, Vidal M, Tokunaga E, et al. Trastuzumab Deruxtecan in Previously Treated HER2-Low Advanced Breast Cancer. N Engl J Med. 2022;387(1):9–20.

55. Zhang H, Katerji H, Turner BM, Hicks DG. HER2-Low Breast Cancers. Am J Clin Pathol. 2022;157(3):328–36.

56. Yin L, Zhang H, Shang Y, Wu S, Jin T. ErbB/HER family in cancer immunology: therapeutic advances and mechanisms. Drug Discovery Today. 2025;30(9):104436.

57. Wolff AC, Somerfield MR, Dowsett M, Hammond MEH, Hayes DF, McShane LM, et al. Human Epidermal Growth Factor Receptor 2 Testing in Breast Cancer. Archives of Pathology & Laboratory Medicine. 2023;147(9):993–1000.

58. Modi S, Park H, Murthy RK, Iwata H, Tamura K, Tsurutani J, et al. Antitumor Activity and Safety of Trastuzumab Deruxtecan in Patients With HER2-Low-Expressing Advanced Breast Cancer: Results From a Phase Ib Study. J Clin Oncol. 2020;38(17):1887–96.

59. Tarantino P, Hamilton E, Tolaney SM, Cortes J, Morganti S, Ferraro E, et al. HER2-Low Breast Cancer: Pathological and Clinical Landscape. Journal of Clinical Oncology. 2020;38(17):1951–62.

60. Denkert C, Seither F, Schneeweiss A, Link T, Blohmer JU, Just M, et al. Clinical and molecular characteristics of HER2-low-positive breast cancer: pooled analysis of individual patient data from four prospective, neoadjuvant clinical trials. Lancet Oncol. 2021;22(8):1151–61.

61. Schettini F, Chic N, Brasó-Maristany F, Paré L, Pascual T, Conte B, et al. Clinical, pathological, and PAM50 gene expression features of HER2-low breast cancer. NPJ Breast Cancer. 2021;7(1):1.

62. Bardia A, Hu X, Dent R, Yonemori K, Barrios CH, O'Shaughnessy JA, et al. Trastuzumab Deruxtecan after Endocrine Therapy in Metastatic Breast Cancer. N Engl J Med. 2024;391(22):2110–22.

63. Hensing WL, Podany EL, Sears JJ, Tapiavala S, Davis AA. Evolving concepts in HER2-low breast cancer: Genomic insights, definitions, and treatment paradigms: Oncotarget. 2025 Jan 20;16:11-27. doi: 10.18632/oncotarget.28680. eCollection 2025.

64. Zhang G, Ren C, Li C, Wang Y, Chen B, Wen L, et al. Distinct clinical and somatic mutational features of breast tumors with high-, low-, or non-expressing human epidermal growth factor receptor 2 status. BMC Medicine. 2022;20(1):142.

65. Heitzer E, Haque IS, Roberts CES, Speicher MR. Current and future perspectives of liquid biopsies in genomics-driven oncology. Nat Rev Genet. 2019;20(2):71–88.

66. Ignatiadis M, Sledge GW, Jeffrey SS. Liquid biopsy enters the clinic - implementation issues and future challenges. Nat Rev Clin Oncol. 2021;18(5):297–312.

67. Nikanjam M, Kato S, Kurzrock R. Liquid biopsy: current technology and clinical applications. Journal of Hematology & Oncology. 2022;15(1):131.

68. Heitzer E, Ulz P, Geigl JB. Circulating tumor DNA as a liquid biopsy for cancer. Clin Chem. 2015;61(1):112–23.
69. Hasenleithner SO, Speicher MR. A clinician's handbook for using ctDNA throughout the patient journey. Mol Cancer. 2022;21(1):81.
70. Diaz LA, Bardelli A. Liquid Biopsies: Genotyping Circulating Tumor DNA. Journal of Clinical Oncology. 2014;32(6):579–86.
71. Wan JCM, Massie C, Garcia-Corbacho J, Mouliere F, Brenton JD, Caldas C, et al. Liquid biopsies come of age: towards implementation of circulating tumour DNA. Nature Reviews Cancer. 2017;17(4):223–38.
72. Moser T, Kühberger S, Lazzeri I, Vlachos G, Heitzer E. Bridging biological cfDNA features and machine learning approaches. Trends Genet. 2023;39(4):285–307.
73. Mandel P, Metais P. [Nuclear Acids In Human Blood Plasma]. C R Seances Soc Biol Fil. 1948;142(3-4):241–3.
74. Tan EM, Schur PH, Carr RI, Kunkel HG. Deoxybonucleic acid (DNA) and antibodies to DNA in the serum of patients with systemic lupus erythematosus. J Clin Invest. 1966;45(11):1732–40.
75. Leon SA, Shapiro B, Sklaroff DM, Yaros MJ. Free DNA in the serum of cancer patients and the effect of therapy. Cancer Res. 1977;37(3):646–50.
76. Stroun M, Anker P, Lyautey J, Lederrey C, Maurice PA. Isolation and characterization of DNA from the plasma of cancer patients. Eur J Cancer Clin Oncol. 1987;23(6):707–12.
77. Stroun M, Anker P, Maurice P, Lyautey J, Lederrey C, Beljanski M. Neoplastic characteristics of the DNA found in the plasma of cancer patients. Oncology. 1989;46(5):318–22.
78. Sidransky D, Von Eschenbach A, Tsai YC, Jones P, Summerhayes I, Marshall F, et al. Identification of p53 gene mutations in bladder cancers and urine samples. Science. 1991;252(5006):706–9.
79. Sidransky D, Tokino T, Hamilton SR, Kinzler KW, Levin B, Frost P, et al. Identification of ras oncogene mutations in the stool of patients with curable colorectal tumors. Science. 1992;256(5053):102–5.
80. Caldas C, Hahn SA, Hruban RH, Redston MS, Yeo CJ, Kern SE. Detection of K-ras mutations in the stool of patients with pancreatic adenocarcinoma and pancreatic ductal hyperplasia. Cancer Res. 1994;54(13):3568–73.

81. Takeda S, Ichii S, Nakamura Y. Detection of K-ras mutation in sputum by mutant-allele-specific amplification (MASA). Hum Mutat. 1993;2(2):112–7.
82. Sorenson GD, Pribish DM, Valone FH, Memoli VA, Bzik DJ, Yao SL. Soluble normal and mutated DNA sequences from single-copy genes in human blood. Cancer Epidemiol Biomarkers Prev. 1994;3(1):67–71.
83. Lo YM, Corbetta N, Chamberlain PF, Rai V, Sargent IL, Redman CW, et al. Presence of fetal DNA in maternal plasma and serum. Lancet. 1997;350(9076):485–7.
84. Rieneck K, Clausen FB, Dziegiel MH. Noninvasive Antenatal Determination of Fetal Blood Group Using Next-Generation Sequencing. Cold Spring Harb Perspect Med. 2015;6(1):a023093.
85. Mennuti MT, Chandrasekaran S, Khalek N, Dugoff L. Cell-free DNA screening and sex chromosome aneuploidies. Prenatal Diagnosis. 2015;35(10):980–5.
86. Chiu RW, Lau TK, Leung TN, Chow KC, Chui DH, Lo YM. Prenatal exclusion of beta thalassaemia major by examination of maternal plasma. Lancet. 2002;360(9338):998–1000.
87. Lo YM, Tein MS, Lau TK, Haines CJ, Leung TN, Poon PM, et al. Quantitative analysis of fetal DNA in maternal plasma and serum: implications for noninvasive prenatal diagnosis. Am J Hum Genet. 1998;62(4):768–75.
88. Thierry AR, El Messaoudi S, Gahan PB, Anker P, Stroun M. Origins, structures, and functions of circulating DNA in oncology. Cancer Metastasis Rev. 2016;35(3):347–76.
89. Hill M, Wright D, Daley R, Lewis C, McKay F, Mason S, et al. Evaluation of non-invasive prenatal testing (NIPT) for aneuploidy in an NHS setting: a reliable accurate prenatal non-invasive diagnosis (RAPID) protocol. BMC Pregnancy Childbirth. 2014;14:229.
90. Heitzer E, Perakis S, Geigl JB, Speicher MR. The potential of liquid biopsies for the early detection of cancer. NPJ Precis Oncol. 2017;1(1):36.
91. Breitbach S, Sterzing B, Magallanes C, Tug S, Simon P. Direct measurement of cell-free DNA from serially collected capillary plasma during incremental exercise. J Appl Physiol (1985). 2014;117(2):119–30.
92. Rodrigues Filho EM, Simon D, Ikuta N, Klovan C, Dannebrock FA, Oliveira de Oliveira C, et al. Elevated cell-free plasma DNA level as an independent predictor of mortality in patients with severe traumatic brain injury. J Neurotrauma. 2014;31(19):1639–46.

93. De Vlaminck I, Valantine HA, Snyder TM, Strehl C, Cohen G, Luikart H, et al. Circulating cell-free DNA enables noninvasive diagnosis of heart transplant rejection. Sci Transl Med. 2014;6(241):241ra77.

94. De Vlaminck I, Martin L, Kertesz M, Patel K, Kowarsky M, Strehl C, et al. Noninvasive monitoring of infection and rejection after lung transplantation. Proc Natl Acad Sci U S A. 2015;112(43):13336–41.

95. Bardelli A, Pantel K. Liquid Biopsies, What We Do Not Know (Yet). Cancer Cell. 2017;31(2):172–9.

96. Brett JO, Spring LM, Bardia A, Wander SA. ESR1 mutation as an emerging clinical biomarker in metastatic hormone receptor-positive breast cancer. Breast Cancer Res. 2021;23(1):85.

97. Robinson DR, Wu YM, Vats P, Su F, Lonigro RJ, Cao X, et al. Activating ESR1 mutations in hormone-resistant metastatic breast cancer. Nat Genet. 2013;45(12):1446–51.

98. Rugo HS, Rumble RB, Macrae E, Barton DL, Connolly HK, Dickler MN, et al. Endocrine Therapy for Hormone Receptor–Positive Metastatic Breast Cancer: American Society of Clinical Oncology Guideline. Journal of Clinical Oncology. 2016;34(25):3069–103.

99. André F, Ciruelos E, Rubovszky G, Campone M, Loibl S, Rugo HS, et al. Alpelisib for PIK3CA-Mutated, Hormone Receptor-Positive Advanced Breast Cancer. N Engl J Med. 2019;380(20):1929–40.

100. Turner NC, Kingston B, Kilburn LS, Kernaghan S, Wardley AM, Macpherson IR, et al. Circulating tumour DNA analysis to direct therapy in advanced breast cancer (plasmaMATCH): a multicentre, multicohort, phase 2a, platform trial. Lancet Oncol. 2020;21(10):1296–308.

101. Bidard F-C, Hardy-Bessard A-C, Dalenc F, Bachelot T, Pierga J-Y, de la Motte Rouge T, et al. Switch to fulvestrant and palbociclib versus no switch in advanced breast cancer with rising ESR1 mutation during aromatase inhibitor and palbociclib therapy (PADA-1): a randomised, open-label, multicentre, phase 3 trial. The Lancet Oncology. 2022;23(11):1367–77.

102. Mamann A, Pradat Y, Bidard FC, Delaloge S, Cabel L, Faull I, et al. Prognostic significance of early on-treatment evolution of circulating tumor DNA in advanced ER-positive/HER2-negative breast cancer. Ann Oncol. 2025;36(11):1342–55.

103. Pontolillo L, Davis AA, Gerratana L, Medford AJ, Wang J, Nicolo E, et al. Circulating genomic landscape following cyclin-dependent kinase 4/6 inhibitors exposure in HR + /HER2- metastatic breast cancer: a retrospective multi-institutional Consortium analysis. NPJ Breast Cancer. 2025;11(1):93.
104. Jongbloed EM, Wortelboer N, de Weerd V, Beaufort CM, Ruigrok-Ritstier K, Van MN, et al. Early versus deferred use of CDK4/6 inhibitors in advanced breast cancer: circulating tumor DNA analysis of a randomized phase 3 trial. Nat Med. 2025.
105. Fuentes-Antrás J, Elliott MJ, Main SC, Echelard P, Dou A, Bedard PL, et al. Personalized ctDNA monitoring in metastatic HR+/HER2− breast cancer patients during endocrine and CDK4/6 inhibitor therapy. npj Breast Cancer. 2025;11(1):74.
106. Dawson S-J, Tsui DWY, Murtaza M, Biggs H, Rueda OM, Chin S-F, et al. Analysis of Circulating Tumor DNA to Monitor Metastatic Breast Cancer. New England Journal of Medicine. 2013;368(13):1199–209.
107. Fribbens C, O'Leary B, Kilburn L, Hrebien S, Garcia-Murillas I, Beaney M, et al. Plasma ESR1 Mutations and the Treatment of Estrogen Receptor-Positive Advanced Breast Cancer. J Clin Oncol. 2016;34(25):2961–8.
108. Pascual J, Gil-Gil M, Proszek P, Zielinski C, Reay A, Ruiz-Borrego M, et al. Baseline Mutations and ctDNA Dynamics as Prognostic and Predictive Factors in ER-Positive/HER2-Negative Metastatic Breast Cancer Patients. Clinical Cancer Research. 2023;29(20):4166–77.
109. Cybulla E, Stover DG. Circulating DNA tumor fraction as a biomarker for advanced breast cancer. Front Oncol. 2025;15:1655415.
110. Harris PA, Taylor R, Minor BL, Elliott V, Fernandez M, O'Neal L, et al. The REDCap consortium: Building an international community of software platform partners. J Biomed Inform. 2019;95:103208.
111. Chakravarty D, Gao J, Phillips SM, Kundra R, Zhang H, Wang J, et al. OncoKB: A Precision Oncology Knowledge Base. JCO Precis Oncol. 2017;2017.
112. Ulz P, Belic J, Graf R, Auer M, Lafer I, Fischereder K, et al. Whole-genome plasma sequencing reveals focal amplifications as a driving force in metastatic prostate cancer. Nat Commun. 2016;7:12008.
113. Belic J, Koch M, Ulz P, Auer M, Gerhalter T, Mohan S, et al. Rapid Identification of Plasma DNA Samples with Increased ctDNA Levels by a Modified FAST-SeqS Approach. Clin Chem. 2015;61(6):838–49.

114. Suppan C, Brcic I, Tiran V, Mueller HD, Posch F, Auer M, et al. Untargeted Assessment of Tumor Fractions in Plasma for Monitoring and Prognostication from Metastatic Breast Cancer Patients Undergoing Systemic Treatment. Cancers (Basel). 2019;11(8).
115. Klocker EV, Dobrić N, Graf R, Beichler C, Hlauschek D, Suppan C, et al. Clinical impact of single-gene vs. panel sequencing in advanced HR + /HER2- breast cancer: insights and implications. NPJ Breast Cancer. 2025;11(1):86.
116. Adalsteinsson VA, Ha G, Freeman SS, Choudhury AD, Stover DG, Parsons HA, et al. Scalable whole-exome sequencing of cell-free DNA reveals high concordance with metastatic tumors. Nat Commun. 2017;8(1):1324.
117. Zhou X, Cheng Z, Dong M, Liu Q, Yang W, Liu M, et al. Tumor fractions deciphered from circulating cell-free DNA methylation for cancer early diagnosis. Nat Commun. 2022;13(1):7694.
118. Rickles-Young M, Tinoco G, Tsuji J, Pollock S, Haynam M, Lefebvre H, et al. Assay Validation of Cell-Free DNA Shallow Whole-Genome Sequencing to Determine Tumor Fraction in Advanced Cancers. J Mol Diagn. 2024;26(5):413–22.
119. Mermel CH, Schumacher SE, Hill B, Meyerson ML, Beroukhim R, Getz G. GISTIC2.0 facilitates sensitive and confident localization of the targets of focal somatic copy-number alteration in human cancers. Genome Biol. 2011;12(4):R41.
120. Mayakonda A, Lin DC, Assenov Y, Plass C, Koeffler HP. Maftools: efficient and comprehensive analysis of somatic variants in cancer. Genome Res. 2018;28(11):1747–56.
121. Schemper M, Smith TL. A note on quantifying follow-up in studies of failure time. Control Clin Trials. 1996;17(4):343–6.
122. Uno H, Cai T, Pencina MJ, D'Agostino RB, Wei LJ. On the C-statistics for evaluating overall adequacy of risk prediction procedures with censored survival data. Stat Med. 2011;30(10):1105–17.
123. Akaike H. Information Theory and an Extension of the Maximum Likelihood Principle. In: Parzen E, Tanabe K, Kitagawa G, editors. Selected Papers of Hirotugu Akaike. New York, NY: Springer New York; 1998. p. 199–213.
124. Dobrić N, Hasenleithner SO, Suppan C, Klocker EV, Hlauschek D, Graf R, et al. Integrating baseline ctDNA-derived tumor metrics enhances risk stratification in HR-positive/HER2-negative advanced breast cancer: a real-world multicenter cohort study from Austria. ESMO Open. 2026;11(4).

125. Davis AA, Luo J, Zheng T, Dai C, Dong X, Tan L, et al. Genomic Complexity Predicts Resistance to Endocrine Therapy and CDK4/6 Inhibition in Hormone Receptor-Positive (HR+)/HER2-Negative Metastatic Breast Cancer. Clin Cancer Res. 2023;29(9):1719–29.
126. Gerratana L, Davis AA, Velimirovic M, Reduzzi C, Clifton K, Bucheit L, et al. Cyclin-Dependent Kinase 4/6 Inhibitors Beyond Progression in Metastatic Breast Cancer: A Retrospective Real-World Biomarker Analysis. JCO Precis Oncol. 2023;7:e2200531.
127. Lefebvre C, Bachelot T, Filleron T, Pedrero M, Campone M, Soria JC, et al. Mutational Profile of Metastatic Breast Cancers: A Retrospective Analysis. PLoS Med. 2016;13(12):e1002201.
128. Huebner H, Wimberger P, Laakmann E, Ruckhäberle E, Ruebner M, Lehle S, et al. Cell-free tumor DNA analysis in advanced or metastatic breast cancer patients: mutation frequencies, testing intention, and clinical impact. Precision Clinical Medicine. 2025;8(1):pbae034.
129. Lv D, Lan B, Guo Q, Yi Z, Qian H, Guan Y, et al. Exploration of the clonal evolution and construction of the tumor clonal evolution rate as a prognostic indicator in metastatic breast cancer. BMC Med. 2025;23(1):122.
130. Murtaza M, Dawson S-J, Tsui DWY, Gale D, Forshew T, Piskorz AM, et al. Non-invasive analysis of acquired resistance to cancer therapy by sequencing of plasma DNA. Nature. 2013;497(7447):108–12.
131. Razavi P, Chang MT, Xu G, Bandlamudi C, Ross DS, Vasan N, et al. The Genomic Landscape of Endocrine-Resistant Advanced Breast Cancers. Cancer Cell. 2018;34(3):427–38.e6.
132. Valenza C, Curigliano G. Positioning oral selective estrogen receptor degraders in patients with metastatic breast cancer. Eur J Cancer. 2025;228:115739.
133. Bertucci F, Ng CKY, Patsouris A, Droin N, Piscuoglio S, Carbuccia N, et al. Genomic characterization of metastatic breast cancers. Nature. 2019;569(7757):560–4.
134. Razavi P, Li BT, Brown DN, Jung B, Hubbell E, Shen R, et al. High-intensity sequencing reveals the sources of plasma circulating cell-free DNA variants. Nat Med. 2019;25(12):1928–37.
135. Coombs CC, Zehir A, Devlin SM, Kishtagari A, Syed A, Jonsson P, et al. Therapy-Related Clonal Hematopoiesis in Patients with Non-hematologic Cancers Is Common and Associated with Adverse Clinical Outcomes. Cell Stem Cell. 2017;21(3):374–82.e4.

136. Hu Y, Ulrich BC, Supplee J, Kuang Y, Lizotte PH, Feeney NB, et al. False-Positive Plasma Genotyping Due to Clonal Hematopoiesis. Clinical Cancer Research. 2018;24(18):4437–43.
137. Li Z, Spoelstra NS, Sikora MJ, Sams SB, Elias A, Richer JK, et al. Mutual exclusivity of ESR1 and TP53 mutations in endocrine resistant metastatic breast cancer. npj Breast Cancer. 2022;8(1):62.
138. Williams MM, Spoelstra NS, Arnesen S, O'Neill KI, Christenson JL, Reese J, et al. Steroid Hormone Receptor and Infiltrating Immune Cell Status Reveals Therapeutic Vulnerabilities of ESR1-Mutant Breast Cancer. Cancer Res. 2021;81(3):732–46.
139. Boscolo Bielo L, Guerini Rocco E, Trapani D, Zagami P, Taurelli Salimbeni B, Esposito A, et al. Genomic and clinical landscape of metastatic hormone receptors-positive breast cancers carrying ESR1 alterations. ESMO Open. 2024;9(10):103731.
140. Christodoulou E, Yellapantula V, O'Halloran K, Xu L, Berry JL, Cotter JA, et al. Combined low-pass whole genome and targeted sequencing in liquid biopsies for pediatric solid tumors. NPJ Precis Oncol. 2023;7(1):21.
141. Mouliere F, Chandrananda D, Piskorz AM, Moore EK, Morris J, Ahlborn LB, et al. Enhanced detection of circulating tumor DNA by fragment size analysis. Sci Transl Med. 2018;10(466).
142. Turner NC, Im SA, Saura C, Juric D, Loibl S, Kalinsky K, et al. Inavolisib-Based Therapy in PIK3CA-Mutated Advanced Breast Cancer. N Engl J Med. 2024;391(17):1584–96.
143. Wortelboer N, Van Ommen-Nijhof A, Konings IR, Van Der Noort V, Van Den Pol E, Páez CG, et al. 487MO Overall survival with first versus second-line use of CDK4/6 inhibitors in HR+/HER2- advanced breast cancer. Annals of Oncology. 2025;36:S402–S3.
144. Yi Z, Feng K, Lv D, Guan Y, Shao Y, Ma F, et al. Genomic landscape of circulating tumor DNA in HER2-low metastatic breast cancer. Signal Transduct Target Ther. 2024;9(1):345.
145. Pearson A, Proszek P, Pascual J, Fribbens C, Shamsher MK, Kingston B, et al. Inactivating NF1 Mutations Are Enriched in Advanced Breast Cancer and Contribute to Endocrine Therapy Resistance. Clinical Cancer Research. 2020;26(3):608–22.
146. Turner N, Pearson A, Sharpe R, Lambros M, Geyer F, Lopez-Garcia MA, et al. FGFR1 amplification drives endocrine therapy resistance and is a therapeutic target in breast cancer. Cancer Res. 2010;70(5):2085–94.
147. Hanf D, Fasching P, Gass P, Matthias W. Beckmann, Hack CC, Heindl F, et al. Impact of CCND1 amplification on the prognosis of hormone receptor–positive, HER2-negative breast

cancer patients—correlation of clinical and pathological markers. Breast Cancer Research and Treatment. 2025;210(1):125–34.

7. APPENDIX

Table 6. List of genes, their targeted regions and alteration types assessed via the AVENIO ctDNA Expanded Kit (Roche).

Gene	Seq Target	SNV	Indel*	Fusion**	CNV**
ABL1	Selected Regions	●			
AKT1	Selected Regions	●			
AKT2	Selected Regions	●			
ALK	Selected Regions	●	●	●	
APC	Selected Regions	●	●		
AR	All Coding Regions	●			
ARAF	Selected Regions	●			
BRAF	Selected Regions	●	●		
BRCA1	All Coding Regions	●			
BRCA2	All Coding Regions	●			
CCND1	All Coding Regions	●			
CCND2	All Coding Regions	●			
CCND3	All Coding Regions	●			
CD274	All Coding Regions	●			
CDK4	All Coding Regions	●			
CDK6	Selected Regions	●			
CDKN2A	All Coding Regions	●			
CSF1R	Selected Regions	●			
CTNNB1	Selected Regions	●	●		
DDR2	Selected Regions	●			
DPYD	Selected Regions	●			
EGFR	All Coding Regions	●	●		●
ERBB2	All Coding Regions	●	●		●
ESR1	All Coding Regions	●			
EZH2	Selected Regions	●			
FBXW7	All Coding Regions	●			
FGFR1	Selected Regions	●			
FGFR2	Selected Regions	●		●	

FGFR3	Selected Regions	●		●	
FLT1	Selected Regions	●			
FLT3	Selected Regions	●			
FLT4	Selected Regions	●			
GATA3	Selected Regions	●			
GNA11	Selected Regions	●			
GNAQ	Selected Regions	●			
GNAS	Selected Regions	●			
IDH1	Selected Regions	●			
IDH2	Selected Regions	●			
JAK2	Selected Regions	●			
JAK3	Selected Regions	●			
KDR	Selected Regions	●			
KEAP1	All Coding Regions	●			
KIT	Selected Regions	●	●		
KRAS	All Coding Regions	●			
MAP2K1	Selected Regions	●			
MAP2K2	Selected Regions	●			
MET	All Coding Regions	●	●		●
MLH1	All Coding Regions	●			
MSH2	All Coding Regions	●			
MSH6	All Coding Regions	●			
MTOR	Selected Regions	●			
NF2	All Coding Regions	●			
NFEL2	Selected Regions	●			
NRAS	Selected Regions	●			
NTRK1	Selected Regions	●		●	
PDC1LG2	All Coding Regions	●			
PDGFRA	Selected Regions	●			
PDGFRB	Selected Regions	●			
PIK3CA	Selected Regions	●	●		
PIK3R1	Selected Regions	●			

PMS2	All Coding Regions	●			
PTCH1	Selected Regions	●			
PTEN	All Coding Regions	●	●		
RAF1	Selected Regions	●			
RB1	All Coding Regions	●			
RET	Selected Regions	●		●	
RNF43	Selected Regions	●			
ROS1	Selected Regions	●		●	
SMAD4	All Coding Regions	●			
SMO	All Coding Regions	●			
STK11	All Coding Regions	●			
TP53	All Coding Regions	●			
TERT promoter	Selected Regions	●			
TSC1	Selected Regions	●	●		
TSC2	Selected Regions	●			
UGT1A1***	Selected Regions	●			
VHL	All Coding Regions	●			

All coding regions are based on the longest transcript from Ensembl build 82.
*Indels are limited to variants in a pre-specified list of positions, referred to as "Loci of Interest", except for EGFR exon 19 long deletions, EGFR exon 20 long insertions and MET long insertions, which are not restricted to a pre-defined set of indels.
**Detection of fusions and CNVs are limited to variants in a pre-specified list of positions, referred to as "Loci of Interest" in the AVENIO analysis software.
*** Certain variants are associated with sensitivity to irinotecan.